CHAPTER EIGHTEEN

OPTICAL SPECTRA AND ELECTRONIC STRUCTURE

Guokui Liu and James V. Beitz

18.1 INTRODUCTION

Much of our knowledge of the electronic properties of actinides in solutions and solids is obtained from optical spectroscopy. One of the features that sets actinide spectra apart from those of other elements in the periodic table, aside from the lanthanide series, is that their f-orbitals can be considered both as containing optically active electrons and as belonging to the core of inner shells. As a result of this dominant characteristic, the spectra of these elements, particularly of the lower valence states, are moderately insensitive to changes in the ionic environment. Although ion–ligand interactions shift and split the energy levels of the f-orbitals, the scale of this crystal-field splitting is generally smaller than the intra-ionic Coulomb interaction and spin–orbit coupling. The relative insensitivity of these f-electrons to external forces also means that for these elements there is a close connection between energy levels in compounds and those in gaseous free atoms and ions. Table 18.1 lists the scales of various mechanisms of electronic interactions that will be discussed in this chapter through analysis and modeling of the optical spectra of the various valence states of actinide ions in solutions and compounds.

Table 18.1 *Energy level scales of actinide ions in crystals.*

Interaction mechanism	*Energy* (cm^{-1})[a]	*Optical probe*
configuration splitting ($5f^N$–$5f^{N-1}6d$)	10^5	visible and UV spectroscopy
splitting within a $5f^N$ configuration		
noncentral electrostatic field	10^4	absorption, fluorescence, and laser excitation spectroscopy
spin–orbit interaction	10^3	
crystal-field interaction	10–10^2	
hyperfine splitting	10^{-3}–10^{-1}	selective and nonlinear laser spectroscopy

[a] 1 eV = 8065.7 cm^{-1}.

For the actinide valence states of most interest to chemists, 1+ through 7+, very few gaseous free-ion spectra have been sufficiently analyzed to provide a basis for guiding theoretical interpretations. From an experimental point of view, optical spectroscopy usually probes energy levels with photon sources in the infrared, visible, and ultraviolet (UV) region with energies below 45 000 cm^{-1}. This situation is responsible for the fact that most of our structural information for the f^N states comes from observation of forced electric dipole absorption and luminescence transitions in optically clear crystals. The latter analysis is much simplified by the fact that only transitions between nominal f^N levels are involved. Electric dipole transitions normally are forbidden by the parity selection rule, but in crystals such as $LaCl_3$ that have no center of symmetry, enough of the character of opposite-parity configurations can be mixed in to induce such transitions. At the same time, the admixture (of the order 0.1%) is small enough for the actinide ions in low-lying states of a $5f^N$ configuration that the f-character of the levels is preserved and level calculations can be made on the assumption of a pure $5f^N$ configuration.

The stability of f-orbitals against changes in the ionic environment results in energy levels of various compounds being closely correlated among themselves as well as with those of the free ion, where known. In consequence, *ab initio* free-ion calculations have proven to be very useful for interpreting spectra of the same ion in a solid, and a parametric model based on these calculations has been developed for systematic analyses of the $4f^N$ (lanthanides) (Crosswhite, 1977; Carnall *et al.*, 1989) and $5f^N$ (actinides) (Carnall, 1992; Liu *et al.*, 1994b) optical spectra. This model can be applied in a consistent way to ions of both the actinide and lanthanide series (Crosswhite and Crosswhite, 1984; Görller-Walrand and Binnemans, 1996; Liu, 2000). The free-ion energy levels for trivalent actinide ions in $5f^N$ ($N = 2$ through 13) configurations may be calculated using the parametric model as shown in Fig. 18.1 by the horizontal lines.

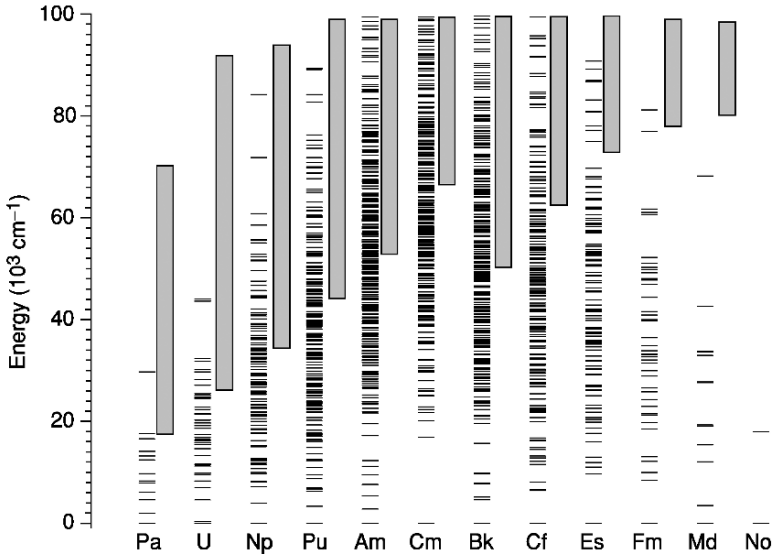

Fig. 18.1 *Calculated free-ion energy levels* (*horizontal lines*) *for the trivalent ions in the* $5f^N$*configurations and the energy range* (*shaded vertical bars*) *for the excited configurations.*

The method of parametric modeling is discussed here to help systematize the overall view of actinide spectra. This chapter is based primarily on Chapter 16 by Carnall and Crosswhite in the second edition of this series. In this review advances in actinide spectroscopy are updated, and in particular, recent progress in the optical spectroscopy of trivalent and tetravalent actinide ions in crystals are included. Our emphasis is on the fundamental understanding of actinide spectra that are interpreted by a parametric model in terms of free-ion and crystal-field interactions (Wybourne, 1965a; Hüfner, 1978; Judd, 1988).

With the experimental techniques used, highly excited states belonging to many different configurations may be produced simultaneously, making interpretation difficult. The estimated energy ranges of the $5f^{N-1}6d$, $5f^{N-1}7s$, and $5f^{N-1}7p$ configurations are plotted in Fig. 18.1 as gray bars for comparison with the calculated energy levels of the free-ion states of the $5f^N$ configurations of trivalent actinide ions (Brewer, 1971a). It is obvious that large portions of the upper states of $5f^N$ configurations overlap with the low-lying states of $5f^{N-1}6d$, $5f^{N-1}7s$, and $5f^{N-1}7p$ configurations. Therefore, a major complicating factor in the theoretical interpretation of $5f^N$ spectra is the extensive inter-configurational mixing, often termed as configurational interaction (Wybourne, 1965a; Dieke, 1968; Goldschmidt, 1978; Hüfner, 1978; Crosswhite and Crosswhite, 1984).

These effects of mixing other configurations into the $5f^N$ states involve not only competing configurations with large overlaps but also cumulative interactions with infinitely many distant electronic configurations. That this is a serious problem is demonstrated by analysis of isotope shifts and hyperfine structure in actinide free-ion spectra (Fred, 1967). The parameters that describe the energy level structure for a configuration would show less variation if the independent-particle model provided a fully accurate description of actinide free-ion spectra. In the parametric model for f-element spectral analysis, the effects of configuration interaction are partially compensated by the use of effective operators in the atomic Hamiltonian for f^N shells (Wybourne, 1965a; Judd, 1966, 1968a,b; Crosswhite *et al.*, 1968; Goldschmidt, 1978; Poon and Newman, 1983; Judd and Crosswhite, 1984; Judd and Suskin, 1984).

Qualitatively, the spectroscopic properties of lanthanides and actinides are very similar because both f-shell electron densities are primarily within already filled s- and p-shells of one higher principal quantum number, which partially shield the f-shells from external influences. A comparison of the Nd^{3+} and U^{3+} analogs is shown in Fig. 18.2, where the squares of the f-electron radial functions are multiplied by an arbitrary factor for emphasis. The same theoretical framework has been used successfully in modeling solid-state spectra of trivalent (Edelstein *et al.*, 1967; Carnall, 1989) and tetravalent actinides (Edelstein, 1987; Krupa, 1987; Liu *et al.*, 1994b; Liu, 2000), as well as for the lanthanide series (Crosswhite, 1977; Carnall *et al.*, 1989; Görller-Walrand and Binnemans, 1996).

Notice that in Fig. 18.2 for U^{3+} (relative to Nd^{3+} $4f^3$) the $5f^3$ peak is considerably displaced toward greater r values with respect to the shielding of s- and p-shells, and the relative magnitude of the 5f electron tail at large r with respect to the rest of the core function is larger and more exposed. Because of the greater extension of the 5f orbitals with respect to those of the shielding 6s and 6p shells, they are more sensitive to changes in the valence electron situation than is the case for the corresponding lanthanide ions. As a result, actinides in solution and in solids, particularly in the first half of the $5f^N$ series, appear in different valence states from 3+ to 6+, making 5f spectroscopy extremely rich and complicated.

18.2 RELATIVE ENERGIES OF ACTINIDE ELECTRONIC CONFIGURATIONS

In order to emphasize the systematic correlations found in the energy level structure of actinide ions both as a function of atomic number Z and for configurations with the same number of f-electrons but different charge states, we begin by considering the types of interactions that have been used successfully to account for observed energy level structures. In the discussion of atomic spectra, attention is focused on identification of the ground (lowest-energy) and

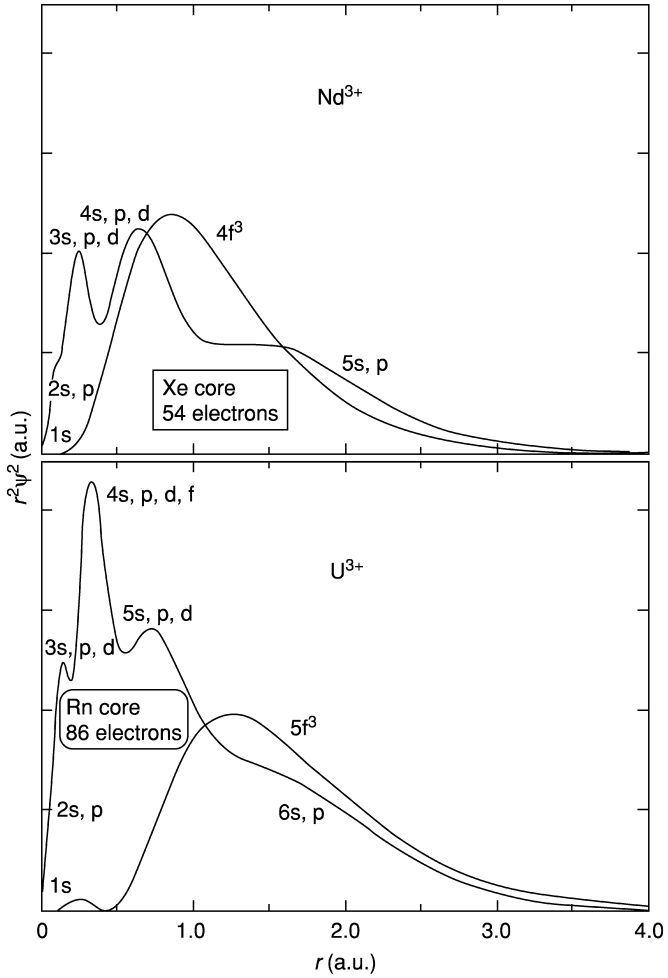

Fig. 18.2 *Comparison of the overlap of* $4f^3$–$5s,p$ *configurations and those of* $5f^3$–$6s,p$ *configurations for* Nd^{3+} *and* U^{3+}, *respectively.*

excited electronic configurations of neutral as well as ionized species. The relative energies of the various electronic configurations thus established provide the basis for extending the interpretation of spectra (and thus electronic structure) to condensed media. In gaseous atomic or ionic species, the energy level structure is attributed primarily to the interactions between electrons in unfilled shells. In condensed media, the additional effect of the ligand field is superimposed. Several summaries of the atomic spectra of the actinides have been published (Kanellakopulos and Fischer, 1973; Peterson, 1976;

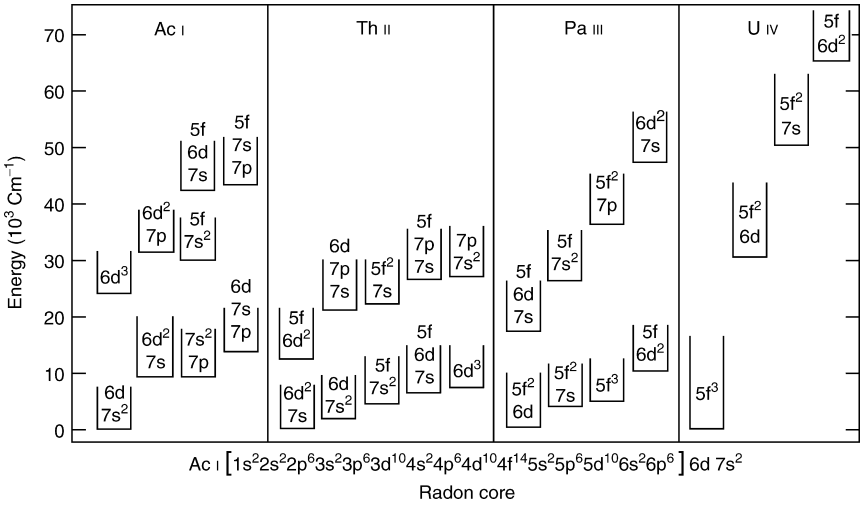

Fig. 18.3 *Three-electron configurations beyond the radon core.*

Crosswhite, 1982; Blaise *et al.*, 1983; Crosswhite and Crosswhite, 1984; Worden *et al.*, 2005).

The progenitor of the actinide (5f) series is actinium. The electronic structure of zero-valent actinium Ac I[1] is represented as three electrons ($6d7s^2$) outside the radon core. This can be written [Rn] ($6d7s^2$), but in the subsequent discussion the core symbol [Rn] will be omitted from the notation. All of the actinide atomic and ionic species are built on the radon core, but the properties of the electronic structure beyond the core depend on the energy with respect to the ground state, atomic number Z, and the state of ionization (Brewer, 1971a,b, 1983). Thus, within the energy range indicated in Fig. 18.3, in addition to configurations involving 6d and 7s electrons, there are those containing 7p and 5f electrons.

Fig. 18.3 is to be interpreted in the following manner. In Ac I the lowest-energy electron states result from the coupling of two 7s electrons and one 6d electron. Further, an energy equivalent to about 9000 cm^{-1} is sufficient to promote a ground-state 7s electron to the 6d shell, thus forming the lowest level of the excited configuration ($6d^27s$). Essentially the same energy is required to promote a ground-state 6d electron to the 7p shell, giving the excited configuration ($7s^27p$). Only the lowest-energy state (relative to the ground state) for each configuration is indicated in the figure. In most cases large numbers of excited states exist within each of the configurations, so that the density of levels from overlapping configurations increases appreciably with

[1] In atomic spectroscopy, Roman letters I, II, III, IV,...refer to ionic oxidation states 0, 1+, 2+, 3+,... respectively, while in some chemistry literature, notations such as An(I) refers to An^+.

excitation energy. However, since the coupling of two 7s electrons result in a filled subshell, the ground configuration in Ac I ($6d7s^2$) is simple in structure, involving only the states of a single 6d electron, $^2D_{3/2}$ and $^2D_{5/2}$. Such states, written in terms of the quantum numbers S, L, and J, are subsequently referred to as free-ion states.

In Th II, the ground state belongs to $6d^27s$, but as Fig. 18.3 indicates, the spectrum at lower energies is very complex due to a number of electronic configurations with nearly the same energy relative to the ground state. In Pa III, the three electrons beyond the Rn core in the ground state belong to the $5f^26d$ configuration. In U IV, further stabilization of the 5f orbital has taken place and excited configurations occur at much higher energies relative to the ground state than was the case in Pa III, Th II, and Ac I. Thus in U IV, the only electronic transitions observed in absorption in the range up to ~30 000 cm^{-1} are those *within* the $5f^3$ configuration.

Experimentally, free-ion spectra (for both neutral and ionic species) usually have been observed in emission, and the underlying energy level structures are deduced from coincidences of energy differences of pairs of spectral lines, subject to verification by isotope shift, hyperfine structure, and magnetic g-factor tests. In condensed phases, spectra are more commonly measured in absorption. Since the application of tunable lasers, laser-induced fluorescence spectra and excitation spectra also have been used in condensed phases to probe energy levels of actinide ions that possess a metastable emitting state. Relative intensities associated with 'parity-allowed' and 'forbidden' transitions are reflected in the nature of two processes: transitions in which the initial and final states belong to electronic configurations of different parity (parity-allowed transitions, e.g. $5f^3 \rightarrow 5f^26d$) and those in which both states belong to the same configuration (parity-forbidden transitions, e.g. $5f^3 \rightarrow 5f^3$). The latter are weak and sharp. The former are much more intense and are associated with broader absorption bands.

The primary purpose of this chapter is to elucidate the electronic energy level structure of the $5f^N$ configurations of actinide ions in condensed phases. The energy levels of trivalent and tetravalent actinide ions in $5f^N$ configurations spread up to ~100 000 cm^{-1} for $4 \leq N \geq 10$, and even extend higher than 150 000 cm^{-1} for $N = 6, 7, 8$. However, as shown in Fig. 18.3, the energy levels of the excited state configurations, specifically, $5f^{N-1}6d$, $5f^{N-1}7s$, and $5f^{N-1}7p$ are present below 100 000 cm^{-1} and thus overlap the energy levels of the $5f^N$ states. This overlap induces complexity in modeling the energy level structures, since the commonly used theory treats the inter-configurational coupling as a perturbation, an approximation that is valid only when the respective configurations are well separated. In this section, a systematic comparison of the energies between the ground states of $5f^N$ configurations and the higher-lying energy configurations that are accessible via optical excitation is given. The energy required to promote an electron from a 5f to a 6d orbital varies rapidly in an irregular manner as the nuclear charge is increased, but a large portion of the

variation and most of the irregularity can be attributed to the pairing energy within the $5f^N$ configuration (Jørgensen, 1975, 1980). A method of using thermodynamic and spectroscopic data for calculating energies of various electronic configurations of lanthanide and actinide ions was developed by Brewer (1971a,b).

For the case of electrons in a 6d orbital, ion–lattice coupling is much stronger than for a 5f orbital. As a result, the energy levels of the $5f^{N-1}6d$ configuration exhibits much stronger host dependence than that of the $5f^N$ configurations. Systematic variation of the $5f^{N-1}6d$ energy level structures for trivalent lanthanide ions in CaF_2 was measured in ultraviolet absorption spectra (Loh, 1966). (van Peterson *et al.*, 2002) conducted further experimental measurements and theoretical modeling of the inter-configuration $4f^N$ to $4f^{N-1}5d$ transitions of rare earth (RE) ions in $LiYF_4$ and YPO_4. For actinide ions, extensive studies of $5f^N$ to $5f^{N-1}6d$ transitions are limited to the $5f^1$ and $5f^2$ configurations. The 6d states of Pa^{4+} in several crystalline hosts were measured based on observed 5f−6d electronic transitions (Piehler *et al.*, 1991; Edelstein *et al.*, 1992). The lowest-energy level of the 6d state is only $\sim$20 000 cm^{-1} above the ground state of Pa^{4+}. In the series of $5f^1$ ions, the differences between the lowest 6d energy level and the ground $5f^1$ level for U^{5+} and Np^{6+} increase as do the total splittings of the 5f energy levels with atomic number (Carnall and Crosswhite, 1985).

18.3 MODELING OF FREE-ION INTERACTIONS

The well-developed theoretical framework for modeling the electronic interactions and analyzing the optical spectra of lanthanide ions has been adopted to modeling the actinides because of the similarities in the electronic properties of actinides in the $5f^N$ configurations and the lanthanides in the $4f^N$ configurations (Crosswhite, 1977; Edelstein, 1979, 1995; Carnall and Crosswhite, 1985; Carnall *et al.*, 1991; Liu *et al.*, 1994b; Liu, 2000). In this section a brief review of the free-ion part of the model theory and its applications to actinide spectroscopy is given.

18.3.1 Central field approximation

Interpretation of optical spectra of actinides in condensed phases follows the general approach in atomic spectroscopy that utilizes the central field approximation and Hartree–Fock method (Hartree, 1957; Slater, 1960; Weissbluth, 1978). In the central field approximation, each electron is assumed to move independently in the field of the nucleus and a central field made up of the spherically averaged potential fields of each of the other electrons. The non-spherical part of the electronic interactions is treated as a perturbation to a spherically symmetric potential, so that the basis of the hydrogen atom wave functions can be used to construct the eigenstates of an N-electron atom (ion). The same method has been used to classify electronic states and evaluate energy levels of lanthanide and actinide ions (Judd, 1963b; Wybourne, 1965a).

The primary terms of the Hamiltonian for an N-electron ion in the absence of external fields are commonly expressed as

$$\mathscr{H} = \mathscr{H}_0 + \mathscr{H}_{\mathrm{C}} + \mathscr{H}_{\mathrm{S-O}}, \tag{18.1}$$

where

$$\mathscr{H}_0 = -\sum_{i=1}^{N} \frac{\hbar^2}{2m} \boldsymbol{\nabla}_i^2 - \sum_{i=1}^{N} \frac{Ze^2}{r_i}, \tag{18.2}$$

$$\mathscr{H}_{\mathrm{C}} = \sum_{i<j}^{N} \frac{e^2}{r_{ij}}, \tag{18.3}$$

$$\mathscr{H}_{\mathrm{S-O}} = \sum_{i}^{N} \xi(r_i) \boldsymbol{l}_i \cdot \boldsymbol{s}_i. \tag{18.4}$$

In equation (18.2), the first term is the kinetic energy and the second term is the potential energy of the electrons in the field of the nucleus. All levels that belong to a particular configuration are shifted equally by this term, which is purely radial, without affecting the energy level structure of the configuration. The term $\mathscr{H}_{\mathrm{C}}$ in equation (18.3) represents the inter-electron Coulombic repulsion between a pair of electrons at a distance of r_{ij}, which varies for different states of the same configuration. The term $\mathscr{H}_{\mathrm{S-O}}$ describes the spin–orbit interactions, which can be understood as magnetic dipole–dipole interactions between the spin and angular momenta of the electrons. In equation (18.4), the spin–orbit coupling constant $\xi(r_i)$ is defined as solely a function of r_i.

Exact solutions of Schrödinger's equation are not possible for systems with more than one electron. In the framework of the central field approximation, one assumes that it is possible to construct a potential energy function $U(r_i)$, which is a spherically symmetric, one-electron operator, and is a good approximation to the actual potential energy of the electron i in the field of the nucleus and the other $N-1$ electrons. Therefore, $\mathscr{H}_0$ can be replaced by (Weissbluth, 1978)

$$\mathscr{H}_0' = \sum_{i=1}^{N} \left[-\frac{\hbar^2}{2m} f \boldsymbol{\nabla}_i^2 + U(r_i) \right], \tag{18.5}$$

with

$$\sum_{i=1}^{N} U(r_i) = -\sum_{i=1}^{N} \frac{Ze^2}{r_i} + \left\langle \sum_{i<j}^{N} \frac{e^2}{r_{ij}} \right\rangle. \tag{18.6}$$

The second term in equation (18.6) is an average over a sphere of the electron repulsion. This term is therefore independent of the angular coordinates. Since $\mathscr{H}_0'$ contains the kinetic energy, the potential energy of N-electrons, and most of the inter-electron repulsion, it is called the Hamiltonian of the central

field. Since most of the inter-electron repulsion is included in the central field Hamiltonian equation (18.5), the second term in equation (18.1) can be rewritten as

$$\mathscr{H}'_{\mathrm{c}} = \sum_{i<j}^{N} \frac{e^2}{r_{ij}} - \left\langle \sum_{i<j}^{N} \frac{e^2}{r_{ij}} \right\rangle, \tag{18.7}$$

which is small enough to be treated, along with the spin–orbit Hamiltonian (equation (18.4)), as a perturbation to the central field potential.

The eigenfunctions of $\mathscr{H}'_0$ for a N-electron ion are obtained as a linear combination of one-electron wave functions that satisfy the Pauli exclusion principle and are subject to the orthonormality condition. This method, known as the Hartree–Fock approach, is generally used for seeking an approximate solution to the N-electron Schrödinger equation (Hartree, 1957; Weissbluth, 1978). All effects of noncentral field interactions including spin–orbit coupling and many-body collective electronic interactions are considered by introducing additional effective operators and diagonalizing the Hamiltonian with parameters determined in comparison with experiments.

In the Hartree–Fock method, the wave function of each electron is expressed as a product of radial functions and angular functions of the spherical harmonics multiplied by a spin function

$$\Psi_{nlm_{\mathrm{l}}m_{\mathrm{s}}}(\mathbf{r}, m_s) = \frac{1}{r} R_{n\mathrm{l}}(r)\, Y_{lm_{\mathrm{l}}}(\theta, \varphi)\sigma(m_{\mathrm{s}}), \tag{18.8}$$

where the radial function $R_{nl}(r)$ depends on the central field potential, which determines the radial charge distribution functions such as that plotted in Fig. 18.2 for U^{3+}. The spherical harmonic function $Y_{lm_{\mathrm{l}}}(\theta, \varphi)$ in equation (18.8) is characterized by the four conventional quantum numbers n, l, m_{l}, and m_{s}, which define a unique state of an electron in an atom. For electrons in a $5f^N$ configuration,

$$\begin{aligned} &n = 5, \\ &l = 3, m_{\mathrm{l}} = -l, -l, +1, ..., l, \\ &m_{\mathrm{s}} = \frac{1}{2} \end{aligned} \tag{18.9}$$

The central field wave function for N-electrons thus may be written in the form of a determinant as

$$\Psi(\lambda_1, \lambda_2, ..., \lambda_N) = \frac{1}{\sqrt{N!}} \begin{vmatrix} \Psi_1(\lambda_1) & \Psi_2(\lambda_1) & \cdots & \Psi_N(\lambda_1) \\ \Psi_1(\lambda_2) & \Psi_2(\lambda_2) & \cdots & \Psi_N(\lambda_2) \\ \vdots & & & \\ \Psi_1(\lambda_N) & \Psi_2(\lambda_N) & \cdots & \Psi_N(\lambda_N) \end{vmatrix}, \tag{18.10}$$

in which $\Psi_i(\lambda_j)$ are spin orbital wave functions in the form of equation (18.8). The subscript i identifies a particular choice of the four quantum numbers n, l,

m_l, and m_s, where λ_j represents the space and spin coordinates of the jth electron. The primary purpose of the central field approximation is to use the N-electron wave functions defined by equation (18.10) as the basis functions for the perturbation terms of a Hamiltonian that includes inter-electron Coulomb (18.3) and spin–orbit interactions (18.4).

18.3.2 *LS* coupling and intermediate coupling

To construct wave functions for a multielectron atom on the basis of the central field approximation, one needs to choose a coupling scheme for angular momentum summation to determine the wave functions of the N-independent electrons defined by equation (18.10). There are two coupling schemes that are commonly used for two extreme cases in atomic spectroscopy (Judd, 1963b; Cowan, 1981). In lighter atoms, where spin–orbit interactions (equation (18.4)) tend to be small compared with the electrostatic interactions between electrons (equation (18.3)), the so-called Russell–Saunders coupling scheme, or LS coupling scheme is a good choice, since L and S are approximately good quantum numbers. With increasing Z, electrostatic interactions decrease and spin–orbit interactions become more important, and in the heavier atoms, spin–orbit interactions become much stronger than the Coulomb interactions. Thus, one should consider the j–j coupling scheme. For f-elements, the Coulomb electrostatic interactions and spin–orbit interactions have the same order of magnitude. Therefore, neither coupling scheme is really appropriate. Calculations of energy levels of actinide ions involve a mathematically more complicated scheme that is called intermediate coupling, which is usually developed from the LS scheme.

In the LS coupling scheme, orbital momentum (l) and spin momentum (s) of individual electrons are summed separately (Weissbluth, 1978; Cowan, 1981). Thus

$$\boldsymbol{L} = \sum_{i=1}^{N} \boldsymbol{l}_i, \quad \boldsymbol{S} = \sum_{i=1}^{N} \boldsymbol{s}_i, \tag{18.11}$$

where $\boldsymbol{L}$ and $\boldsymbol{S}$ are the total orbital and total spin momentum operators, respectively. $\boldsymbol{J}$ defined as

$$\boldsymbol{J} = \boldsymbol{L} + \boldsymbol{S}, \tag{18.12}$$

is the total angular momentum operator which has $2J+1$ eigenstates represented by the magnetic quantum number $M = -J, -J+1, \ldots, J$.

In the LS coupling scheme, the electronic states of an actinide ion may be specified completely by writing the basis states as

$$\Psi = |nl\tau LSJM\rangle, \tag{18.13}$$

where nl, which is 5f or 6d for actinide ions, represents the radial part of the basis states. Usually, the symbol ${}^{2S+1}L_J$ is used to label a free-ion state that is

Table 18.2 *Electronic configurations and ground states of divalent (An^{2+}), trivalent (An^{3+}), and tetravalent (An^{4+}) actinide ions.*

Atomic number	*Element*	An^{2+}	An^{3+}	An^{4+}
89	Ac actinium	$5f^1$, $^2S_{1/2}$	$5f^0$, $^1S_0$	
90	Th thorium	$6d^2$, $^3F_2$	$6d^1$, $^2D_{3/2}$	$5f^0$, $^1S_0$
91	Pa protactinium	$5f^26d^1$, $^4I_{11/2}$	$5f^2$, $^3H_4$	$5f^1$, $^2F_{5/2}$
92	U uranium	$5f^36d^1$, $^5L_6$	$5f^3$, $^4I_{9/2}$	$5f^2$, $^3H_4$
93	Np neptunium	$5f^5$, $^6H_{5/2}$	$5f^4$, $^5I_4$	$5f^3$, $^4I_{9/2}$
94	Pu plutonium	$5f^6$, $^7F_0$	$5f^5$, $^6H_{5/2}$	$5f^4$, $^5I_4$
95	Am americium	$5f^7$, $^8S_{7/2}$	$5f^6$, $^7F_0$	$5f^5$, $^6H_{5/2}$
96	Cm curium	$5f^8$, $^7F_6$	$5f^7$, $^8S_{7/2}$	$5f^6$, $^7F_0$
97	Bk berkelium	$5f^9$, $^6H_{15/2}$	$5f^8$, $^7F_6$	$5f^7$, $^8S_{7/2}$
98	Cf californium	$5f^{10}$, $^5I_8$	$5f^9$, $^6H_{15/2}$	$5f^8$, $^7F_6$
99	Es einsteinium	$5f^{11}$, $^4I_{15/2}$	$5f^{11}$, $^5I_8$	$5f^9$, $^6H_{15/2}$
100	Fm fermium	$5f^{12}$, $^3H_6$	$5f^{11}$, $^4I_{15/2}$	$5f^{11}$, $^5I_8$
101	Md mendelevium	$5f^{13}$, $^2F_{7/2}$	$5f^{12}$, $^3H_6$	$5f^{11}$, $^4I_{15/2}$
102	No nobelium	$5f^{14}$, $^1S_0$	$5f^{13}$, $^2F_{7/2}$	$5f^{12}$, $^3H_6$

called a multiplet. Whereas S and J are specified with numbers $(0, \frac{1}{2}, 1, ...)$, L is traditionally specified with letters S, P, D, F, G, H, ... respectively, for $L = 0$, 1, 2, 3, 4, 5, ... Table 18.2 lists the electronic configurations and ground states identified by $^{2S+1}L_J$ for divalent, trivalent, and tetravalent ions in the actinide series. All tetravalent ions (An^{4+}) have the lowest spectroscopic energies in $5f^N$ configurations, however, this is not true for the lighter divalent ions. For Th^{3+}, the ground state in known compounds is $6d^1$, $^2D_{3/2}$ instead of the calculated $5f^1$, $^2F_{5/2}$ (Brewer, 1971a,b).

An additional quantum number τ, the seniority number, is needed for distinguishing the states that have the same L and S quantum numbers. In fact, two more quantum numbers are needed to completely define the states of an f^N configuration. One such classification number is $W = (w_1w_2w_3)$, with three integers for characterizing the irreducible representations of the seven-dimensional rotational group R_7. The other classification number is $U = (u_1u_2)$ for characterizing the irreducible representations of the group G_2. Details as to classification of the f^N states are given by Judd (1963b) and Wybourne (1965a). Table 18.3 lists the classification of the states for the f^N configurations with $N \leq 7$. Columns 5 and 11 list the LS terms with the same S, and columns 6 and 12 list the number of $^{2S+1}L_J$ multiplets in the classification. The LS terms of the $5f^{14-N}$ configuration are identical for those of the $5f^N$ configuration ($N \leq 7$), although the seniority of the states is different.

Inclusion of spin–orbit coupling breaks the symmetry of the LS coupling scheme. In this case,

$$\begin{aligned} \left[\mathscr{H}_{\text{S–O}}, \boldsymbol{L}\right] \neq 0, \left[\mathscr{H}_{\text{S–O}}, \boldsymbol{S}\right] \neq 0, \\ \left[\mathscr{H}_{\text{S–O}}, J^2\right] = \left[\mathscr{H}_{\text{S–O}}, J_Z\right] = 0, \end{aligned} \tag{18.14}$$

Table 18.3 *Classification of the free-ion states of the f^N configurations* (*Wybourne,* 1965a).

N	τ	W	U	^{2S+1}L	N_J	N	τ	W	U	^{2S+1}L	N_J
1	1	(100)	(10)	^{2}F	2				(20)	^{5}DGI	15
2	2	(110)	(10)	^{3}F	3		6	(221)	(10)	^{3}F	3
			(11)	^{3}PH	6				(11)	^{3}PH	6
	2	(200)	(20)	^{1}DGI	3				(20)	^{3}DGI	9
	0	(000)	(00)	^{1}S	1				(21)	^{3}DFGHKL	18
3	3	(111)	(00)	^{4}S	1				(30)	^{3}PFGHIKM	21
			(10)	^{4}F	4				(31)	^{3}PDFFGHHIIK-KLMNO	45
			(20)	^{4}DGI	12		4	(211)	(10)	^{3}F	3
	3	(210)	(11)	^{2}PH	4				(11)	^{3}PH	6
			(20)	^{2}DGI	6				(20)	^{3}DGI	9
			(21)	^{2}DFGHKL	12				(21)	^{3}DFGHKL	18
	1	(100)	(10)	^{2}F	2				(30)	^{3}PFGHIKM	21
4	4	(111)	(00)	^{5}S	1		2	(110)	(10)	^{3}F	3
			(10)	^{5}F	5				(11)	^{3}PH	6
			(20)	^{5}DGI	15		6	(222)	(00)	^{1}S	1
	4	(211)	(10)	^{3}F	3				(20)	^{1}DGL	3
			(11)	^{3}PH	6				(30)	^{1}PFGHIKM	7
			(20)	^{3}DGI	9				(40)	^{1}SDFGGHIIK-LLMNQ	14
			(21)	^{3}DFGHKL	18		4	(220)	(20)	^{1}DGI	3
			(30)	^{3}PFGHIKM	21				(21)	^{1}DFGHKL	6
	2	(110)	(10)	^{3}F	3				(22)	^{1}SDGHILN	7
			(11)	^{3}PH	6		2	(200)	(20)	^{1}DGI	3
	4	(220)	(20)	^{1}DGI	3		0	(000)	(00)	^{1}S	1
			(21)	^{1}DFGHKL	6	7	7	(000)	(00)	^{8}S	1
			(22)	^{1}SDGHILN	7		7	(200)	(20)	^{6}DGI	17
	2	(200)	(20)	^{1}DGI	3		5	(110)	(10)	^{6}F	6
	0	(000)	(00)	^{1}S	1				(11)	^{6}PH	9
5	5	(110)	(10)	^{6}F	6		7	(220)	(20)	^{4}DGI	12
			(11)	^{6}PH	9				(21)	^{4}DFGHKL	24
	5	(211)	(10)	^{4}F	4				(22)	^{4}SDGHILN	25
			(11)	^{4}PH	7		5	(211)	(10)	^{4}F	4
			(20)	^{4}DGI	12				(11)	^{4}PH	7
			(21)	^{4}DFGHKL	24				(20)	^{4}DGI	12
			(30)	^{4}PFGHIKM	27				(21)	^{4}DFGHKI	24
	3	(111)	(00)	^{4}S	1				(30)	^{4}PFGHIKM	27
			(10)	^{4}F	4		3	(111)	(00)	^{4}S	1
			(20)	^{4}DGI	12				(10)	^{4}F	4
	5	(221)	(10)	^{2}F	2				(20)	^{4}DGI	12
			(11)	^{2}PH	4		7	(222)	(00)	^{2}S	1
			(20)	^{2}DGI	6				(10)	^{2}F	2
			(21)	^{2}DFGHKL	12				(20)	^{2}DGI	6
			(30)	^{2}PFGHIKM	14				(30)	^{2}PFGHIKM	14
			(31)	^{2}PDFFGHH-IIKKLMNO	30				(40)	^{2}SDFGGHII-KLLMNQ	27
	3	(210)	(11)	^{2}PH	4		5	(221)	(10)	^{2}F	2
			(20)	^{2}DGI	6				(11)	^{2}PH	4

Table 18.3 (*Contd.*)

N	τ	W	U	^{2S+1}L	N_J	N	τ	W	U	^{2S+1}L	N_J
			(21)	^{2}DFGHKL	12				(20)	^{2}DGI	6
	1	(100)	(10)	^{2}F	2				(21)	^{2}DFGHKL	12
6	6	(100)	(10)	^{7}F	7				(30)	^{2}PFGHIKM	14
	6	(210)	(11)	^{5}PH	8				(31)	^{2}PDFFGHHII-KKLMNO	30
			(20)	^{5}DGI	15		3	(210)	(11)	^{2}PH	4
			(21)	^{5}DFGHKL	30				(20)	^{2}DGI	6
	4	(111)	(00)	^{5}S	1				(21)	^{2}DFGHKL	12
			(10)	^{5}F	5		1	(100)	(10)	^{2}F	2

namely, J^2 and M still commute, but $\boldsymbol{L}$ and $\boldsymbol{S}$ do not. Thus L and S are no longer good quantum numbers, but J and M are still good; therefore, the wave functions $|nl\tau LSJM\rangle$ are not eigenfunctions of the Hamiltonian shown in equation (18.1). One may obtain a new set of eigenfunctions by diagonalizing the primary terms of the Hamiltonian defined by equations (18.4) and (18.7) with the basis set in terms of $|nl\tau LSJM\rangle$ based on perturbation theory and the concept of the central field approximation. As a result, the new eigenfunctions are linear combinations of the LS basis sets, and are known as the free-ion wave functions in the intermediate coupling scheme. If we do not include inter-configurational coupling, the eigenfunctions in the intermediate coupling scheme are expressed as

$$\Psi(nlJ) = \sum_{\tau LS} a_{\tau LSJ} |nl\tau LSJ\rangle, \tag{18.15}$$

where the coefficients $a_{\tau LSJ}$ are determined by the matrix elements

$$a_{\tau LSJ} = \sum_{\tau' L' S'} \langle nl\tau LSJ| \mathscr{H}_{\mathrm{C}} + \mathscr{H}_{\mathrm{S-O}} |nl\tau' L' S' J'\rangle \delta_{JJ'}. \tag{18.16}$$

The energy levels of the free-ion states are independent of M, so they are $(2J+1)$-fold degenerate. The new basis set (equation (18.15)) in the intermediate coupling scheme describes the energy states of a Hamiltonian that includes Coulomb and spin–orbit interactions and is obtained from the mixing of all LS terms with the same J in a given $5f^N$ configuration. The transformation coefficients of $a_{\tau SLJ}$ are the components of the eigenvector pertaining to the basis state in the LS coupling (Judd, 1963b).

18.3.3 Effective-operator Hamiltonian

In spectroscopy, a powerful method for evaluating atomic energy level structure is to define and diagonalize an effective-operator Hamiltonian with the wave functions of the central field Hamiltonian. Racah (1949) used this method for

calculating the matrix elements of tensor operators of the electronic angular momentum (Racah, 1949). Since then, many developments have been made, particularly for applications of the effective-operator method to rare earth spectroscopy (Judd, 1963b; Wybourne, 1965a). An essential part of the effective-operator method is to determine the matrix elements of irreducible tensor operators using the Wigner–Eckart theorem. According to the Wigner–Eckart theorem, for a tensor operator $\mathbf{T}^{(k)}$ of rank k with $2k+1$ components $T_q^{(k)}(q = -k, -k+1, \ldots, k)$ that acts on a set of basis functions $|\tau LSJM\rangle$, each of which is an eigenfunction of the operators J^2 and J_z, the matrix elements of $T_q^{(k)}$ can be reduced as

$$\left\langle \tau LSJM \middle| T_q^{(k)} \middle| \tau' L' S' J' M' \right\rangle = (-1)^{J-M} \begin{bmatrix} J & k & J' \\ -M & q & M' \end{bmatrix} \left\langle \tau LSJ \middle\| \mathbf{T}^{(k)} \middle\| \tau' L' S' J' \right\rangle, \tag{18.17}$$

where the $3-j$ symbols involve only geometrical properties of the tensor operator (Rotenberg *et al.*, 1959). The physical nature of the operator is contained entirely in the reduced matrix elements $\left\langle \tau LSJ \middle\| T^{(k)} \middle\| \tau' L' S' J' \right\rangle$. Information on the use of tensor operators in atomic spectroscopy is provided in several textbooks (Judd, 1963b, 1975; Weissbluth, 1978).

In central field approximation, the orbital electronic wave functions of an actinide ion are represented by products of radial and angular parts as shown in equation (18.8). The effective operator for Coulomb electrostatic intra-ion interaction may be expressed by expanding $1/r_{ij}$ into scalar products of tensor operators of spherical harmonics. Therefore, for N-equivalent electrons in orbital nl, the matrix elements of the effective-operator Hamiltonian for the Coulomb electrostatic interaction may be expressed as:

$$\left\langle l^N \tau LS \middle| \sum_{i>j}^{N} \frac{e^2}{r_{ij}} \middle| l^N \tau' \; L' S' \right\rangle = \sum_k f_k(l,l) F^{(k)}(nl, nl), \tag{18.18}$$

where $F^k(nl, nl)$, with $k = 0, 2, 4, 6$, are the Slater radial integrals for the radial part of the electrostatic interaction, which is defined as:

$$F^k(nl, nl) = e^2 \int_0^\infty \int_0^\infty \frac{r_<^k}{r_>^{k+1}} [R_{nl}(r_i)]^2 \left[R_{nl}\left(r_j\right)\right]^2 \mathrm{d}r_i \mathrm{d}r_j \tag{18.19}$$

The value of F^k may be calculated using the Hartree–Fock method, but in analyses of actinide-ion spectra, F^k is considered as an experimentally determined parameter.

The angular part of the matrix element in equation (18.18) is defined as

$$f_k(l,l) = \left\langle l^N \tau LS \middle| \sum_{i>j} \mathbf{C}^{(k)}(i) \cdot \mathbf{C}^{(k)}(j) \middle| l^N \tau' L' S' \right\rangle. \tag{18.20}$$

Using the Wigner–Eckart theorem, the matrix elements in equation (18.20) are best handled by introducing the tensor operator $\mathbf{U}^{(k)}$. In combination with the symmetry properties of angular momentum, f_k can be expressed in terms of the reduced matrix elements of $\mathbf{U}^{(k)}$ as:

$$f_k(l,l) = \frac{1}{2}(2l+1)^2 \begin{pmatrix} l & k & l \\ 0 & 0 & 0 \end{pmatrix}^2 \left\{ \frac{1}{2L+1} \sum_{\tau' L'} \left| \left\langle l^N \tau L S \middle\| \mathbf{U}^{(k)} \middle\| l^N \tau' L' S \right\rangle \right|^2 - \frac{N}{2l+1} \right\}. \tag{18.21}$$

In the particular case of $k = 0$, it is easy to find that

$$f_0(l,l) = N(N-1)/2. \tag{18.22}$$

For the d^N and f^N configurations, the values for the reduced matrix elements of tensor operator $\mathbf{U}^{(k)}$ have been tabulated (Nielson and Koster, 1963). Because of the symmetry properties of the $3-j$ symbol, $f_k(l,l)$ has nonzero values only if $l+l \geq k \geq |l-l|$; and k is even. For f-electrons, $l = 3$, thus f_k vanishes except for $k = 0, 2, 4, 6$.

As defined in equation (18.4), the Hamiltonian for spin–orbit coupling for N-electrons in an actinide ion is a linear summation of the independent spin–orbit interaction for a single electron. In LS coupling, the N-equivalent electronic matrix element of the spin–orbit interaction is expressible in terms of the tensor operator $\mathbf{V}^{(11)}$. Hence the matrix element of spin–orbit interaction for N-equivalent electrons can be expressed as

$$\left\langle nl^N \tau L S J \middle| \sum_{i=1}^{N} \xi(r_i) \boldsymbol{l}_i \cdot \boldsymbol{s}_i \middle| nl^N \tau' L' S' J' \right\rangle = \zeta_{nl} A_{nl}(ls), \tag{18.23}$$

where ζ_{nl} is the spin–orbit interaction parameter defined as a radial integral

$$\zeta_{nl} = \int_0^\infty [R_{nl}(r)]^2 \xi(r) \mathrm{d}r. \tag{18.24}$$

where $R_{nl}(r)$ is the radial wave function.

The spin–orbit parameter can be evaluated numerically using the Hartree–Fock central field potential, but it is usually adjusted to obtain the experimentally observed energies. The matrix element in equation (18.23) can be expressed as (Sobelman, 1972)

$$A_{nl}(ls) = (-1)^{L+S'+J} \sqrt{(2l+1)(l+1)l} \delta_{JJ'} \delta_{MM'} \begin{Bmatrix} L & S & J \\ S' & L' & 1 \end{Bmatrix} \left\langle \tau L S \middle\| \mathbf{V}^{(11)} \middle\| \tau' L' S' \right\rangle, \tag{18.25}$$

where $\{\ldots\}$ is a $6-j$ symbol, and the values for the reduced matrix elements of the tensor operators $\mathbf{V}^{(11)}$ have been tabulated by Slater (1960), Sobelman (1972), and Nielson and Koster (1963).

The electrostatic and spin–orbit interactions usually give the right order for the energy level splitting of the f^N configurations. However, these primary terms of the free-ion Hamiltonian do not accurately reproduce the experimentally measured energy level structures. The reason is the parameters F^k and ζ_{nf}, which are associated with interactions within a f^N configuration, cannot absorb all the effects of additional mechanisms such as relativistic effects and configuration interactions. Introduction of new terms in the effective-operator Hamiltonian is required to better interpret the experimental data. It was demonstrated (Judd and Crosswhite, 1984) that, in fitting the experimental free-ion energy levels of Pr^{3+} (f^2 configuration), the standard deviation between observed and calculated f-state energies could be reduced from 733 to 24 cm^{-1} by adding nine more parameterized effective operators into the Hamiltonian.

Among several corrective terms included in the effective-operator Hamiltonian, a significant contribution to the f^N energy level structure is from configuration interactions between configurations of the same parity. This contribution can be taken into account by a set of three two-electron operators (Wybourne, 1965a):

$$\mathscr{H}_{c1} = \alpha L(L+1) + \beta G(G_2) + \gamma G(R_7) \tag{18.26}$$

where α, β, and γ are the parameters associated with the continuous groups $G(G_2)$ and $G(R_7)$ (Rajnak and Wybourne, 1963, 1964) the latter being eigenvalues of Casimir operators for the groups G_2 and R_7 (Judd, 1963a).

For f^N configurations of $N \geq 3$, three-body interaction terms were introduced by Judd (1966) and Crosswhite *et al.* (1968) as

$$\mathscr{H}_{c2} = \sum_{i=2,3,4,6,7,8} T^i t_i \tag{18.27}$$

where T^i are parameters associated with three-particle operators t^i. This set of effective operators scaled with respect to the total spin $\boldsymbol{S}$ and total orbital angular momentum $\boldsymbol{L}$ are needed in the Hamiltonian to represent the coupling of the f^N states to those in the higher energy configurations (d, p, s) via inter-electron Coulombic interactions. It is common to include six three-electron operators $t^i (i = 2, 3, 4, 6, 7, 8)$. When perturbation theory is carried beyond the second order, an additional eight three-electron operators t^i ($11 \leq i \leq 19$, with $i = 13$ excluded) are required (Judd and Lo, 1996). A complete table of matrix elements of the 14 three-electron operators for the f-shell have been published (Hansen *et al.*, 1996).

In addition to the magnetic spin–orbit interaction parameterized by ζ_{nf}, relativistic effects including spin–spin and spin–other–orbit, both being

parameterized by the Marvin integrals M^0, M^2, and M^4 (Marvin, 1947), are included as the third corrective term of the effective-operator Hamiltonian (Judd *et al.*, 1968).

$$\mathscr{H}_{c3} = \sum_{i=0,2,4} M^i m_i, \tag{18.28}$$

where m_i is the effective operator and M^i is the radial parameter associated with m_i.

As demonstrated (Judd *et al.*, 1968; Carnall *et al.*, 1983), for improving the parametric fitting of the f-element spectra, two-body effective operators can be introduced to account for configuration interaction through electrostatically correlated magnetic interactions. This effect can be characterized by introducing three more effective operators as

$$\mathscr{H}_{c4} = \sum_{i=2,4,6} P^i p_i, \tag{18.29}$$

where p_i is the operator and P^i is the radial parameter.

In summary, 20 effective operators are utilized for fitting spectra, including those for two- and three-electron interactions. The total effective-operator Hamiltonian for free-ion interactions is

$$\begin{aligned}\mathscr{H}_{FI} = &\sum_{k=0,2,4,6} F^k f_k + \zeta_{nl} A_{nl} + \alpha L(L+1) + \beta G(G_2) + \gamma G(R_7) \\ &+ \sum_{i=2,3,4,6,7,8} T^i t_i + \sum_{i=0,2,4} M^i m_i + \sum_{i=2,4,6} p_i P^i.\end{aligned} \tag{18.30}$$

This effective-operator Hamiltonian has been used as the most comprehensive free-ion Hamiltonian in previous spectroscopic analyses of f-element ions in solids (Crosswhite, 1977; Crosswhite and Crosswhite, 1984; Carnall *et al.*, 1989; Liu, 2000). The 20 parameters associated with the free-ion operators are adjusted in the fitting of experimental energy levels.

18.3.4 Reduced matrices and free-ion state representation

In equation (18.30), all effective operators for the free-ion interactions have well-defined group-theoretical properties (Judd, 1963b; Wybourne, 1965a). Within the intermediate coupling scheme, all matrix elements can be reduced, using the Wigner–Eckart theorem, to new forms that are independent of J, viz.

$$\langle \tau SLJ | \mathscr{H}_i | \tau' S' L' J' \rangle = P_i \delta_{JJ'} c(SLS'L'J) \langle \tau SL \| O_i \| \tau' S' L' \rangle, \tag{18.31}$$

where P_i is the parameter, $c(SLS'L'J)$ is a numerical coefficient, and $\langle \tau SL \| O_i \| \tau' S' L' \rangle$ is the reduced matrix element of the effective-operator O_i. Once the reduced matrix elements are calculated, it is not difficult to diagonalize the entire free-ion Hamiltonian with the wave functions in the LS basis set. The free-ion eigenfunctions are thus obtained in the form of the intermediate

coupling representation. All matrix elements of the effective-operator Hamiltonian are evaluated in terms of the parameters of the effective operators.

Because the reduced matrix elements are independent of J, the matrix of the free-ion Hamiltonian thus can be reduced into a maximum of 13 independent submatrices for $J = 0, 1, 2, \ldots, 12$ for even N and $J = \frac{1}{2}, \frac{3}{2}, \frac{5}{2}, \ldots, \frac{25}{2}$ *for odd N* in an f^N configuration. The number of submatrices and their size can be determined from the values of N_J (the number of J levels for a given SL multiplet) given in Table 18.3. Separation of the free-ion matrix into submatrices greatly facilitates the evaluation of free-ion energy levels. However, evaluation of matrix elements is still a considerable effort, particularly with inclusion of the corrective terms in the Hamiltonian. For an f^N configuration with $3 < N < 11$, there are more than 10^4 free-ion matrix elements and each of them may have as many as 20 terms to be evaluated on the basis of angular momentum operations. Fortunately, several groups have calculated the matrix elements that are available on web sites (http://chemistry.anl.gov) from which one may download a MS-Windows based computer program named SPECTRA to calculate the eigenvalues and eigenfunctions of the free-ion Hamiltonian defined in equation (18.30). As discussed in the following sections, SPECTRA can also be used for nonlinear least-squares fitting of observed levels to determine values of the Hamiltonian parameters.

Due to the SL–$S'L'$ mixing in the intermediate coupling scheme, labeling a multiplet as $^{2S+1}L_J$ is incomplete. In most cases, the nominal labeling of a free-ion state as $^{2S+1}L_J$ only indicates that this multiplet has a leading component from the pure LS basis $|LSJ\rangle$. Diagonalization of each of the submatrices produces free-ion eigenfunctions in the form of equation (18.15). As an example, the leading LS terms for the free-ion wave functions of the nominal $^4I_{9/2}$ ground state of the $4f^3$ ion Nd^{3+} and the $5f^3$ ion $U^{3+}$are:

$$\Psi(4f^3, {}^4I_{9/2}) = 0.984\,{}^4I - 0.174\,{}^2H - 0.017\,{}^2G + \text{etc.}$$

$$\Psi(5f^3, {}^2I_{9/2}) = 0.912\,{}^4I - 0.391\,{}^2H - 0.081\,{}^2G + 0.048\,{}^4G + 0.032\,{}^4F + \text{etc.}$$

In general, SL–$S'L'$ mixing becomes more significant in the excited multiplets.

18.3.5 Parameterization of the free-ion Hamiltonian

In an empirical approach to interpretation of the experimentally observed energy level structure of an f-element ion in solids, establishing accurate parameters for the model Hamiltonian essentially relies on systematic analyses that encompass theoretical calculations for incorporating trends of parameter variation across the f-element series. In the previous work that led to the establishment of the free-ion parameters for the trivalent actinide ions (Carnall, 1992) and the tetravalent actinide ions (Carnall *et al.*, 1991; Liu *et al.*, 1994b), the results of analyses of simpler spectra were carried over to more complex ones through consideration of their systematic trends and symmetry properties.

Table 18.4 lists values of the free-ion interaction parameters obtained from analyses of the spectra of An^{3+}:$LaCl_3$.

In early attempts to develop a systematic interpretation of trivalent actinide and lanthanide spectra, initial sets of F^k and ζ_{nf} for some members of the series had to be estimated. This was done by a linear extrapolation based on the fitted parameters that were available from the analyses of other individual spectra. As more extensive data and improved modeling yielded better determined and more consistent F^k and ζ_{nf} values for the 3+ actinides (and lanthanides), it became apparent that the variation in the parameters was nonlinear, as indicated for F^2(5f,5f) in Fig. 18.4. This nonlinearity could also be observed in the values of parameters of the *ab initio* calculations. The difference between the *ab initio* and fitted values of parameters (ΔF) appears to exhibit a much more linear variation with Z than do the parameter values. Consequently, ΔF has been adopted as the basis for a useful predictive model.

For the trivalent actinides, the values of ΔF are not constant over the series, but use of a single average value over a group of four or five elements is not an unreasonable approximation. Thus, in developing a predictive model for the F^k and ζ_{nf} parameters, an attempt is made to establish average values of ΔF for a particular valence state and type of crystal-field interaction. The energy level structure computation based on the predicted parameters can be compared to that observed, and then appropriate modifications sought by a fitting procedure where necessary.

Detailed results of Hartree–Fock calculations on f-electrons were previously analyzed (Carnall *et al.*, 1983; Crosswhite and Crosswhite, 1984). The most important trends are those of the electrostatic-interaction parameters F^k and spin–orbit parameters ζ_{nf} which increase with the number of f-electrons, N. The experimentally determined values of F^k and ζ_{nf} for trivalent actinides in $LaCl_3$ are shown as a function of N in Figs. 18.4 and 18.5, respectively. These values were obtained from the systematic analyses of experimental spectra (Carnall, 1992). Fig. 18.5 also shows the systematic trends for ζ_{nf} for the trivalent actinide ions that were obtained from Hartree–Fock calculations. Although the Hartree–Fock calculations predict the same trends across the series, the Hartree–Fock values for F^k and ζ_{nf} are always larger than the empirical parameters obtained by allowing them to vary in fitting experimental data. The relativistic Hartree–Fock (HFR) values of ζ_{nf} agree remarkably well with empirical values, whereas the F^k values remain considerably larger than the empirical values. Presumably, this is because, in addition to relativistic effects, f-electron coupling with orbitals of higher-lying energies reduces the radial integrals assumed in the HFR approximation. Moreover, the experimental results are obtained for ions in condensed phases, not in a gaseous phase, which leads on average to an ~5% change (Crosswhite, 1977). Because of the absence of mechanisms that absorb these effects in the HFR model, HFR values of F^ks cannot be used directly as initial parameters for the least-squares fitting process. Scaling of HFR values to the experimentally determined ones is

Table 18.4 *Energy-level parameters for trivalent actinide ions in* $LaCl_3$ (*in* cm^{-1}), *from Carnall* (1992).[a]

	U^{3+}	Np^{3+}	Pu^{3+}	Am^{3+}	Cm^{3+}	Bk^{3+}	Cf^{3+}	Es^{3+}	Fm^{3+}	Md^{3+}
F^2	39 611(222)	45 382(80)	48 679(89)	[51 900]	[55 055]	[57 697]	[60 464]	63 174(142)	65 850	68 454
F^4	32 960(418)	37 242(215)	[39 333 R]	[41 600]	43 938(148)	[45 969]	[48 026]	[50 034 R]	52 044	54 048
F^6	23 084(352)	25 644(196)	27 647(89)	[29 400]	32 876(154)	[32 876]	[34 592]	[36 199 R]	37 756	39 283
ζ	1626(3)	1937(2)	2242(2)	2564(3)	2889(4)	3210(4)	3572(2)	3944(3)	4326	4715
α	29.26(0.44)	31.78(0.30)	30.00(0.16)	26.71(0.31)	29.42(0.32)	29.56(0.42)	27.36(0.26)	30.21(1.1)	30	30
β	–824.6(29)	–728.0(18)	–678.3(12)	–426.6(42)	–362.9(51)	–564.9(47)	–587.5(21)	–761.0(55)	–600	–600
γ	1093(105)	840.2(61)	1022(31)	977.9(28)	[500]	839.8(28)	753.5(14)	488.2(39)	450	450
T^2	306(64)	[200]	190(8)	150(20)	[275]	127(15)	105(11)	[110]	100	100
T^3	42(14)	45(7)	54(10)	[45]	[45]	24(59)	48(11)	[45]	45	
T^4	188(20)	50(6)	[45]	[45]	[60]	70(54)	59(21)	[50]	50	
T^6	–242(40)	–361(18)	–368(19)	–487(31)	–289(22)	–388(44)	–529(31)	–256(43)	–300	
T^7	447(61)	427(23)	363(14)	489(28)	546(95)	525(29)	630(34)	648(66)	640	
T^8	[300]	340(17)	322(10)	228(32)	528(52)	378(34)	270(14)	408(44)	400	
M^0	[0.672]	[0.773]	[0.877]	[0.985]	[1.097]	[1.213]	[1.334]	[1.458]	1.587	1.720
M^2	[0.372]	[0.428]	[0.486]	[0.546]	[0.608]	[0.672]	[0.738]	[0.807]	0.878	0.951
M^4	[0.258]	[0.297]	[0.388]	[0.379]	[0.423]	[0.468]	[0.514]	[0.562]	0.612	0.662
P^{2b}	1 216(77)	1009(30)	949(24)	613(42)	1054(36)	667(83)	820(42)	506(102)	600	600
B_0^2	287(32)	164(26)	197(22)	242(34)	[280]	280(40)	306(29)	[306]	306	306
B_0^4	–662(93)	–559(44)	–586(38)	–582(80)	[–884]	–884(62)	–1062(56)	[–1062]	–1062	–1062
B_0^6	–1 340(89)	–1 673(49)	–1723(39)	–1 887(83)	[–1 293]	–1293(68)	–1441(48)	[–1441]	–1441	–1441
B_6^6	1070(63)	1033(34)	1011(34)	1122(49)	[990]	990(40)	941(36)	[941]	941	941
σ^c	29	22	18	21	23	22	19	22		
η^c	82	167	193	79	84	83	110	47		

[a] The values in parentheses are errors in the indicated parameters. The values in brackets were either not allowed to vary in the parameter fitting, or if followed by an *R*, were constrained: For Pu^{3+}, $F^4/F^2 = 0.808$; for Es^{3+}, $F^4/F^2 = 0.792$, $F^6/F^2 = 0.573$. All parameters for Fm^{3+} and Md^{3+} are extrapolated values.
[b] P^2 was varied freely, P^4 and P^6 were constrained by ratios $P^4 = 0.5P^2$, $P^6 = 0.1P^2$.

[c] Deviation $\sigma = \sqrt{\sum_i \Delta_i^2/(n-p)}$, where i is an index that runs over the assigned levels, Δ_i is the difference between observed and calculated energies for the ith assigned level, n is the number of levels fit, and p is the number of parameters freely varied.

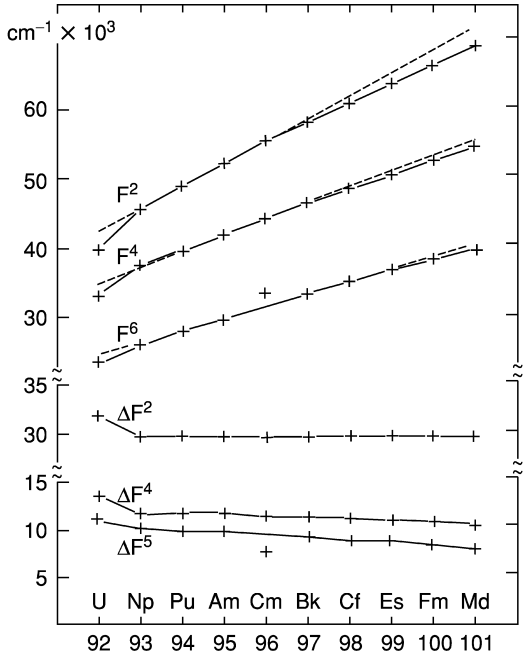

Fig. 18.4 *Variation of the parameters* F^2, F^4, F^6, ΔF^2, ΔF^4, ΔF^6 *where* $\Delta F^N = F^N$ (*HFR*) $-F^4$ (*expt*) *in* cm^{-1} *for* An^{3+}:$LaCl_3$ *as a function of atomic number.* (*Reprinted with permission from Carnall,* 1992. *Copyright* 1992, *American Institute of Physics.*)

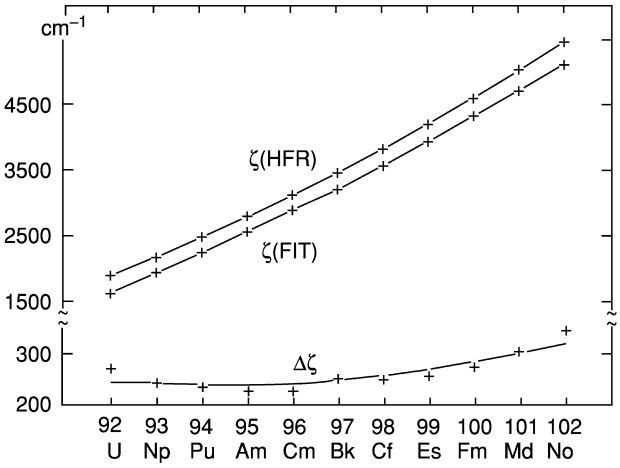

Fig. 18.5 *Variation of the parameter* ζ(*expt*), ζ(*expt*), *and* $\Delta\zeta$(*expt*) *in* cm^{-1} *for* An^{3+}: $LaCl_3$ *as a function of atomic number.* (*Reprinted with permission from Carnall,* 1992. *Copyright* 1992, *American Institute of Physics.*)

necessary to establish a systematic trend for a specific parameter. With this procedure, linear extrapolations of model parameters from one ion to another lead to values consistent with those obtained in the actual fitting process.

In addition to HFR calculations of F^ks and ζ_{nf}, estimated values for $M^k (k = 0, 2, 4)$ can also be computed using the HFR method (Judd *et al.*, 1968). These parameters do not vary dramatically across the f-series. In practice, experience has shown that they can be taken as given or varied as a single parameter while maintaining the HFR ratios $M^2/M^0 = 0.56$ and $M^4/M^0 = 0.31$ (Carnall, 1989). For actinide ions, the ratio M^4/M^0 may be maintained at 0.38−0.4 (see Table 18.4).

For the rest of the free-ion effective operators introduced above, no direct Hartree–Fock calculated values can be derived. Only a term-by-term HFR calculation is possible to give additional guidance for parameter estimates. For example, the HFR values of P^ks for Pr^{2+} and Pr^{3+} have been determined by Copland *et al.* (1971). In establishing systematic trends of parameters for An^{3+}:$LaCl_3$, Carnall (1989) constrained the P^k parameters by the ratios $P^4 = 0.5P^2$ and $P^6 = 0.1P^2$ whereas P^2 was varied freely along with other parameters. These ratios are consistent with the HFR estimation. The variation of these parameters across the series is not significant, and no obvious systematic trends have been established.

Once the systematic trends of free-ion parameters are established, constraints can be imposed on other parameters that are relatively insensitive to the available experimental data. Some parameters such as T^i, M^k, and P^k do not vary significantly across the series and as a good approximation can be fixed at the same values for neighboring ions in the same series. In fact, most of the free-ion parameters are not host sensitive. Typically, there are changes of ~1% in the values of the free-ion parameters between different lattice environments. The free-ion parameters given in Table 18.4 can be used as initial inputs for least-squares fitting of the energy level structure of a trivalent f-element ion in any crystalline lattice. If there is a limited number of experimentally determined levels, one may allow only the F^k and ζ_{nf} parameters to vary freely along with the crystal field parameters and keep the other free-ion parameters fixed. For further improvement of the fits, α, β, and γ can be released. For a final refinement, M^0 and P^2 may be varied freely with $M^{2,4}$ and $P^{4,6}$ varied following M^0 and P^2, respectively, at fixed ratios.

Multiconfiguration calculations have shown that similar values of these effective-operator parameters are to be expected at both ends of the lanthanide sequence (Morrison, 1972), and empirical evaluations are in agreement with this for both the lanthanides and actinides. For three (or 11) electrons, similar arguments show the need for additional (three-body) operators to parameterize the electrostatic interactions completely. If consideration is limited to the interactions arising from second-order perturbation theory, only six new operators are needed (Judd *et al.*, 1968; Judd and Suskin, 1984), and their experimental

evaluation is consistent with results expected from first-principles calculations (Poon and Newman, 1983).

Similar arguments hold for corrections to the spin–orbit interaction, as well as additional terms of relativistic origin such as the spin–other–orbit and spin–spin interactions. Hartree–Fock calculations give good estimates of the Marvin radial integrals $M^k(k = 0, 2, 4)$ associated with spin–other-orbit and spin–spin interactions (Judd *et al.*, 1968). Experimental investigations are needed for evaluation of the magnetic corrections associated with configuration interactions, but experience has shown that a single set of parameters $P^k\left(k = 2, 4, 6 \text{ with } P^4 = 0.75P^2 \text{ and } P^6 = 0.50P^2\right)$ accounts for a large part of this class of corrections (Judd *et al.*, 1968). Use of sets of all of the foregoing parameters has been explored in detail for all of the trivalent ions from U^{3+} through Es^{3+}, and values are shown in Table 18.4 for An^{3+}: $LaCl_3$.

18.4 MODELING OF CRYSTAL-FIELD INTERACTION

When an actinide or lanthanide ion occurs in a condensed-phase medium, the spherical symmetry of its electronic structure is destroyed, and ionic energy levels shift and split under the influence of the electric field produced by the crystalline environment. The energy level shifts and splittings depend on the nature and strength of the interaction with the environment. Some of this interaction can be absorbed by the nominal 'free-ion' parameters themselves and a measure of this contribution would give clues as to the nature of the interactions. Unfortunately, mainly because of the different methods by which the free-ion and condensed-phase levels are determined, there are very few cases in which both sets of parameters are known well enough for meaningful comparisons to be drawn.

In addition to modifications of the atomic parameters, there are medium-related effects that must be taken into account explicitly. The broken spherical symmetry that normally results when an isolated free gaseous ion is placed in a ligand field gives rise to a splitting of the free-ion level into a maximum of $(2J+1)$ components. A single-particle crystal field model has had remarkable success for lanthanide ions and a somewhat qualified, but nevertheless satisfactory, success for the trivalent actinide ions in providing an interpretation of experimental data (Dieke, 1968; Hüfner, 1978; Carnall, 1992; Liu, 2000). The degree to which the $2J+1$ fold degeneracy of a free-ion state is removed depends only on the point symmetry about the ion. The magnitude of crystal-field splittings is determined primarily by the crystal field strength that is expressed in terms of the crystal field parameters of the effective-operator Hamiltonian. The 5f electrons of actinide ions, which participate primarily in ionic bonding with surrounding ligands, have localized states that are conventionally described in the framework of crystal field theory (Stevens, 1952; Wybourne, 1965a). Using effective-operator techniques and the parameterization method,

the framework of crystal field theory has been developed with the same basis set of eigenfunctions of the effective-operator Hamiltonian for the free-ion interactions discussed in Section 18.3.5.

Because electronic interactions in solids are complex, various interaction mechanisms that influence the electronic states of an actinide ion in a solid environment may not be accurately calculated in the framework of current crystal field theory. Evaluation of the crystal field parameters, however, is theoretically much more difficult than predicting the number of energy levels for each free-ion state. To date, an empirical approach has been the most effective method for evaluation of the crystal field parameters of f-states of actinide ions (Krupa, 1987; Carnall, 1992; Liu *et al*., 1994b). Phenomenological modeling and *ab initio* calculations of ion–ligand interactions are able to provide theoretical guidance for the analysis of crystal field spectra. From theoretical approaches, analytical expressions of crystal field parameters using phenomenological models are available for calculating the crystal field parameters of actinide and lanthanide ions in a specific crystalline lattice. The exchange charge model (Malkin *et al*., 1970; Malkin, 1987) and the superposition model (Newman, 1971; Newman and Ng, 1989a) are two crystal field models that have achieved significant success and are useful for guiding spectral analyses. In addition, *ab initio* calculations of the solid-state electronic energy level structure have advanced significantly along with the rapid development of computer technology and are likely to be increasingly important in future studies (Matsika *et al*., 2001; Seijo and Barandiaran, 2001).

18.4.1 Correlation of free-ion and condensed-phase energy level structures

It was pointed out earlier that, because of the different techniques used in studying condensed-phase and free-ion spectra, the configurations available for direct comparison in the two cases have very little overlap. When crystals or solutions are cooled to near 4 K so that only the lowest (ground) electronic state is populated, the resultant absorption spectrum is directly interpretable in terms of energy levels, and, except for complications of superimposed vibronic bands and the added perturbations of crystal field effects themselves, the analysis can proceed to energy level assignments and parametric fitting. In free-ion emission studies, on the other hand, many overlapping transition arrays between the multiple configurations displayed in Fig. 18.1 are obtained simultaneously, and one must first analyze this complex structure. This can only be done with the aid of additional tags on the energy levels such as isotope shift, hyperfine structure, or Landé *g*-factor information, which requires that multiple experiments be performed. Of the many configurations that finally result, most are too heavily involved with s-, p-, and d-orbitals for easy comparison with the f-shell cases discussed here. See Chapter 16 for a detailed discussion of free-atom and free-ion spectra. Nevertheless, with some assistance from theory,

cases are available from which to begin constructing a useful interpretative and predictive model.

Considering the analogous lanthanide situation, nearly all the $4f^2$ atomic levels are known for Pr^{3+} as a free-ion (Pr IV; Crosswhite *et al.*, 1965) and as an ion in $LaCl_3$ (Crosswhite *et al.*, 1965; Rana *et al.*, 1984) and LaF_3 (Carnall *et al.*, 1969, 1989) hosts. The corresponding parametric results are given in Table 18.5. This is the only example now available in either the lanthanide or actinide series for which this direct comparison can be made. For this reason, this case will be examined more closely. Columns 2 (free-ion) and 3 ($LaCl_3$ crystal) in the upper part of Table 18.5 give the results found for the parametric model. Comparing the two cases line-by-line, significant differences can be seen for the major parameters F^k and ζ_{4f}, and lesser ones for α and β. Any possible differences in the M^k and P^k values are masked by the statistical uncertainties. The parameter shifts attributed to the Pr^{3+} environment are given in column 4 and the relative change of the crystal values, compared to those of the free ion, in column 5. Note that the most important change, nearly 5%, occurs for F^2, and about half of this for F^4, F^6, and ζ_{4f}. Also α is in the same range, but with a large uncertainty. The most striking change seems to be for β, which shows an increase in magnitude of some 10–15%.

The $5f^2$ free-ion configurations are completely known for both Th III (deBruin *et al.*, 1941) and U V (Wyart *et al.*, 1980; Van Deurzen *et al.*, 1984), but the Th^{2+} condensed-phase analog is not known, and analyzed data for U^{4+} are limited in scope. The $4f^3$ Pr III configuration is nearly completely known (Suger, 1963), but

Table 18.5 *Medium shift of free-ion parameters for selected f-element ions.*

	Pr IV (cm^{-1})	Pr^{3+}:$LaCl_3$ (cm^{-1})	*Medium shift* (cm^{-1})	*Relative change* (%)
F^2	71 822(41)	68 498(20)	–3324	–4.63 ± 0.08
F^4	51 829(112)	50 317(50)	–1512	–2.92 ± 0.33
F^6	33 889(72)	33 127(38)	–762	–2.25 ± 0.32
α	23 939(322)	22 866(173)	–1073	–4.5 ± 2.1
β	–599(19)	–678(9)	–79	+13 ± 5
ζ	766(3)	749(1)	–17	–2.0 ± 0.5
M^0	2.0(0.4)	1.7(0.2)	0	
P^2	168(58)	248(32)	0	

	Pu II $5f^5 7s^2$ (exp.) (cm^{-1})	*Pu IV* $5f^5$ (est.) (cm^{-1})	Pu^{3+}:$LaCl_3$ (exp.) (cm^{-1})	*Medium shift* (cm^{-1})	*Relative change* (%)
F^2	49 066(770)	50 015	48 670(154)	–1345(924)	–2.7 ± 1.8
F^4	39 640(719)	40 322	39 188(294)	–1134(1 013)	–2.8 ± 2.5
F^6	26 946(785)	27 466	27 493(153)	+27(938)	+0.1 ± 3.4
ζ	2275(27)	2305	2241(2)	–64(29)	–2.8 ± 1.3

there is no corresponding divalent crystal case for comparison. On the other hand, both the Nd^{3+}:$LaCl_3$ (Crosswhite *et al.*, 1976) and U^{3+}:$LaCl_3$ (Crosswhite *et al.*, 1980) spectra are very well documented, but experimental work for both Nd IV and U IV are incomplete. In fact, except for thorium, no doubly or triply ionized actinide free-ion analyses are known.

Although the parametric analyses are incomplete, enough free-ion data are available in a few cases to permit a determination of one or both of the major parameters F^k and ζ_{nf}. For the actinides, these are all neutral atomic and singly ionized cases, for which, again, no condensed-phase analogs are available. These are U I $5f^47s^2$, U II $5f^37s^2$, Pu I $5f^67s^2$, Pu II $5f^57s^2$, and Cf I $5f^{10}7s^2$, all of which contain the closed shell $7s^2$. Using Hartree–Fock (Cowan and Griffin, 1976) results to make corrections for the removal of the $7s^2$ shells, parametric values for the divalent U III, Pu III, and Cf III, and trivalent U IV and Pu IV cases can be inferred. The best example is for Pu IV. A comparison of estimated free-ion parameters with the Pu^{3+}:$LaCl_3$ results is given in Table 18.5. Although the statistical uncertainties are large, the relative changes are consistent with those for Pr^{3+} in the same host.

Because the shifts due to the crystalline environment and those due to the addition of the $7s^2$ shell are nearly the same, it has turned out that, for initial identification, the crystal absorption lines can be related directly to the free-ion spectral lines, at least in those cases for which the crystal field can be treated in the weak-field approximation.

18.4.2 Crystal-field Hamiltonian and matrix element evaluation

Based on the concept that the crystal-field interaction can be treated approximately as a point-charge perturbation on the free-ion energy states, which have their eigenfunctions constructed with the basis of spherical harmonic functions, the effective operators of crystal-field interaction may be defined with the tensor operators of the spherical harmonics $\mathbf{C}^{(k)}$. Following Wybourne's formalism (Wybourne, 1965a,b), the crystal field potential may be defined by:

$$\mathscr{H}_{\mathrm{CF}} = \sum_{k,q,i} B_q^k C_q^{(k)}(i), \tag{18.32}$$

where the summation involving i is over all the equivalent electrons of the open shell of the ion of interest; where the B_q^k are crystal field parameters and the $C_q^{(k)}$ are components of the tensor operators $\mathbf{C}^{(k)}$ that transform like spherical harmonics.

In addition to Wybourne's formalism for crystal field parameters, the Stevens' notation of crystal field parameters $A_k^q\langle r^k\rangle$ are often found in the literature. The crystal-field interaction is often characterized by quantitative comparison of the crystal field strength defined as (Wybourne, 1965a; Auzel and Malta, 1983):

$$N_v = \left[\frac{1}{4\pi}\sum_{q,k}\frac{\left(B_q^k\right)^2}{2k+1}\right]^{1/2}, \tag{18.33}$$

With tensor operators, evaluation of the crystal field matrix elements can be performed with the same methods used for the free-ion matrix elements. Upon application of the Wigner–Eckart theorem, the matrix elements of the crystal-field interaction can be expressed with the reduced matrix elements of a unit tensor $\mathbf{U}^{(k)}$ (Wybourne, 1965a; Weissbluth, 1978):

$$\left\langle l\tau SLJM\left|\sum_i C_q^k(i)\right|l\tau' L'J'M'\right\rangle = (-1)^{J-M}\begin{pmatrix} J & k & J' \\ -M & q & M'\end{pmatrix} \left\langle l\tau SLJ\|\boldsymbol{U}^{(k)}\|l'\tau' S'L'J'\right\rangle\left\langle l\left\|\boldsymbol{C}^{(k)}\right\|l\right\rangle. \tag{18.34}$$

In *LS* coupling, the matrix elements of the unit tensor can be further reduced to

$$\left\langle l\tau LSJ\|\mathbf{U}^{(k)}\|l\tau' L'S'J'\right\rangle = (-1)^{S+L'+J+k}[(2J+1)(2J'+1)]^{1/2} \begin{Bmatrix} J & J' & k \\ L' & L & S\end{Bmatrix}\left\langle l\tau LS\|\boldsymbol{U}^{(k)}\|l\tau' L'S'\right\rangle \tag{18.35}$$

With equations (18.34) and (18.35), the reduced matrix elements of the crystal-field Hamiltonian can be written as:

$$\langle l\tau SLJM\,|\,\mathscr{H}_{\mathrm{CF}}|l\tau' S'L'J'M'\rangle = \sum_{k,q} B_q^k(-1)^{J-M}\begin{pmatrix} J & k & J' \\ -M & q & M'\end{pmatrix} D_J^k, \tag{18.36}$$

where

$$D_J^k = (-1)^{S+L'+J+k}[(2J+1)(2J'+1)]^{1/2}\begin{Bmatrix} J & J' & k \\ L' & L & S\end{Bmatrix} \left\langle l\tau SL\|\mathbf{U}^{(k)}\|l\tau' S'L'\right\rangle(-1)^l(2l+1)\begin{pmatrix} l & k & l \\ 0 & 0 & 0\end{pmatrix} \tag{18.37}$$

where $l = 3$ for f^N configurations. Since all the coefficients, including the values of the $3{-}j$ and $6{-}j$ symbols and the doubly reduced matrix elements of the unit tensor, are known for a given free-ion multiplet, it is obvious that evaluation of crystal-field splittings can be performed by fitting the crystal field parameters B_q^k.

The doubly reduced matrix elements of $\mathbf{U}^{(k)}$ may be obtained directly from Nielson and Koster (1963) or from the SPECTRA program. The values of the $3{-}j$ ( ) and $6{-}j$ { } symbols can be obtained from the compilation of Rotenberg *et al*. (1959) or by direct computer evaluation. The values of k and q for which the matrix elements are nonzero are determined by the symmetry of the crystal

field and the f-electron angular momentum. For f^N configurations ($l = 3$), the $3-j$ symbols in equation (18.37) require that $k = 0, 2, 4, 6$, and $|q| \leq k$. The values of q are also restricted by the point group of the f-ion site, because the crystal-field Hamiltonian has to be invariant under all symmetry operations of the point group. Restrictions due to point group symmetry properties on the nonzero matrix elements of the crystal-field Hamiltonian are discussed later in this section.

For the matrix element of $k = q = 0$, the zero-order of crystal-field interaction is spherically symmetric and does not split the free-ion energy levels, but induces a shift to all energy levels in the same f^N configuration. In general, B_0^0 is not included in evaluation of the crystal-field splitting. Therefore, its contribution to energy level shift is combined with the spherically symmetric component of the free-ion electrostatic interactions. One parameter, namely F^0, absorbs contributions from spherically symmetric components of free-ion and crystal-field interactions.

Once the matrix elements in equation (18.36) are evaluated, the Hamiltonian of the crystal-field interaction may be diagonalized together with the free-ion Hamiltonian to obtain the crystal-field splittings as a function of crystal field parameters. For spectral analysis, the free-ion parameters may also be considered as variables for fitting an experimental spectrum. As a result of the crystal-field interactions, each of the $^{2S+1}L_J$ multiplets splits into crystal field levels. Because the off-diagonal matrix elements of the crystal field between different J-multiplets may not be zero, crystal field operators induce J-mixing. In consequence, for actinide ions in crystals, both J and M are no longer good quantum numbers.

As a result of J-mixing, the eigenfunction of a crystal field level is expressed as

$$|\mu\rangle = \sum_{J,M} a_{JM} |JM\rangle, \tag{18.38}$$

where, in principle, the summation is over all JM terms of a given f^N configuration. However, inclusion of all J-multiplets results in extremely large matrices, particularly, for the configurations with $4 \leq N \leq 10$. Diagonalization of the effective-operator Hamiltonian on the entire $LSJM$ basis could be very time-consuming in an analysis of an experimental spectrum from optical spectroscopy. Such spectra usually cover energy levels that are less than 40 000 cm^{-1} above the ground state (Carnall, 1992; Liu *et al.*, 1994b). Off-diagonal matrix elements between free-ion states separated by a large energy gap are small. As an approximation, crystal field calculations without including J-mixing is appropriate only for the isolated multiplets, such as the first $^5D_1$ excited state of Am^{3+} or the $^8S_{7/2}$ ground state of Cm^{3+}. In practice, the crystal field energy level structure of a $5f^N$ configuration is usually calculated over the restricted energy region in which experimental data are available. Free-ion multiplets with energy

levels far from this region usually are not be included in the calculation. Namely, the free-ion eigenfunction basis may be truncated before diagonalizing the matrix of crystal-field Hamiltonian. Theoretically, this truncation of free-ion states is justified because crystal-field coupling diminishes between two free-ion multiplets as their energy gap increases. From the perturbation point of view, the leading contribution of J-mixing to the energy level splitting of the J-multiplets is proportional to $1/\Delta E_{JJ'}$. Given that the crystal-field splitting of a free-ion multiplet is about 100−1000 cm^{-1}, multiplets that are separated by 10^4 cm^{-1} should have no significant influence on each other.

In computational analyses of experimental spectra, one may truncate the free-ion states whose energy levels are far from the region of interest. This is readily accomplished after diagonalization of the free-ion matrix to produce a calculated free-ion energy level structure. These levels are considered to be the centers of gravity for the crystal-field splitting (Carnall *et al.*, 1983; Carnall, 1992). One chooses the numbers of J-multiplets to be included in the crystal-field matrices for each J-value. Therefore, the chosen J-multiplets are still complete sets of free-ion eigenfunctions that contain all SL components of the given J. This way of free-ion state truncation ensures that no contribution from the free-ion interactions is lost when constructing the free-ion wave functions for each J-multiplet.

One example is the $^8S_{7/2}$ ground state of ions in a $5f^7$ configuration for Am^{2+}, Cm^{3+}, or Bk^{4+} in which both diagonal and off-diagonal matrix elements of the crystal field operators vanish (Wybourne, 1966; Newman, 1970; Liu *et al.*, 1993; Newman and Ng, 2000). The observed crystal-field splittings must be attributed to the contributions of the mixture of other LS terms in the ground state free-ion wave function and nonzero off-diagonal matrix elements between different J values (Liu *et al.*, 1993, 1998; Murdoch *et al.*, 1996, 1998). Because of large energy gaps from the ground state to the excited multiplets ($\sim$16 000 cm^{-1}), J-mixing is negligible in this case. It has been shown that for the $^8S_{7/2}$ ground state splitting, the leading contributions are from the fourth and higher orders of the coupled matrix elements between the spin–orbit ($\mathbf{V}^{(11)}$) and crystal field ($\mathbf{U}^{(k)}$) operators (Liu *et al.*, 1993; Brito and Liu, 2000). Without inclusion of J-mixing, the leading contributions to the crystal-field splitting of the $^8S_{7/2}$ multiplet of an f_7 configuration are from the mixed matrix elements such as

$$\begin{aligned}&\left\langle {}^8S\middle|\mathbf{V}^{(11)}\middle|{}^6P\right\rangle\left\langle {}^6P\middle|\mathbf{U}^{(2)}\middle|{}^6D\right\rangle\left\langle {}^6D\middle|\mathbf{U}^{(2)}\middle|{}^6P\right\rangle\left\langle {}^6P\middle|\mathbf{V}^{(11)}\middle|{}^8S\right\rangle\\&\left\langle {}^8S\middle|\mathbf{V}^{(11)}\middle|{}^6P\right\rangle\left\langle {}^6P\middle|\mathbf{U}^{(11)}\middle|{}^6I\right\rangle\left\langle {}^6I\middle|\mathbf{U}^{(6)}\middle|{}^6P\right\rangle\left\langle {}^6P\middle|\mathbf{V}^{(11)}\middle|{}^8S\right\rangle.\end{aligned} \tag{18.39}$$

It is obvious that truncation of LS terms in the $J = 7/2$ multiplets should affect the scale of the coupled matrix elements, and thus affect the calculated crystal-field splitting. The same situation occurs for the off-diagonal matrix elements between different J-levels, but is less important because of the large energy gap between the ground state and the first excited state.

18.4.3 Symmetry rules

The geometric properties of the crystal field operators will now be discussed in more detail. In addition to the angular momentum of the f-ions that restricts k and q for a set of nonvanishing crystal field operators, the site symmetry in a crystalline lattice also imposes limits on crystal field operators. The tensor operators for the crystal-field interaction must be invariant under the point group symmetry operations imposed by the site symmetry of the ion in question. Here the interest is to identify the nonvanishing components of crystal field operators and their matrix elements. First, for states of the same parity, namely $l = l'$, k must be even. It is also required that B_q^k must be real in any symmetry group that contains a rotation operation about the y-axis by π or a reflection through the $x-z$ plane; otherwise B_q^k ($q \neq 0$) is complex. In the latter case, one of the B_q^k can be made real by a rotation of the coordinate system about the z-axis. The B_q^k for $q < 0$ are related to those of $q > 0$ by

$$B_{-q}^k = (-1)^q B_q^{k*}. \tag{18.40}$$

Also under the invariant conditions of the point group theory, the crystallographic axis of the lowest symmetry determines the values of q for the nonvanishing crystal field operators. For example, at a site of C_{3v} symmetry, there is a three-fold axis of rotational symmetry with a reflection plane that contains the C_3 axis (Tinkham, 1964; Hüfner, 1978). The ligand field must exhibit this symmetry. Hence, if a $2\pi/3$ rotation is performed on the crystal field potential followed by a reflection with regard to the plane, the potential is invariant only if $q = 0$, ± 3, and ± 6. Thus, within an f^N configuration, the crystal-field Hamiltonian may be written as

$$\begin{aligned}\mathscr{H}(C_{3v}) = \sum_i [&B_0^2 C_0^{(2)}(i) + B_0^4 C_0^{(4)}(i) + B_3^4 (C_{-3}^{(4)}(i) - C_3^{(4)}(i)) \\ &+ B_0^6 C_0^{(6)}(i) + B_3^6 (C_{-3}^{(6)}(i) - C_3^{(6)}(i)) + B_6^6 (C_{-6}^{(6)}(i) + C_6^{(6)}(i))].\end{aligned} \tag{18.41}$$

If the reflection plane is perpendicular to the C_3 axis, the site symmetry becomes C_{3h}, which occurs for doped f^N impurity ions in lanthanum ethylsulfate, $LaCl_3$, and $LaBr_3$ (Morosin, 1968). This potential invariant property requires $q = 0$, ± 6 only, but, since there is no rotation symmetry about the y-axis by π or a reflection through the x–z plane for the C_{3h} site, there is an imaginary noncylindrical term in the Hamiltonian:

$$\begin{aligned}\mathscr{H}(C_{3h}) = \sum_j [&B_0^2 C_0^{(2)}(j) + B_0^4 C_0^{(4)}(j) + B_0^6 C_0^{(6)}(j) + B_6^6 (C_{-6}^{(6)}(j) \\ &+ C_6^{(6)}(j)) + iB_6'^6 (C_6^{(6)}(j) - C_{-6}^{(6)}(j))].\end{aligned} \tag{18.42}$$

D_{3h} is a symmetry group that includes all rotation and reflection operations of C_{3h} (Tinkham, 1964; Hüfner, 1978). The crystal field operators for ions at a

D_{3h} site are the real terms for C_{3h} without the imaginary term $iB_6'^6(C_6^{(6)} - C_{-6}^{(6)})$. The nonvanishing terms of crystal field operators for various lattice sites of f-ions in crystals are listed in Table 18.6.

The free-ion degeneracy in M may be partially or completely removed by the crystal-field interaction. In the crystal-field energy matrix using the JM basis set, the terms for which $M-M' = q$ for the operator $C_q^{(k)}$ are nonzero. Otherwise the crystal-field matrix elements are zero. Based on this property, the crystal-field matrix may be reduced into several independent submatrices, each of which is characterized by a crystal quantum number μ (or γ). Each μ represents a group of M, such that $M-M' = q(0, 2, 3, 4, 6)$ belongs to the same submatrix (Hüfner, 1978). All matrix elements between the submatrices are zero. The crystal field quantum number may be used to classify the crystal field energy levels even when J and M are not good quantum numbers. Considering C_{3h} (and D_{3h}) as an example, the JM and $J'M'$ (J may be equal to J') with $M-M' = 6$ belong to the same crystal field submatrix. For an even number of f-electrons, there are four independent submatrices, and for an odd number of f-electrons, there are three independent submatrices. The parameters of nonvanishing crystal field terms for symmetries of common crystal hosts of f-element ions are given in Table 18.6 along with the numbers of reduced crystal-field matrices.

Without a magnetic field, the electrostatic crystal field alone does not completely remove the free-ion degeneracy for the odd-numbered electronic configurations. Known as Kramers' degeneracy (Kramers, 1930; Hüfner, 1978), all crystal field levels are at least doubly degenerate. The crystal quantum number and JM classification schemes are given for D_{3h} symmetry in Table 18.7. In calculation of energy level structure for degenerate doublets, one may cut off half of the submatrix elements. In many cases, calculations of crystal field energy levels have been carried out usefully by assuming a higher site symmetry than the real one so that fewer parameters are required. In some cases, this approach was used because actinide ions in many solids occupy a low-symmetry site and the limited number of observed energy levels could not accurately determine a large number of crystal field parameters (Carnall *et al.*, 1991). In other cases, a crystal lattice that does not have mirror symmetries in its coordinates requires complex crystal field parameters for the $q \neq 0$ terms (Table 18.6). If one uses as an approximation only the real part of the crystal field operators, energy level calculation becomes much easier. Because the use of high symmetry as an approximation is equivalent to upgrading a lower-symmetry site to a higher one within the same crystal symmetry group, this approach has been called the descent-of-symmetry method (Görller-Walrand and Binnemans, 1996). This method may be applied to the groups of monoclinic, trigonal, and tetragonal structures listed in Table 18.6. For example, the C_{3h} symmetry of $LaCl_3$ was replaced by D_{3h} (Morrison and Leavitt, 1982); the S_4 site symmetry of trivalent lanthanide ions in $LiYF_4$ is often treated as D_{2d} (Esterowitz *et al.*, 1979; Görller-Walrand *et al.*, 1985; Liu *et al.*, 1994a). Similarly, the actual C_2 symmetry of LaF_3 was replaced by C_{2v} (Carnall *et al.*, 1989).

Table 18.6 *Nonvanishing terms of crystal field (CF) parameters B_q^k, numbers of reduced matrices and crystal field quantum number μ for f^N configurations in crystals of various symmetries.*[a,b]

Crystal structure	*Site symmetry*	*Example*	B_q^{kc}	μ *for even* N[d]	*μ for odd* N[d]
monoclinic	C_s, C_2,C_{2h}	LaF_3	$B_0^2, B_0^4, B_0^6, \mathrm{Re}(B_2^2), B_2^4, B_2^6, B_4^4, B_4^6, B_6^6$	±0, ±1 (S)	1/2 (D)
rhombic	C_{2v}, D_2, D_{2h}	$Y_3Al_5O_{12}$	$B_0^2, B_0^4, B_0^6, \mathrm{Re}\left(B_2^2, B_2^4, B_2^6, B_4^4, B_4^6, B_6^6\right)$		
trigonal	C_3, $S_6(C_{3i})$	$LiNbO_3$	$B_0^2, B_0^4, B_0^6, \mathrm{Re}(B_3^4), B_3^6, B_6^6$	±0 (S), 1 (D)	1/2, 3/2 (D)
	C_{3v}, D_3, D_{3d}	Y_2O_2S	$B_0^2, B_0^4, B_0^6, \mathrm{Re}\left(B_3^4, B_3^6, B_6^6\right)$		
tetragonal	C_4, S_4, C_{4h}	$LiYF_4$	$B_0^2, B_0^4, B_0^6, \mathrm{Re}\left(B_4^4\right), B_4^6$	±0, ±2 (S), 1 (D)	1/2, 3/2 (D)
	D_4,C_{4v}, D_{2d}, D_{4h}	YPO_4	$B_0^2, B_0^4, B_0^6, \mathrm{Re}\left(B_4^4, B_4^6\right)$		
hexagonal	C_6,C_{3h}, C_{6h},D_6, C_{6v}, D_{3h}, D_{6h}	$LaCl_3$	$B_0^2, B_0^4, B_0^6, \mathrm{Re}\left(B_6^6\right)$	±0, ±3 (S), 1, 2 (D)	1/2, 3/2, 5/2 (D)
cubic	T, T_d, T_h, O, O_h	CeO_2	$B_0^4, B_0^6, \mathrm{Re}\left(B_4^4, B_4^6\right)$[e]	±0, ±4 (S), 2, 6 (D), 1 (T)	1/2, 7/2 (D), 3/2 (Q)

[a] Morrison and Leavitt (1982).
[b] Hüfner (1978).
[c] For $q \neq 0$, $B_q^k$are complex except for the real terms $\mathrm{Re}\left(B_q^k\right)$.
[d] S, singlet; D, doublet; T, triplet; Q, quartet.
[e] $B_4^4 = \frac{5}{\sqrt{70}} B_0^4, \quad B_4^6 = -\sqrt{\frac{7}{2}} B_0^6$

Table 18.7 *Classification of crystal field energy levels for D_{3h} symmetry.*

(*a*) *Even number of electrons*

	$\mu = 0\ (^1\Gamma_{1,\,2})$	$\mu = \pm 1\ (^2\Gamma_5)$	$\mu = \pm 2\ (^2\Gamma_6)$	$\mu = 3\ (^1\Gamma_{3,\,4})$	*No. levels*
J	*M*	*M*	*M*	*M*	
0	0				1
1	0	± 1			2
2	0	± 1	± 2		3
3	0	± 1	± 2	$3, -3$	5
4	0	± 1	$\pm 2, \mp 4$	$3, -3$	6
5	0	$\pm 1, \mp 5$	$\pm 2, \mp 4$	$3, -3$	7
6	$-6, 0, 6$	$\pm 1, \mp 5$	$\pm 2, \mp 4$	$3, -3$	9
7	$-6, 0, 6$	$\pm 7, \pm 1, \mp 5$	$\pm 2, \mp 4$	$3, -3$	10
8	$-6, 0, 6$	$\pm 7, \pm 1, \mp 5$	$\pm 8, \pm 2, \mp 4$	$3, -3$	11

(*b*) *Odd number of electrons*

	$\mu = \pm 1/2\ (^2\Gamma_7)$	$\mu = \pm 3/2\ (^2\Gamma_8)$	$\mu = \pm 5/2\ (^2\Gamma_9)$	*No. levels*
J	*M*	*M*	*M*	
1/2	$\pm 1/2$			1
3/2	$\pm 1/2$	$\pm 3/2$		2
5/2	$\pm 1/2$	$\pm 3/2$	$\pm 5/2$	3
7/2	$\pm 1/2$	$\pm 3/2$	$\pm 5/2, \mp 7/2$	4
9/2	$\pm 1/2$	$\pm 3/2, \mp 9/2$	$\pm 5/2, \mp 7/2$	5
11/2	$\pm 1/2, \mp 11/2$	$\pm 3/2, \mp 9/2$	$\pm 5/2, \mp 7/2$	6
13/2	$\pm 13/2, \pm 1/2, \mp 11/2$	$\pm 3/2, \mp 9/2$	$\pm 5/2, \mp 7/2$	7
15/2	$\pm 13/2, \pm 1/2, \mp 11/2$	$\pm 15/2, \pm 3/2, \mp 9/2$	$\pm 5/2, \mp 7/2$	8

In general, use of the descent-of-symmetry method may have more complicated consequences than that of the above examples. For a specific symmetry modification, one may estimate the changes in crystal field parameters based on the rotational symmetry of point charges in polar coordinates (θ,ϕ) and assuming that the ligand ions in each coordination shell are at the same distance from the f-element ion. For an arbitrary rotation, the B_0^k parameters should only depend on the θ-coordinates, whereas the B_q^k parameters ($q \neq 0$) depend on both θ- and ϕ-coordinates. Changes in the ϕ-coordinates have no influence on B_0^k and $|B_q^k| = [(\mathrm{Re}B_q^k)^2 + (\mathrm{Im}B_q^k)^2]^{1/2}$. Descent-of-symmetry operations that have this property are $C_{n\mathrm{h}} \rightarrow D_{n\mathrm{h}}$, $S_4 \rightarrow D_{2\mathrm{d}}$, and $C_n \rightarrow C_{n\mathrm{v}}$. The symmetry changes that incorporate a change in θ-coordinates will change all parameters, such as $D_{n\mathrm{h}} \rightarrow C_{n\mathrm{v}}$ and $D_{n\mathrm{h}} \rightarrow C_n$. If the symmetry of the f-element site is lowered, not only are additional parameters required, but there are also changes in the crystal field parameters found in the higher symmetry. In consequence, there is far less rationale for using D_n has an approximation for C_n and $C_{n\mathrm{v}}$.

Site distortion is a common phenomenon when f-element ions are doped into crystals. A dopant ion may have site symmetry lower than that of the host ion it replaces. This is especially true if the charge on the dopant ion and/or its ionic radius is different from that of the host ion. Accordingly, both the sign and magnitude of crystal field parameters are subject to change. As discussed above, different crystal structures may undergo different types of distortion that reflect the properties of the specific coordination polyhedron in a given crystal. Görller-Walrand and Binnemans (1996) give a detailed description of the effects of structural distortion in terms of changes in the θ- and ϕ-coordinates. However, changes in radial distances may occur as well. For ions at a distorted site that further reduces the degeneracy of electronic states, analyses of crystal field spectra must be conducted using a lower symmetry.

18.4.4 Empirical evaluation of crystal field parameters

Extensive mixing of *SL*-basis states, brought about by the spin–orbit and crystal-field interactions for each *J*-multiplet, can result in the least-squares method for empirical evaluation of crystal field parameters converging to a false solution. A false solution can be recognized if there is sufficient characterization of the states from supplementary data, such as Zeeman splitting factors or polarized spectra. However, this in itself may not produce the true solution. The latter can only be found if sufficiently accurate initial parameters are available for the least-squares fitting process to be effective. Therefore, establishing accurate parameters for the model Hamiltonian essentially relies on systematic analyses that encompass theoretical calculations for incorporating trends of parameter variation across the f-element series (Carnall, 1989; Liu *et al.*, 1994b; Liu, 2000). The results of analyses of simpler spectra are carried over to more complex ones through consideration of their symmetry properties.

For f-element ions in crystals of well-defined site symmetry, crystal field theory is widely used along with group theory for predicting the number of energy levels and determining selection rules for electronic transitions between crystal field levels. Whereas the number of nonvanishing crystal field parameters can be determined by the symmetry arguments, their values are usually determined by analyzing the experimentally observed crystal-field splittings. Experimental data that carry supplementary spectroscopic information, such as polarized transitions allowed by electric or magnetic dipolar selection rules, ensure the accuracy of the experimentally fitted crystal field parameters (Liu *et al.*, 1992, 1994a, 1998). In addition, the temperature dependence of observed crystal-field splittings may be analyzed to distinguish pure electronic lines from vibronic features. Properties such as magnetic susceptibility as a function of temperature may be calculated from the empirical wave functions as a further check on the accuracy of the crystal field parameters. If multiple sites exist, site-resolved spectra are required to distinguish energy levels of ions at different sites (Tissue and Wright, 1987; Liu *et al.*, 1994b; Murdoch *et al.*, 1996). Accordingly, as a procedure of

parametric modeling, correct assignment of observed energy levels is crucial to avoid a false solution. For spectra that lack sufficient experimental information to achieve unambiguous assignment, this procedure may involve several iterations of trial calculations and analyses that require a firm understanding of the basics of crystal-field splitting of free-ion states (Carnall, 1989, 1992).

For setting initial parameters of the crystal-field Hamiltonian to be fit by observed energy levels, one may simply use the previously established parameters for different f-element ions in the same or similar host materials. For the series of trivalent actinide ions in $LaCl_3$, one of the most extensively studied host crystals, the parameters of free-ion and crystal-field interactions are listed in Table 18.4. Comprehensive summaries of previously studied lanthanide systems are given (Morrison and Leavitt, 1982; Görller-Walrand and Binnemans, 1996). Alternatively, the signs and magnitudes of crystal field parameters can be predicted according to the coordination of the f-element ion using the point charge model of the electrostatic crystal field potential. For this purpose, only the nearest ligand (NL) atoms need to be considered. As a function of the radial and angular coordinates, the expressions for the B_q^k parameters are given in the following section. The signs of the crystal field parameters are determined by the angular part of the electrostatic potential and may be obtained by symmetry analysis. The predicted signs are important for checking the signs of the parameters obtained by the fitting procedure. Some sign combinations may correspond to a coordination that is physically impossible. Generally, determination of the magnitudes requires more quantitative calculations of the overlap integrals between the f-electrons and the electrons of the ligands. The electrostatic interactions beyond the nearest ligands may bring about significant contributions to the parameters with $k = 2$. For these parameters, the total contribution from the long-range interactions may exceed that of the NL so that a change in the sign of B_q^2 determined by the NL atoms is possible (Zhorin and Liu, 1998). Moreover, the electrostatic point charge model is not realistic in describing the short-range interactions between the f-element ion and its nearest ligands. Charge exchange interactions including covalency may dominate the crystal field parameters with $k = 4$ and 6. For these reasons, an empirical approach with theoretical guidance is necessary to ensure that the parameterization is within the limitations of physical interactions.

In a nonlinear least-squares fitting process, the magnitudes and signs of crystal field parameters are varied to best reproduce the observed energy level structure. This is actually a process of optimizing crystalline structure within a given restriction through variation of the crystal field parameters. The parameters that have higher weight are better determined than the parameters that have less influence on the observed energy levels. Adding an imaginary parameter may only change the real part of the term that has the same q and k but does not have much influence on other parameters. If the values of the crystal field parameters for a system of higher symmetry are used as initial values of the parameters for a different system of lower symmetry, the fitting may either

fall into a false solution or leave the added parameters less accurately determined. In this case, one should assign the unambiguously observed energy levels, most likely the isolated multiplets, and only allow the most significant crystal field parameters to vary freely. Once these weighted parameters converge, further fitting should be performed on the entire set of crystal field parameters, along with the variation of the free-ion parameters.

18.4.5 Theoretical evaluation of crystal field parameters

Quantum mechanical calculations of crystal field energies and corresponding crystal field parameters for f-element ions in compounds with different chemical characteristics were carried out by several groups in the framework of the cluster approximation. For an f-ion and its nearest ligands (chlorine, fluorine, or oxygen ions), the fully antisymmetric and orthonormalized wave functions of zero-order are constructed as linear combinations of products of individual ion wave functions, and the energy matrix is built with the complete Hamiltonian that contains one- and two-electron operators including the interaction with the electrostatic field created by the rest of the crystal. The first-order contributions to the energy matrix include integrals over one-electron wave functions of the occupied states of the cluster. Higher-order contributions correspond to configuration mixing. The procedure and details of calculations have been described in several original and review papers (Newman, 1971; Eremin, 1989; Garcia and Faucher, 1995; Shen and Bray, 1998; Zhorin and Liu, 1998; Newman and Ng, 2000). Here we present only a brief description of the results of *ab initio* simulations that are important for modeling of the main physical mechanisms responsible for crystal-field splittings.

The first-order terms in the energy matrix include Coulombic, exchange, and overlap integrals over 5f orbitals of the actinide ion and outer orbitals of ligand ions. From these terms, the 5f-electron energy in the electrostatic field of the ligand point multipole moments and the charge penetration contribution may be singled out. The second-order terms may be classified according to intermediate (virtual) excited states of the cluster. In this regard, the following electronic excitations should be considered:

(1) Intra-ion excitations from the filled electronic shell of the actinide ion to the empty excited shell (in particular, $6p^6 \rightarrow 6p^5 6d^1$). These processes shield the inner valence $5f^N$ shell and may be accounted for, at least partly, by introducing shielding (or antishielding) factors into the multipole moments of the valence electron $\left(\langle 5f|r^k|5f\rangle \rightarrow (1-\sigma_k)\langle 5f|r^k|5f\rangle\right)$ (Rajnak and Wybourne, 1964).
(2) Intra-ion excitations from the valence shell into empty shells and from the filled shells into the valence shell (in particular, $5f^N \rightarrow 5f^{N-1}6d^1$ or $6p^6 \rightarrow 6p^5 5f^{N+1}$). These processes contribute to the linear shielding and cause additional corrections to parameters of the effective Hamiltonian bilinear in parameters of the electrostatic field.

(3) Inter-ion excitations, mainly into the charge-transfer states of the actinide ion with the extra electron in the valence shell promoted from the outer-filled shell of the ligand. Actually, mixing of the ground configuration with the charge-transfer states corresponds to a partially covalent character in the chemical bonding between an actinide ion and its ligands.

It should be noted that the effective-operator Hamiltonian (equation (18.32)) with a single set of crystal field parameters, operating within the total space of wave functions of $5f^N$ configuration, can be introduced if all excited configurations of the cluster under consideration are separated from the ground configuration by an energy gap that is much larger than the width of the energy spectrum of the ground configuration. Otherwise the crystal field parameters become term (*LSJ*) dependent. In particular, a crystal field analysis carried out on an extended basis containing the ground $4f^2$ and excited 4f5d, 4f6p configurations of Pr^{3+} in YPO_4 (Moune *et al*., 2002) greatly improved the agreement between the experimental data and the calculated energy levels. For the $5f^N$ configurations, the inter-configuration coupling is anticipated to be much stronger because of smaller gaps between the ground and excited state configurations, particularly, for the lighter actinides in the first half of the $5f^N$ series.

A general conclusion about the dominant role of overlap and covalent contributions to the crystal field parameters B_q^4 and B_q^6 follows from all *ab initio* calculations carried out up to the present time. When Hartree–Fock one-electron wave functions of free ions are used in simulations, relative differences between the theoretical and experimental values of these parameters do not exceed 50%. However, for the quadrupole component of the crystal field parameters B_q^2, contributions from the long-range interactions of valence electrons with point charges, dipole, and quadrupole moments of ions in the crystal lattice are comparable to contributions from the interactions with the nearest ligand ions, and the theoretical estimations differ substantially from the experimental data.

Whereas the free-ion parameters vary smoothly across the 5f series, trends in crystal field parameters, particularly B_q^4 and B_q^6, usually break at the f^7 configuration. Experimental evidence for this effect is evident in the systematic analysis of the spectra of trivalent actinides doped into single-crystal $LaCl_3$ (Carnall, 1992) and trivalent lanthanides in LaF_3 (Carnall *et al*., 1989). An abrupt change in the magnitude of parameters with $k = 4$ and 6 occurs at the center of the series. Judd (1979) has interpreted this effect as a problem of the one-electron operators of the crystal-field Hamiltonian. One-electron operators, $\mathbf{U}^k$, change sign at the center of the series. Inclusion of two-electron operators in the crystal-field Hamiltonian would likely remove this discontinuity.

Although extensive Hartree–Fock calculations have been utilized for establishing systematic trends of free-ion interactions that lead to the determination of the parameters of the effective-operator Hamiltonian, most analyses of crystal-field interactions are carried out with the crystal field parameters determined by the fitting of experimental data. Attempts to calculate the crystal field

parameters from first principles may not be realistic. Given the complexity of electronic interactions in solids, *ab initio* calculations of electronic structure of heavy element ions in solids currently are not capable of achieving accuracy that is comparable to experimental results. Therefore, theoretical models, more or less phenomenological on the basis of the point-charge approximation, are essential in providing a clear theoretical understanding of electronic interactions of the f-element ions in solids. Model calculations do not only generate the phenomenological crystal field parameters that provide guidance to parametric modeling of the crystal field spectra of f-element ions in solids, but also reveal more fundamental aspects of the ion–ligand interactions that are poorly characterized by the point-charge approximation itself. Among the crystal field models introduced in the literature, the angular overlap model (Jørgensen *et al.*, 1963), the exchange charge model (Malkin *et al.*, 1970; Malkin, 1987), and the superposition model (Newman, 1971; Newman and Ng, 1989b, 2000) have been used for calculations of crystal field parameters for both 4f elements and 5f elements in various crystals.

Detailed discussions of the superposition model of the crystal field and its application to analysis of experimental spectra were provided by Newman and Ng (1989b, 2000). The superposition model neglects the ligand–ligand overlap effects and reflects the total crystal-field interaction as a linear 'superposition' of local ion–ligand pair-wise electrostatic interactions. The crystal field parameters are expressed as a sum of individual contributions from ions in the host crystal lattice,

$$B_q^k = \sum_L \bar{B}_k(R_L) g_{k,q}(\theta_L, \varphi_L), \tag{18.43}$$

where $g_{k,q}$ are normalized spherical harmonic functions, and R_L, θ_L, φ_L locate the position of ligand L in the lattice coordination environment. The distance-dependent parameters $\bar{B}_k(R_L)$ are referred to as intrinsic crystal field parameters, which by definition are dependent only on the radial distance between the f-ion and the ligand L. Based on the assumption of the point charge model that the ion–ligand electrostatic interaction has a specific power law dependence, the intrinsic parameters can be defined as

$$\bar{B}_k(R) = \bar{B}_k(R_0)(R_0/R)^{t_k}, \tag{18.44}$$

where R_0 is the distance between the f-ion and a reference ligand located on the z-axis of the crystalline lattice, and τ_k are power law exponents that reflect the distance dependence of the ion–ligand interaction (Newman and Ng, 2000). $\bar{B}_k(R_0)$and τ_k can be empirically determined as phenomenological parameters. It should be noted that the parameters τ_k are not generally in agreement with the electrostatic power law components $\tau_2 = 3$, $\tau_4 = 5$, $\tau_6 = 7$. For chloride ligands, in particular, $\tau_4 = 12 - 16$, $\tau_6 = 5 - 7$ for different RE ions (Reid and Richardson, 1985). Values of the rank 4 and 6 parameters quickly decrease with R, and the corresponding sums (equation (18.43)) are limited to the nearest neighbors of the f-ion. Because of their long-range effect, values of the rank 2

parameters are often difficult to determine. One may break the rank 2 operator into two terms, labeled as p and s (Levin and Cherpanov, 1983):

$$\bar{B}_2(R_L) = \bar{B}_2^p(R_0)(R_0/R_L)^3 + \bar{B}_2^s(R_0)(R_0/R_L)^{10} \tag{18.45}$$

to represent, respectively, the ligand point charge contribution and the short-range contribution.

Apparently, model calculations of crystal field parameters result in less discrepancies for some systems than for others. This is mainly due to uncertainties in structure information to which crystal field calculations, particularly of the rank 4 and 6 parameters, are extremely sensitive. Crystal lattice constants determined from X-ray diffraction or neutron scattering may be of very high resolution only for intrinsic sites. For impurity f-element ions doped into host materials, an unknown structural distortion is induced in most cases. The doping-induced site distortion depends in part on the ionic radius difference between the host ion and the doped f-element ion. If a model calculation is conducted based on the structure of the host, the calculated crystal field parameters are expected to be more or less different from those determined by fitting experimental data for the system.

The exchange charge model (ECM) (Malkin *et al.*, 1970; Larionov and Malkin, 1975; Malkin, 1987) is an extension of the angular overlap model (Jørgensen, 1962). It considers both long-range and short-range interactions between the actinide or lanthanide ion and lattice ions. The effective crystal-field Hamiltonian is assumed to be a sum

$$\mathscr{H}_{\mathrm{CF}} = \mathscr{H}^{\mathrm{pm}} + \mathscr{H}^{\mathrm{ec}} \tag{18.46}$$

where the first term corresponds to the electrostatic interaction of valence electrons localized on the f-element ion with point multipole moments of the lattice ions. The second term approximates all contributions due to the spatial distribution of electron density. Both terms have the form of equation (18.44) with parameters $B_q^{(\mathrm{pm})k}$ and $B_q^{(\mathrm{ec})k}$. Matrix elements of the effective-operator Hamiltonian $\mathscr{H}^{\mathrm{ec}}$ in the basis of one-electron wave functions of the metal ion interacting with spherical ligand ions may be calculated (Malkin *et al.*, 1970; Malkin, 1987).

To gain a greater insight into the energy level calculations, it is instructive to compare contributions to the electrostatic crystal field parameters with those from overlap and covalency effects. The ECM introduces the renormalization of the parameters of the electrostatic crystal field only and does not change the structure of the Hamiltonian $\mathscr{H}^{\mathrm{pm}}$. This renormalization may be considered to be a result of the 'nonlocal' interaction of the valence electron with the exchange charges localized at the bonds connecting the metal ion with its nearest neighbor ions. The concept of exchange charge, for which the crystal field model under consideration was named, and was first introduced by Dick and Overhauser (1958) in the theory of dielectric properties of solids. Values of exchange charges are proportional to the linear combinations of the overlap integrals and depend on the rank k of the corresponding tensor $\boldsymbol{B}^{(k)}$ of crystal field parameters. It is

Table 18.8 *Crystal field parameters from ECM calculation and experimental fit* (cm^{-1}).[a]

	Nd^{3+}:$LaCl_3$	(C_{3h} *symmetry*)	Cm^{3+}:$LuPO_4$	(D_{2d} *symmetry*)
	Calculated[b]	*Experimental*[b] (*fit to* D_{3h})	*Calculated*[c]	*Experimental*[c]
B_0^2	−78(39)	81	450(180)	399
B_0^4	−78(−57)	−42	370(230)	363
B_0^6	−44(−41)	−44	−2500(−2050)	−2470
ReB_4^4			2400(1200)	2261
ReB_4^6			200(185)	167
ReB_6^6	299(279)	439		
ImB_6^6	−239(−226)			

[a] The values in parentheses are the contribution from exchange-charge interactions.
[b] Zhorin and Liu (1998).
[c] Liu *et al.* (1998).

important that the ECM allows for consideration of both even and odd components of the crystal field. In particular, integral intensities of spectral lines in the intra-configurational $5f^N-5f^N$ spectra and their frequencies may be fitted in the framework of a single model.

As an example of ECM calculation, Table 18.8 lists the values of crystal field parameters calculated by using the ECM in comparison with the experimentally determined ones. It is evident that the dominant contributions to B_q^2 are from electrostatic interactions, whereas those to B_q^4 and B_q^6 are from short-range interactions. It is generally realized that the second-order parameters B_q^k with $k = 2$ are less accurately determined by the model calculation, particularly for a disordered lattice. This is because the second-order parameters characterize the long-range electrostatic interactions that are difficult to calculate accurately. It should be noted that the contradiction between the calculated and experimental values of the B_0^2 parameter in Nd^{3+}:$LaCl_3$ (in particular, different signs) may be removed when taking into account large contributions due to point dipole and quadrupole moments of chlorine ions (Eremin, 1989).

18.4.6 Corrections to the crystal-field Hamiltonian

As described in earlier sections, the parameterization approach is able to reproduce the crystal field energy level structures of actinide or lanthanide ions in satisfactory agreement with high-resolution absorption and luminescence spectra. The standard deviation in a nonlinear least-squares fit to experimental spectra in the low-lying energy levels (40 000 cm^{-1}) can be less than 10 cm^{-1} for lanthanide ions (Liu *et al.*, 1994a). However, crystal field modeling of energy levels for some particular states in the 4f configurations is invariably poor as, for instance, in the cases of the $^2H_{11/2}$ multiplet of Nd^{3+} and $^3K_8$ of Ho^{3+}. The discrepancies are much larger for the actinides in $5f^N$ configurations

(Edelstein, 1979; Carnall, 1992; Liu *et al*., 1994b; Murdoch *et al*., 1997; Liu, 2000). Faucher *et al*. (1996) reported in energy level analysis of U^{4+} in the octahedral sites of Cs_2UBr_6 and Cs_2ZrBr_6 evidence of strong interaction between the $5f^2$ and $5f^17p^1$ configurations. Adjustment of the parameters in the free-ion Hamiltonian does not result in much improvement. This problem is primarily due to the exclusion of the electron correlation effect in the one-electron crystal field model. The effects of electron–electron interaction cannot be completely absorbed into the effective-operator Hamiltonian of the one-electron crystal field model. Reid and coworkers (Reid, 2000) have reviewed progress in the modification of the one-electron crystal field theory with inclusion of correlation crystal field operators in the Hamiltonian.

There are various physical mechanisms that contribute to multiplet-dependent crystal-field splittings that can be described generally as correlation effects. The two obvious mechanisms, namely, the spin-correlated crystal field potential (Newman, 1971; Judd, 1977b) and the anisotropic ligand polarization effect, also known as nephelauxetic effect (Jørgensen, 1962; Gerloch and Slade, 1973), have been identified as large contributors, although, it is not clear what physical mechanisms produce the dominant contribution to shift the f-electron energy levels. To correct the discrepancy that appears in analyses of optical spectra with the one-electron crystal field model, it becomes necessary to introduce a full parameterization of the anisotropic two-electron interaction. To facilitate calculations of the matrix elements with the same basis for the one-electron operator Hamiltonian, Judd's $\mathbf{g}_{iq}^{(k)}$ operators (Judd, 1977a), which are orthogonal over the complete f^N basis sets, are used to define the correlation crystal field (CCF) Hamiltonian (Reid, 1987):

$$\mathscr{H}_{\mathrm{CCF}} = \sum_{ikq} G_{iq}^{k} \mathbf{g}_{iq}^{(k)}, \tag{18.47}$$

where G_{iq}^{k} are parameters of CCF. The index k runs through the even integers from 0 to 12 ($4l$, for f^N configurations). The parameter q is restricted by symmetry, and the number of operators varies with k. The operators $\mathbf{g}_{i}^{(k)}$with $k = 0$ correspond to Coulomb interactions and those with $i = 1$ to one-electron operators, in fact $\mathbf{g}_{1}^{(k)} \equiv \mathbf{U}^{(k)}$.

The main problem in the application of the CCF Hamiltonian is the very large number of parameters that are necessary to account for electron–electron correlation. However, the successful parameterization of f-ion crystal field energy level structure is largely dependent on the accuracy and the number of observed and properly assigned energy levels. In general, nonlinear least-square fitting requires that the number of assigned energy levels should be much larger than the total number of freely varied parameters. Expansion of the effective-operator Hamiltonian by including the operators for the correlation crystal-field interaction is effective only if there are sufficient experimental data and correctly determined parameters for the free-ion and one-electron crystal-field Hamiltonian for initial input. Otherwise, fits may fall into false minima and

produce inconsistent parameters. To correct the one-electron crystal field discrepancy by adding more terms to the crystal-field interaction, one should always consider restrictions on operators and introduce constraints based on physical relationships to reduce the number of freely varied parameters.

As discussed in Section 18.3, the effective-operator Hamiltonian for the free-ion interaction includes a corrective term (equation (18.26)) due to configuration interaction. In crystal field theory, the effect of configuration interaction was also considered (Rajnak and Wybourne, 1964). For a configuration of equivalent electrons l^N, most mechanisms of configuration interaction lead to a simple scaling of the crystal field parameters B_q^k. However, a one-electron excitation, either from the l^N shell to unfilled orbitals or from closed shells into the l^N shell, also results in effects that cannot be accommodated by a scaling of the B_q^k parameters alone. As a result, the crystal field parameters are expected to vary from one multiplet to another.

For the weak crystal-field interaction of the f-element ions in crystals, the usual method of a second-order perturbation theory can be used to characterize the configuration interaction (Judd, 1963a; Rajnak and Wybourne, 1963, 1964). The single particle operator $C_q^{(k)}$ in equation (18.32) can only couple configurations that differ by the excitation of a single electron. Thus, for an nl^N-type configuration, only three types of configurations are coupled:

(1) $nl^N n'l'^{4l'+1}$ with $nl^N n'l'^{4l'+1}n'l''$;
(2) nl^N with $nl^{N-1}n'l'$;
(3) $nl^N n'l'^{4l'+2}$ with $nl^{N+1}n'l'^{4l'+2}$.

As a result of the interaction between these configurations, each matrix element of equation (18.32) must be replaced by

$$(1+\Delta)\left\langle l^N\tau SLJM\left|B_q^k C_q^{(k)}\right|l^N\tau' S'L'J,M'\right\rangle \tag{18.48}$$

where Δ is known as the configuration interaction correction factor. This factor is the sum of two terms Δ_1 and Δ_2, where

$$\Delta_1 = \frac{-1}{E}\sum_m \frac{\langle nl^N\psi|\mathscr{H}_{\mathrm{CF}}|m\rangle\langle m|\mathscr{H}_{\mathrm{CF}}|nl^N\psi'\rangle}{\langle nl^N\psi|\mathscr{H}_{\mathrm{CF}}|nl^N\psi'\rangle}, \tag{18.49}$$

and

$$\Delta_2 = \frac{-2}{E}\sum_m \frac{\langle nl^N\psi|\mathscr{H}_{\mathrm{CF}}|m\rangle\langle m|\mathscr{H}_{C}|nl^N\psi'\rangle}{\langle nl^N\psi|\mathscr{H}_{\mathrm{CF}}|nl^N\psi'\rangle} \tag{18.50}$$

and E is the mean excitation energy of the excited electron, m is a state of the perturbing configuration, $\mathscr{H}_{\mathrm{CF}}$ is the crystal-field Hamiltonian, and $\mathscr{H}_{\mathrm{C}}$ is the Coulomb interaction in the free-ion Hamiltonian.

The first correction factor Δ_1 corresponds to configuration mixing purely by the crystal field, whereas the second factor Δ_2 represents an electrostatically correlated crystal-field interaction between the configurations. Methods for

evaluating the matrix elements have been discussed in detail in previous work (Judd, 1963a; Rajnak and Wybourne, 1964). It has been shown that the primary effect of configuration interaction is simply to scale the crystal field parameters B_q^k. The individual parameters are shielded (or antishielded) by different amounts depending on the perturbing configuration. This overall scaling effect is absorbed into the crystal field parameters determined from the experimental data. However, it has been shown that the second factor Δ_2 may be different for different *SL* states. This means that the crystal field parameters are no longer independent of free-ion states. If this mechanism is important, the crystal field parameters determined in fitting observed states in the narrow energy range of the low-lying multiplets give an inadequate description of the crystal-field splittings of the multiplets at higher energies.

18.5 INTERPRETATION OF THE OBSERVED SPECTRA OF TRIVALENT ACTINIDE IONS

Most of the actinide elements may be easily stabilized as trivalent ions in solids. Accordingly, a majority of the spectroscopic studies of actinides has been performed on the trivalent ions in $5f^N$ configurations. Whereas higher oxidation states can be stabilized for the lighter members in the first half of the actinide series, the 3+ oxidation state is most stable for the spectroscopically studied heavier actinides in condensed phases. Spectroscopic analyses and empirical modeling of the free-ion and crystal-field Hamiltonian were successfully conducted first on the trivalent ions using the model Hamiltonian reviewed in Section 18.4.6. Similarities are found between the series of trivalent actinide and lanthanide ions in terms of free-ion interactions and crystal-field splittings of the energy levels of the f-electrons.

When the results of a Hartree–Fock calculation are compared to those of a parametric analysis of experimentally identified levels for a given element, the magnitude of the computed energies, particularly those for F^k, are generally found to be too high. For a more realistic Hamiltonian, using parametric approach, one can apply subtractive corrections to the estimates derived from *ab initio* calculations. These corrections turn out to be essentially constant over the series and almost identical for both $4f^N$ and $5f^N$ shells (Crosswhite, 1977; Liu, 2000). The significance of this is that mixing with high configurations can be taken as essentially a fixed contribution to a global parametric model (Crosswhite and Crosswhite, 1984; Carnall, 1992; Liu *et al*., 1994b).

Many of the early spectroscopic studies of actinides in solids were conducted on actinide chlorides or trivalent actinide ions doped into crystals of $LaCl_3$ (Carnall, 1992), which can incorporate the actinide series from U^{3+} through Es^{3+} as impurities that substitute at the La^{3+} lattice site (C_{3h} symmetry). These studies, supplemented by Zeeman-effect studies of the influence of applied magnetic fields on the energy levels, provided the basis for experimental

characterization of the observed transitions in terms of the free-ion *SLJ* and crystal field quantum numbers. The available data for the $5f^N$ energy levels of trivalent actinide ions in $LaCl_3$ and actinide chlorides have enabled a systematic analysis and modeling of the $5f^N$ energy level structure (Carnall, 1992). The significance of such a systematic analysis and theoretical modeling, like that for the lanthanide series in $LaCl_3$ and LaF_3, is to provide a fundamental understanding of the electronic properties of actinides in solids along with values of free-ion interaction parameters that can be used for analyzing the spectra of the actinide ions in other compounds and solutions.

The relative energies of some of the low-lying states in U^{3+}:$LaCl_3$ are shown in Fig. 18.6 (Crosswhite *et al.*, 1980). As indicated, each free-ion state is split by the crystal field. When measured at the temperature of liquid He (~4 K), only transitions from the lowest state (taken as the zero of energy and having a

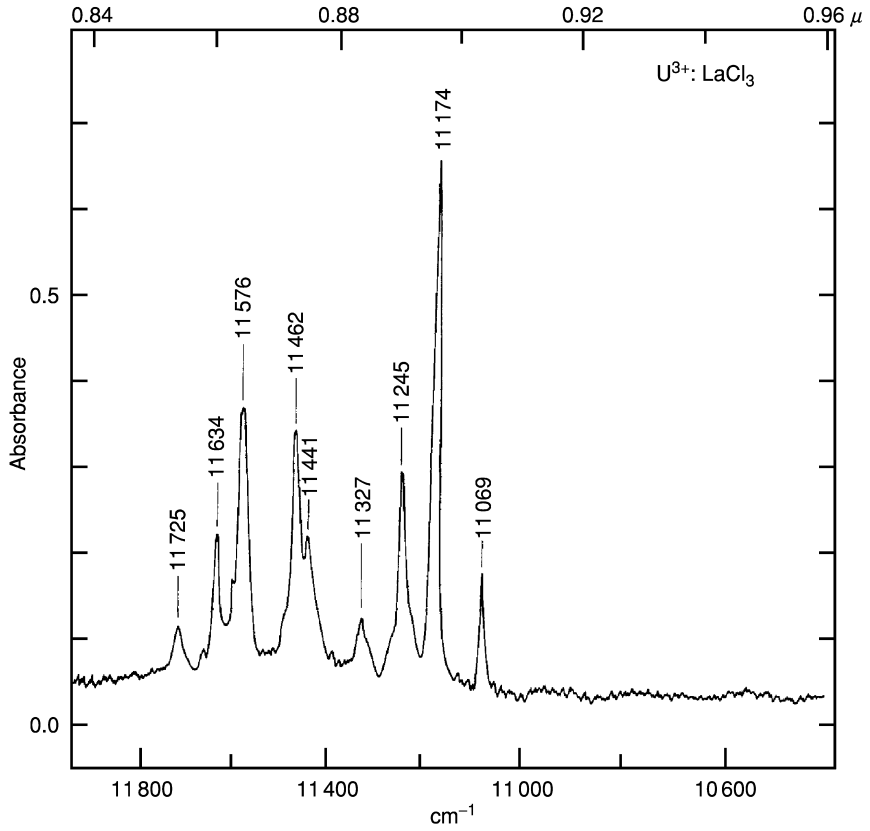

Fig. 18.6 *Absorption spectrum of the crystal-field splittings of* U^{3+}*:*$LaCl_3$ *in the range* 11 000–11 800 cm^{-1} *at* 4 K. (*Reprinted with permission from Crosswhite* et al., 1980. *Copyright* 1980, *American Institute of Physics.*)

crystal field quantum number $\mu = 5/2$ in this case) are observed. Most of the experimental results that have been reported were photographed using high-resolution grating spectrographs. Transitions to only three levels $^4I_{11/2}$ were readily observed in absorption; that to a $\mu = 1/2$ state (found by other techniques near 4580 cm^{-1}) were too weak to be apparent. Fig. 18.6 shows the absorption spectrum of U^{3+}:$LaCl_3$ in the range of 11 000 cm^{-1}. Lines in this spectrum are attributed the multiplets of $^4G_{5/2}$, $^4I_{15/2}$, $^4S_{3/2}$, and $^4F_{7/2}$ (Carnall, 1992). Electric dipole selection rules between the ground (μ=5/2) and excited (μ=5/2) states show that absorption transitions are forbidden, so the levels that would have corresponded to absorption transitions at 4556 and 4608 cm^{-1} had to be established by fluorescence methods. Assigning energies corresponding to the centers of these components, thus defining the 'free-ion' levels for the ion in a particular medium yields the energy level scheme indicated at the left in Fig. 18.7. Although the levels are shifted to somewhat lower energies than those of the true gaseous free-ion states, the basic structure appears to be preserved and is usually only moderately changed from medium to medium for trivalent lanthanides and actinides. For example, the center of gravity of the $^4I_{11/2}$ state in U^{3+}:$LaCl_3$ in Fig. 18.7 is 4544 cm^{-1}.

As the energies of the components of various groups are established experimentally, the model free-ion and crystal field parameters that reproduce the splittings can be computed by a suitable (nonlinear least-squares) fitting procedure. The computed values are then used to predict the splitting patterns in other groups where not all of the allowed components can be observed. Thus in the analysis of such spectral data there is a continual interplay between theory and experiment. When large numbers of levels have been experimentally confirmed, most (in some cases, all) of the parameters of the model can be varied simultaneously to establish the final values (Table 18.4). Fig. 18.8 shows the calculated energy levels that result from crystal-field splitting for An^{3+} in $LaCl_3$ (Carnall, 1992).

In typical analyses of actinide and lanthanide spectra in condensed phases, the range of observation may extend well into the near-ultraviolet region. The number of assignments made to different multiplets and states is usually sufficient to determine most of the energy level parameters. However, in Fig. 18.8 some of the observations on which this diagram is based were limited to less than 50% of the total extent of the f^N configurations. The accuracy of predicted energy level in the ultraviolet range clearly remains to be thoroughly tested. The Slater parameters in An^{3+} are typically only two-thirds as large as those for the Ln^{3+}, but ζ_{5f} is a factor of 2 larger than ζ_{4f}; so while the total energy range of the $5f^N$ configuration is reduced, the states are significantly more mixed in character because of the increased spin–orbit interaction.

The lanthanide orthophosphates, such as $LuPO_4$ and YPO_4, are good hosts for the incorporation of dilute f^N impurities. A wide variety of lanthanide and actinide ions, diluted in these materials, have been produced to carry out fundamental spectroscopic investigations (Morrison and Leavitt, 1982; Görller-Walrand and Binnemans, 1996). For the actinide series, Cm^{3+} doped

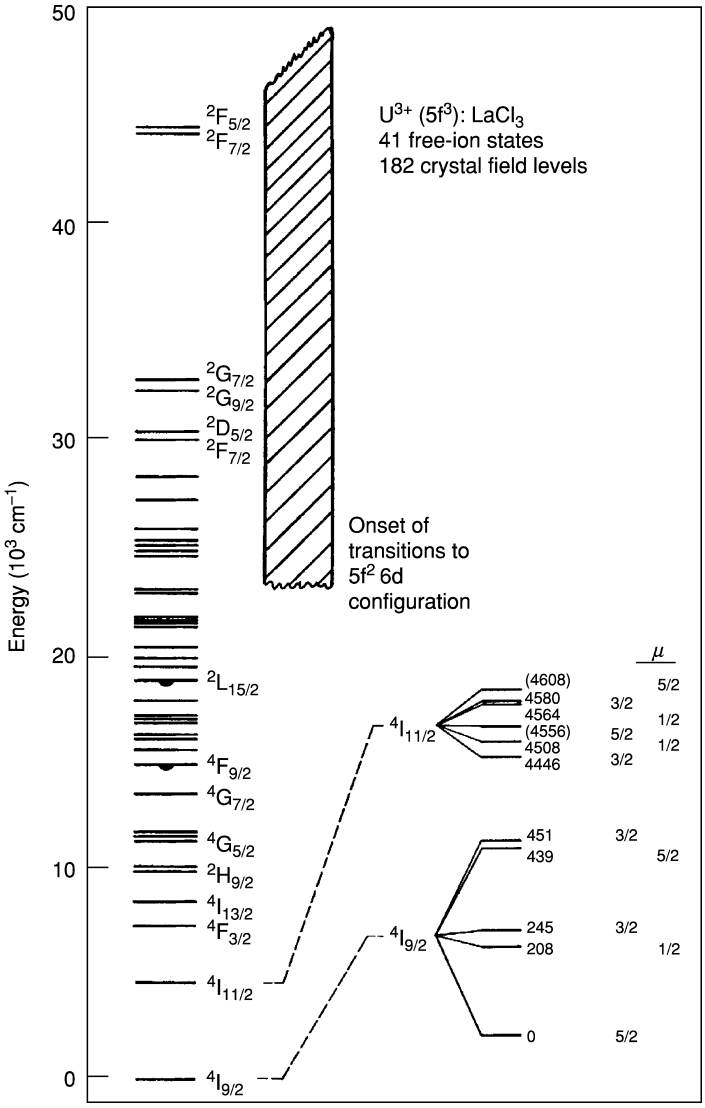

Fig. 18.7 *Energy level structure for* U^{3+}*:*$LaCl_3$.

into $LuPO_4$ and YPO_4, has been the most extensively studied system (Murdoch *et al.*, 1996, 1997; Liu *et al.*, 1998). The greater spatial extent of the 5f electron shell results in a smaller electrostatic interaction between equivalent electrons in the 5f shell than in the 4f shell. Thus for Cm^{3+}, the energy level of the first excited multiplet ($J = 7/2$) is at $\sim$16 000 cm^{-1}. Utilizing this metastable emitting state, excited state absorption studies allowed the collection of data to

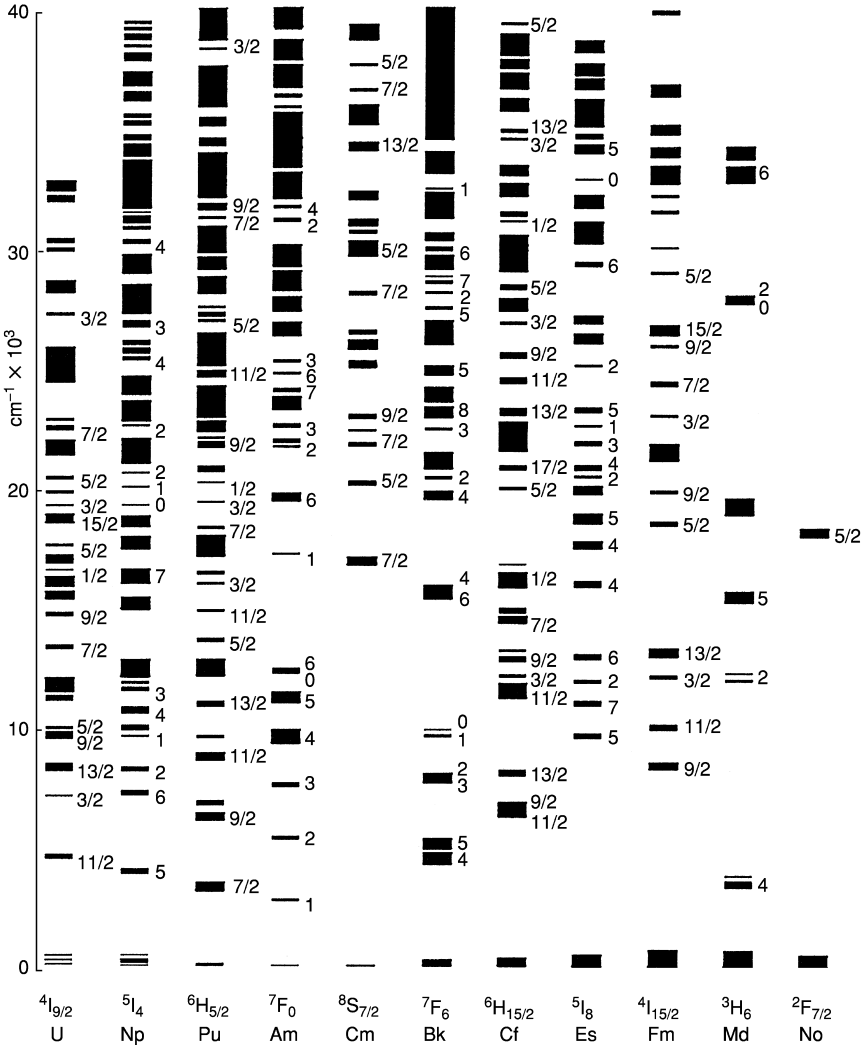

Fig. 18.8 *Energy level structure of An^{3+}:$LaCl_3$ based on computed crystal field energies in the range* 0–40 000 cm^{-1}. (*Reprinted with permission from Carnall,* 1992. *Copyright* 1992, *American Institute of Physics.*)

40 000 cm^{-1} using two visible lasers (Murdoch *et al.*, 1997). The ground term multiplet splitting is small, because the largest component of the ground multiplet has zero angular momentum. Early detailed studies of the Cm^{3+} optical spectra were performed with the ^{244}Cm isotope. During the past decade or so, multimilligram quantities of ^{248}Cm have become available. Several single crystals were doped with the ^{248}Cm isotope and optical studies of these samples

were performed using laser-selective excitation and fluorescence techniques. Edelstein (2002) has recently published a review of the spectroscopic studies of Cm^{3+} in various hosts.

The free-ion model based on studies of the 3+ actinide ions in $LaCl_3$ has been used in analysis of the optical spectra of Cm^{3+} in $LuPO_4$. For the crystal-field splitting, because the metal ion site is D_{2d} in the phosphates instead of C_{3h} in $LaCl_3$, a different set of crystal field parameters must be established. Fig. 18.9 shows the excitation spectra of Cm^{3+} in $LuPO_4$ (Fig. 18.9a) and YPO_4

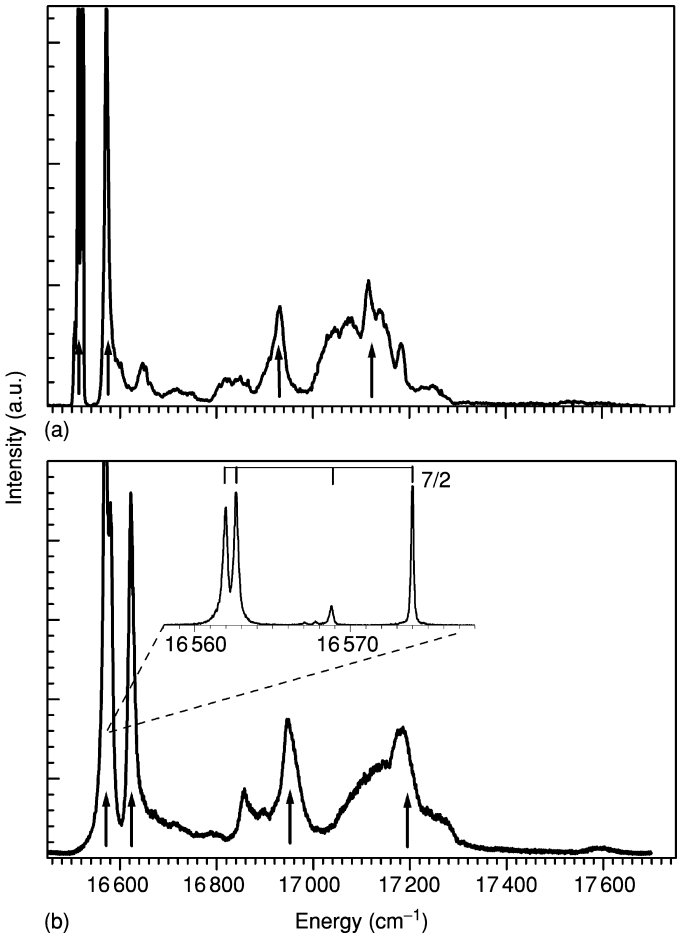

Fig. 18.9 *Excitation spectra of transitions from the* $^8S_{7/2}$ *ground state multiplets to the* $^6D_{7/2}$ *excited state of the* Cm^{3+} *ion in* (*a*) $LuPO_4$ *and* (*b*) YPO_4 *at* 4 K. (*Reprinted with permission from Liu* et al., 1998. *Copyright* 1998, *American Institute of Physics.*) *The emission was monitored at* 16 563.0 cm^{-1} *for* Cm^{3+}:YPO_4 *and* 16 519.5 cm^{-1} *for* Cm^{3+}:$LuPO_4$. *The insert shows the crystal-field splitting of the ground state of* Cm^{3+} *in* YPO_4.

(Fig. 18.9b) in which the crystal field energy levels for the first excited multiplet (nominal $^6D_{7/2}$) were observed to extend from 16 560 to 17 200 cm^{-1}. In addition to the zero-phonon lines (ZPL) indicated by the vertical arrows, vibronic sidebands have intensities comparable to those of the upper ZPLs. The insert in Fig. 18.9b shows the crystal-field splitting in the ground state which also is a $J = 7/2$ (nominal $^8S_{7/2}$). Whereas the excited state crystal-field splitting is more than 800 cm^{-1}, the ground state splitting is only 12 cm^{-1}. As pointed out in Section 18.4.2, the crystal-field interaction vanishes in the ground state of an f^7 configuration unless a fourth-order coupling to the excited states is considered (Liu *et al.*, 1993). Although the excited $^6D_{7/2}$ also has no first-order crystal-field splitting, the more significant mixture of *LS* terms in its wave functions results in much larger crystal-field splitting. Many experimental results of the ground state splitting of actinide ions in the $5f^7$ configuration, which include Am^{2+}, Cm^{3+}, and Bk^{4+} in different crystalline hosts, have been reported (Edelstein and Easley, 1968; Liu *et al.*, 1996; Murdoch *et al.*, 1996; Brito and Liu, 2000).

In different hosts, the values for the An^{3+} free-ion parameters listed in Table 18.4 may vary 1% or less. In fitting the Cm^{3+}:$LuPO_4$ (or YPO_4) data, the parameters of three-body coupling operators, T^k, were kept fixed at the values for Cm^{3+} in $LaCl_3$ (Murdoch *et al.*, 1996, 1997). The energy levels of Cm^{3+} in $LuPO_4$ up to 35 000 cm^{-1} were probed by high-resolution techniques using two-step excited state absorption and one color two-phonon absorption methods (Murdoch *et al.*, 1997). The modeling of the Cm^{3+}:$LuPO_4$ energy level structure with the experimental data up to 35 000 cm^{-1} did not result in significant changes in the free-ion parameters determined in the systematic analysis of the $5f^N$ ions in $LaCl_3$. This consistency leads to two important conclusions as regards the applications of the free-ion and crystal field model: (a) the free-ion interaction parameters are relatively insensitive to host lattice; and (b) the parameters determined by analysis of the low-lying energy states can reproduce energy levels of high-lying states with satisfactory accuracy.

In appropriate hosts, the $^5D_1$ state of Am^{3+} ($5f^6$ configuration) is a metastable emitting state as is the $^6D_{7/2}$ state of Cm^{3+} ($5f^7$ configuration) (Carnall, 1992). In such cases, both ions emit visible luminescence so they are very suitable for laser-induced fluorescence excitation studies. In addition to $LaCl_3$ and $LuPO_4$, these two ions in other crystalline hosts such as Cs_2NaYCl_6 (Murdoch *et al.*, 1998), ThO_2 (Hubert *et al.*, 1993; Thouvenot *et al.*, 1993a, 1994), and $CaWO_4$ (Liu *et al.*, 1997a,b) have been investigated using laser spectroscopic methods. These studies showed that Am^{3+} and Cm^{3+} exhibit spectroscopic properties that are similar to those found in studies in $LaCl_3$, although the strength of the crystal-field interaction may be significantly different. Table 18.9 provides a comparison between the free-ion and crystal-field interactions of Eu^{3+} and Am^{3+} both of which have the f^6 configuration.

The ratios of free-ion interactions and crystal field strength for the 4f and 5f ions listed in Table 18.9 indicate that the electrostatic interaction is reduced approximately to 60% and the spin–orbit coupling is increased by 190%

Table 18.9 *Comparison of interaction parameters of* Am^{3+} $(5f^6)$ *and* $Eu^{3+}(4f^6)$ (cm^{-1}).

	$LaCl_3$[a]	ThO_2[b]
$F^2(Eu^{3+})$	84 400	80 335
$F^2(Am^{3+})$	51 900	48 038
$\boldsymbol{F^2(Am^{3+})/F^2(Eu^{3+})}$	**0.62**	**0.60**
$\zeta_{4f}(Eu^{3+})$	1 328	1 337
$\zeta_{5f}(Am^{3+})$	2 564	2 511
$\boldsymbol{\zeta_{5f}(Am^{3+})/\zeta_{4f}(Eu^{3+})}$	**1.93**	**1.88**
$N\nu(Eu^{3+})$	329	1 231
$N\nu(Am^{3+})$	628	2 953
$\boldsymbol{N\nu(Am^{3+})/N\nu(Eu^{3+})}$	**1.9**	**2.4**

[a] Carnall (1992) and Crosswhite (1977).
[b] Hubert *et al.* (1993).

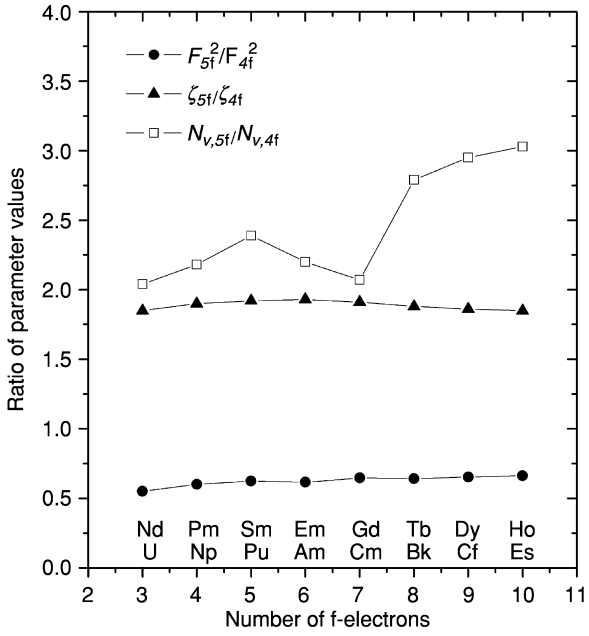

Fig. 18.10 *Comparison of the parameter ratios for trivalent lanthanide and actinide ions in* $LaCl_3$ (*Data from Crosswhite*, 1977 *and Carnall, 1992*).

(Edelstein and Easley, 1968) for the values of the lanthanide analogs in the same f^N configuration. These changes are attributed to the more extended 5f orbitals of Am^{3+} in comparison with the 4f orbitals of Eu^{3+}. In addition, the strength of the crystal-field interaction is doubled for the actinide ion. This trend of

variations is shown systematically in Fig. 18.10 for the two series of ions in the $LaCl_3$ crystal lattice (Liu, 2000).

Edelstein and Easley (1968) observed the trivalent state for ^{243}Am and ^{244}Cm doped into CaF_2 when the crystals were initially grown. However, due to the high level of radioactivity caused mainly by the alpha decay of ^{244}Cm ($t_{1/2}$ = 18.1 years) part of the Am^{3+} was reduced to Am^{2+} and part of the Cm^{3+} was oxidized to Cm^{4+}. It was observed that the ratio of Am^{2+} to Am^{3+} in the cubic sites of CaF_2 was approximately 10:1. The energy level structures of Am^{2+} and Cm^{3+} in CaF_2 were probed and analyzed based on the crystal field model for $5f^7$ configuration (Edelstein *et al.*, 1966; Edelstein and Easley, 1968). A recent study (Beitz *et al.*, 1998) reported that Es^{3+} ($5f^{10}$) can be stabilized in LaF_3 and its spectroscopic properties in terms of free-ion interactions are very similar to Es^{3+} in $LaCl_3$, although a crystal field strength approximately twice of that for Ho^{3+} ($4f^{10}$) in LaF_3 is expected. Although the spectra of several organometallic 3+ actinides, such as plutonium tricyclopentadienide, have been measured, the analysis of data is still quite incomplete (Carnall, 1979b). Nevertheless, it seems apparent that now the energy level parameters for such systems can be approximated by those characteristics of the trivalent actinide in the $LaCl_3$ host.

There have been several recent laser spectroscopic studies on U^{3+} ions in various ternary chloride and bromide crystalline systems. Because of relatively low-phonon energies of lattice vibration, strong luminescence from U^{3+} can be observed in these crystals. Using effective-operator Hamiltonian and parameterization method, Karbowiak and colleagues have analyzed the absorption and emission spectra of U^{3+} in Ba_2YCl_7, $CsCdBr_3$, and Cs_2NaYBr_6, respectively. Both U^{3+} and U^{4+} were observed in the Ba_2YCl_7 system, which possesses monoclinic symmetry. For uranium ions at a C_1 site, a total of 27 crystal field parameters are required to calculate the energy levels (Karbowiak *et al.*, 1997, 2003). Using time-resolved and site-selected laser excitation methods, this group has investigated the spectroscopic and excited state dynamics of U^{3+} in RbY_2Cl_7. The strength of the free-ion and crystal-field interaction in these systems is generally consistent with that for the U^{3+}:$LaCl_3$ systems. A general correlation between the magnitudes of crystal field parameters and the U^{3+} luminescence decay rate has been realized in the analyses of the site-selected spectra and luminescence dynamics.

18.6 INTERPRETATION OF THE OBSERVED SPECTRA OF TETRAVALENT ACTINIDE IONS

It is well known that a major difference between the lanthanide and actinide series is the greater stability of 4+ and higher valance states of the actinides, particularly in the first half of the respective series. There have been numerous analyses of the spectra of tetravalent uranium compounds, whereas the number

of published spectroscopic analyses rapidly decreases as heavier members of the actinide series in the 4+ valence states are considered. The reasons are, first of all, differences in stability of the tetravalent state for actinide compounds are such that reducing and then oxidizing conditions become necessary as the actinide atomic number increases. Secondly, the low specific radioactivity of uranium of natural isotopic abundance makes the doped crystalline materials easy to handle and limits radiolytic degradation. Moreover, the f^2 configuration of U^{4+} provides experimental features that are suitable for theoretical analyses and constitute a useful basis for extending the interpretation of spectra of other An^{4+} ions in condensed media. There is a series of crystalline hosts, notably ThX_4 and Cs_2MX_6 (M = Zr, Th; X = Cl, Br), $ThSiO_4$, and $ZrSiO_4$, in which $Pa^{4+}(5f)$ and $U^{4+}(5f^2)$ can be doped for spectroscopic studies (Krupa, 1987). In addition, Np^{4+}, Pu^{4+}, and Am^{4+} have been successfully doped into $ThSiO_4$ (Krupa *et al.*, 1983; Krupa and Carnall, 1993). However, in contrast to most other binary compounds, the tetravalent actinides as fluorides are sufficiently stable and PaF_4 through CfF_4 can be prepared and are isostructural to UF_4 and CeF_4 (Brown, 1968; Morss, 2005).

Since 1986, significant progress in analyses of the crystal field spectra of tetravalent actinide ions in solids has been reported. The structural characteristic of f→f transitions has been observed and analyzed using the theoretical model of free-ion and crystal-field interactions that was discussed in Sections 18.3 and 18.4. The observations are consistent with trends indicated in Fig. 18.1, which suggest that transitions to the $f^{N-1}d$ configurations in An v will lie even higher in energy relative to the lowest-energy f^N state than in the corresponding transitions for An iv. The lowest f→d transition in the atomic spectrum of U v was assigned at 59 183 cm^{-1} (Van Deurzen *et al.*, 1984). Consequently, broad and intense band structure in the spectra of An^{4+} compounds beginning near 40 000–45 000 cm^{-1} would be consistent with the onset of f→d transitions. The energy level structure of the free-ion U^{4+} ($5f^2$) configuration has provided a valuable basis for comparison in developing the analysis of An^{4+} spectra in solids.

Krupa (1987) reviewed spectroscopic properties of $Pa^{4+}(5f^1)$, $U^{4+}(5f^2)$, and $Np^{4+}(5f^3)$ in crystalline host $ThBr_4$, $ThCl_4$, and $ThSiO_4$. For Pa^{4+} in Cs_2ZrCl_6, electron paramagnetic resonance and near-infrared absorption spectra were measured and the data analyzed by Axe *et al.* (1961) in terms of the crystal-field and spin–orbit interactions for a $5f^1$ electron. Additional optical studies have been reported for pure Pa^{4+} hexahalo compounds and Pa^{4+} diluted into Cs_2ZrCl_6 (Brown *et al.*, 1974, 1976; Edelstein *et al.*, 1974, 1992; Piehler *et al.*, 1991). For this one-electron system, there are no electrostatic terms for the free-ion interactions, thus the splitting of the free-ion energy states, which consist of the $^2F_{5/2}$ ground state and the $^2F_{7/2}$ excited state, is solely due to spin–orbit coupling. Crystal-field splittings in the tetravalent ions are much larger than those of the trivalent ions. Table 18.10 lists the spectroscopic parameters of Pa^{4+} in $ThCl_4$ and $ThBr_4$ in D_{2d} symmetry (Malek and Krupa, 1986; Krupa,

Table 18.10 *Energy parameters of Pa^{4+} and U^{4+} in $ThCl_4$, $ThBr_4$, and $ThSiO_4$ in D_{2d} symmetry* (cm^{-1}).[a]

	Pa^{4+}		U^{4+}		
	$ThCl_4$	$ThBr_4$	$ThCl_4$	$ThBr_4$	$ThSiO_4$
F^2			42 752(162)	42 253(127)	43 110(245)
F^4			39 925(502)	40 458(489)	40 929(199)
F^6			24 519(479)	25 881(383)	23 834(639)
ζ	1524.4(5)	1532.8(5)	1808(8)	1783(7)	1840(2)
α			30.4(2)	31(1)	32.3(0.4)
β			−492(84)	−644(75)	−663(144)
γ			[1200]	[1200]	[1200]
B_0^2	−1405(50)	−1047(52)	−1054(117)	−1096(80)	−1003(127)
B_0^4	1749(94)	1366(138)	1146(200)	1316(146)	1147(281)
B_4^4	−2440(98)	−1990(102)	−2767(147)	−2230(85)	−2698(251)
B_0^6	−2404(607)	−1162(541)	−2315(404)	−3170(379)	−2889(557)
B_4^6	−195(267)	623(174)	−312(227)	686(246)	−208(333)
n[b]	7	7	25	26	25
σ[b]	23.6	19.4	46	36	71

[a] Krupa (1987).
[b] Number of assigned levels (n) and deviation (σ), see Table 18.4, footnote c.

1987). The data for Pa^{4+} in Cs_2ZrCl_6 are considerably better than for the ThX_4 systems. Also some data are given for the excited 6d system.

Analysis of the spectra of U^{4+} in both high-symmetry (O_h) and relatively low-symmetry (D_{2d} and D_2) sites have been published. Somewhat in contrast to observations made with trivalent ions, the magnitude of the crystal-field splitting in the two cases differs significantly. An example of the high-symmetry case is that of U^{4+} in Cs_2UCl_6 (Johnston *et al.*, 1966a,b). The low-symmetry (D_{2d}) case is illustrated in the analysis of U^{4+}:$ThBr_4$ (Delamoye *et al.*, 1983). Recently, spectroscopic analyses were reported by Karbowiak *et al.* (2003) for U^{4+} in Ba_2YCl_7. In this work, values of the 27 crystal field parameters of the Hamiltonian were determined in fitting a total of 60 observed crystal field energy levels to the model Hamiltonian. The crystal-field splitting in the Cs_2UCl_6 is over twice as large as that in U^{4+}:$ThBr_4$. As a result, much more complex structure caused by the mixing of states of different J in close proximity occurs within a given energy range in Cs_2UCl_6 compared to the U^{4+}:$ThBr_4$ case. In the analyses of the crystal field spectrum of U^{4+} on the octahedral sites of Cs_2UBr_6 and Cs_2ZrBr_6, Faucher *et al.* (1996) reported that there is a strong coupling between the $5f^2$ and $5f^17p^1$ configurations. Therefore, additional effective operators for the configuration interaction are necessary to better interpret the observed energy level structure.

The extensive analysis of the data for U^{4+}:$ThBr_4$ and the similar crystal field parameters deduced for Pa^{4+}:$ThCl_4$ (Krupa *et al.*, 1983) have provided a new

basis for examining other An^{4+} spectra. As Auzel and coworkers have shown (Auzel *et al.*, 1982), band intensities in the spectrum of aquated U^{4+} can be assigned in terms of crystal-field split *SLJ* levels similar to those deduced for U^{4+}:$ThBr_4$. Using the method of extrapolation discussed in Sections 18.3 and 18.4, energy level parameters that are consistent with those for Pa^{4+}:$ThCl_4$ and U^{4+}:$ThBr_4$ can be extrapolated to obtain a set for Np^{4+}, and a good correlation is found between this energy level structure and the band structure observed for aquated Np^{4+}. That the apparent correlation between band structure observed for the iso-f-electron configurations of aquated An^{4+} and aquated An^{3+} ions continues along the series is evident when comparing the spectra of aquated Pu^{4+} and aquated Np^{3+}. Jørgensen called attention to this apparent correlation in the band structure observed for the iso-f-electron configurations An^{3+} and An^{4+} spectra at a time when little was known about the extent of the ligand fields involved (Jørgensen, 1959). Concern that the data for aquated An^{4+} should be interpreted in terms of large ligand-field splitting characteristic of Cs_2UCl_6, instead of a weaker-field case may have been partially responsible for the slow pace in exploration of Jørgensen's insight. Of course, development of this An^{3+}/An^{4+} spectral correlation also required an understanding of the energy level structures in An^{3+}, which was not well understood in 1959. Adopting the electrostatic and spin–orbit parameters for U^{4+}:$ThBr_4$ as a basis for estimating parameters for the An^{4+} ions, the general character of the spectra of the An^{4+} ions can be interpreted (Conway, 1964).

In solid compounds such as Cs_2UCl_6, where the 4+ ions occupy sites of inversion symmetry, the observed structure is almost exclusively vibronic in character, as contrasted with the electronic transitions characteristic of 3+ compounds. The electronic origins were deduced from progressions in the vibronic structure, because the electronic transitions themselves were symmetry-forbidden. An analysis of the intensities of vibronic bands has been reported (Satten *et al.*, 1983; Reid and Richardson, 1984). Other extensive analyses of the spectra of U^{4+} in crystalline hosts include those for U^{4+}:$ZrSiO_4$ (Richman *et al.*, 1967; Mackey *et al.*, 1975).

Because of much stronger ion–lattice coupling for the 6d orbitals, in contrast to the 5f−5f transitions in which vibronic coupling is relatively weak, the spectra of 5f↔6d transitions, however, are often dominated by the vibronic bands associated with the f−d electronic transitions in both absorption and emission spectra even when there is no inversion symmetry. The assignment and analyses of the crystal field spectra become difficult, because the pure electronic transitions (ZPL) may be obscured by the broad and intense vibronic sidebands. Fig. 18.11 shows the emission spectrum of the $6d^2D_{3/2}$ (Γ_{8g}) $\rightarrow 5f^2F_{5/2}$ (Γ_{8u}) electronic transition of Pa^{4+}:Cs_2ZrCl_6, with the zero-phonon line at 17 847 cm^{-1} accompanied by various vibronic sidebands (Piehler *et al.*, 1991). From the optical spectra, the vibrational frequencies of different modes can be measured and assigned to the local and lattice modes that couple to the electronic transitions. In the 5f−6d spectra (see Fig. 18.11), and also in charge-transfer spectra

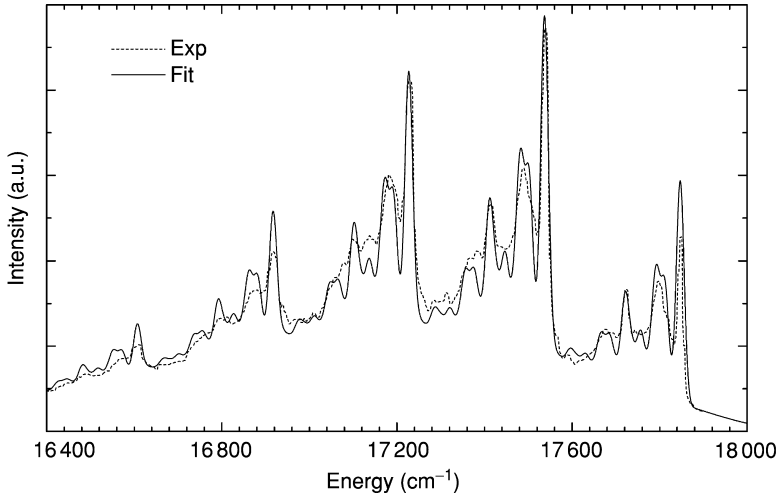

Fig. 18.11 *The emission spectrum of the* $6d^2D_{3/2}(\Gamma_{8g}) \rightarrow 5f^2F_{5/2}(\Gamma_{8u})$*electronic vibronic transitions for* Pa^{4+} *in* Cs_2ZrCl_6 *at* 4.2 K (*experimental data from Piehler* et al., 1991). *The energy of the zero-phonon line of the electronic transition is* 17 847 cm^{-1}. *The vibrational frequencies obtained from fitting the spectrum are* $\nu_1(A_{1g}) = 310$ cm^{-1}, ν_5 $(T_{2g}) = 123$ cm^{-1}, ν_{L1} $(T_{1g}) = 35$ cm^{-1}, *and* ν_{L2} $(T_{2g}) = 55$ cm^{-1}.

(discussed later), certain vibrational progression frequencies have harmonics up to fifth order, whereas others appears only to first order. Liu *et al*. (2002) demonstrated recently that the progressions of multiple vibrational frequencies can be simulated using a modified model of the Huang–Rhys theory of electron–phonon interaction (Huang and Rhys, 1950). The dashed line in Fig. 18.11 is a model fit to the experimental spectrum.

A systematic analysis of crystal field spectra has been reported for tetravalent actinide ions from U^{4+} through Bk^{4+} in AnF_4 and An^{4+}:CeF_4 (Carnall *et al*., 1991; Liu *et al*., 1994b). The tetravalent fluorides were chosen because An^{4+} (An = U to Cf) can be stabilized and they all, including CeF_4, which has no f-electron in the lowest-energy configuration, are isostructural. The absorption spectrum of UF_4 is plotted in Fig. 18.12 in comparison with that of U^{4+} ion in aqueous solution, and the liquid helium temperature absorption spectra of NpF_4 and PuF_4 are shown in Fig. 18.13 (Carnall *et al*., 1991). Crystal structure data for UF_4 established that there are two different low-symmetry sites, C_1 and C_2, for the An^{4+} ion. Both sites have eight nearest neighbor fluorine ions arranged in a slightly distorted antiprismatic configuration; however, there are twice as many C_1 as C_2 sites in the unit cell which aids in identifying sites in the site-resolved spectra. The site-selective excitation spectra of the $^7F_0 - ^5L_6$ transitions are shown in Fig. 18.14 for a 0.1% Cm^{4+}:CeF_4 sample at 4.3 K. Crystal field modeling was conducted based on an approximate C_2 site symmetry. The spectra have similar characteristics as those of An^{3+} ions in crystals

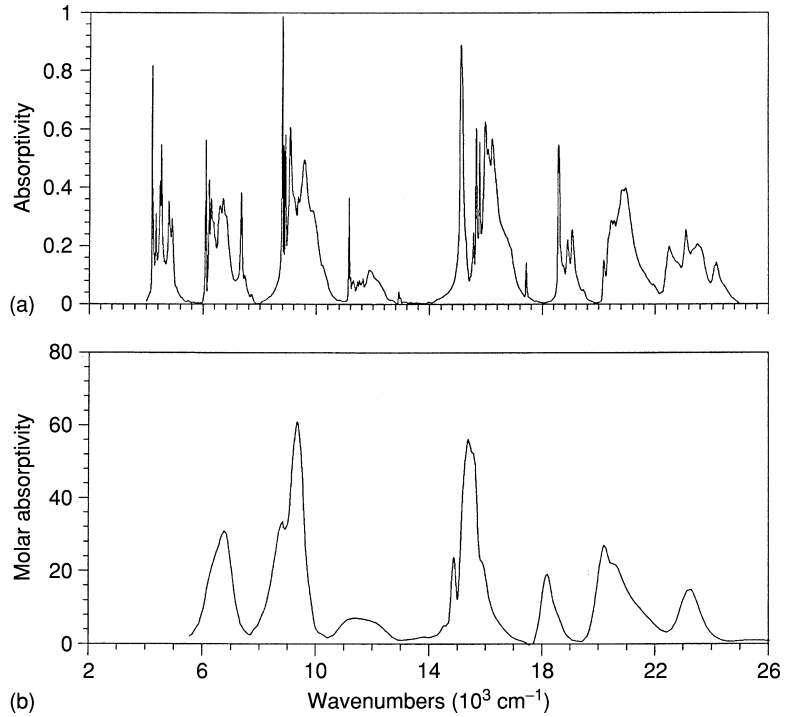

Fig. 18.12 *Absorption spectra of* (*a*) UF_4 *in a KBr pellet at* ~4 K*;* (*b*) *aquated* U^{4+} *at* 298 K *both in the near-infrared to visible range.* (*Reprinted with permission from Carnall* et al., 1991. *Copyright* 1991*, American Institute of Physics.*)

(see Fig. 18.9 for Cm^{3+}:$LuPO_4$). Sharp ZPL are resolved in the low-energy region and broad vibronic transitions that span ~800 cm^{-1} with the strongest features ~400 cm^{-1} above the first ZPL are also found. The vibronic lines in the An^{4+} spectra are relatively stronger than those in An^{3+} spectra. This suggests a stronger ion–ligand coupling for tetravalent ions, which is consistent with the larger crystal-field splittings in the An^{4+} systems.

Optical spectroscopic data, including low-temperature absorption (see Figs. 18.12 and 18.13) and laser excitation and luminescence spectra of tetravalent actinides in fluoride compounds, have provided adequate experimental information for a systematic analysis and parameterization of the free-ion and crystal-field interactions. The Hamiltonian of the free-ion and crystal-field interactions has been established through the same parameterization method used for the trivalent ions that was discussed in Section 18.5. The Hamiltonian parameters for An^{4+} in CeF_4 are listed in Table 18.11. The parameterization method ensures a consistent set of free-ion and crystal field parameters from one ion to the next. Given the limited number of energy levels that could be assigned

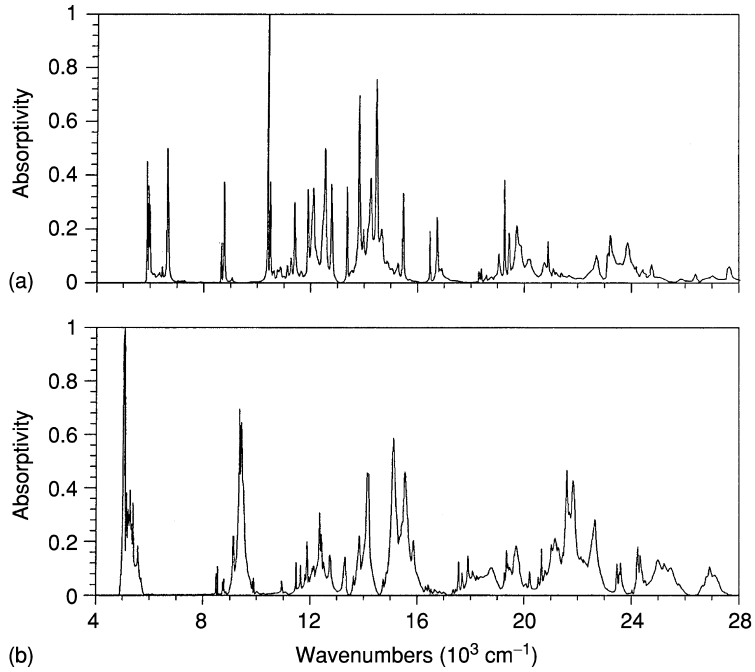

Fig. 18.13 *Absorption spectra of* (*a*) NpF_4 *in a KBr pellet at* ~4 K*;* (*b*) PuF_4 *in KBr pellet at* ~4 K *in the range* 4000–30 000 cm^{-1}. (*Reprinted with permission from Carnall* et al., 1991. *Copyright* 1991, *American Institute of Physics.*)

without ambiguity, the observed spectra of AnF_4 were modeled based on the standard model crystal field with constrained parameters. For instance, the three-body parameters T^i were fixed at average values determined in the analysis of An^{3+}:$LaCl_3$ spectra (Carnall, 1992). The M^h values were assigned in each case based on *ab initio* calculations and were not varied. Although P^2 was varied, in all cases P^4 and P^6 were constrained by the ratios $P^4 = 0.5P^2$ and $P^6 = 0.1P^2$. In fitting experimental data, the modeling, therefore, relied on the systematic variations of F^k and ζ_{5f}. In UF_4, it was pointed out that the magnitude of the crystal-field interaction was relatively large, and *J*-mixing was very significant in higher energy states, the ground crystal field state remained more than 95% pure in terms of *J*-character. Although the excited states above 50 000 cm^{-1} were truncated in the construction of the free-ion wave functions for Pu^{4+}, Am^{4+}, Cm^{4+}, and Bk^{4+}, the ground state eigenfunctions had relatively pure *J*-character, fully consistent with the results for U^{4+} and Np^{4+}. The nominal $^6H_{5/2}$ ground state in Am^{4+} is more than 96% $J = 5/2$, whereas the $^7F_0$ ground state in Cm^{4+} is more than 98% $J = 0$ character. Thus the experimental problem of interpreting magnetic susceptibility measurements in CmF_4 where temperature-dependent results are not consistent with a $J = 0$ ground state (Nave

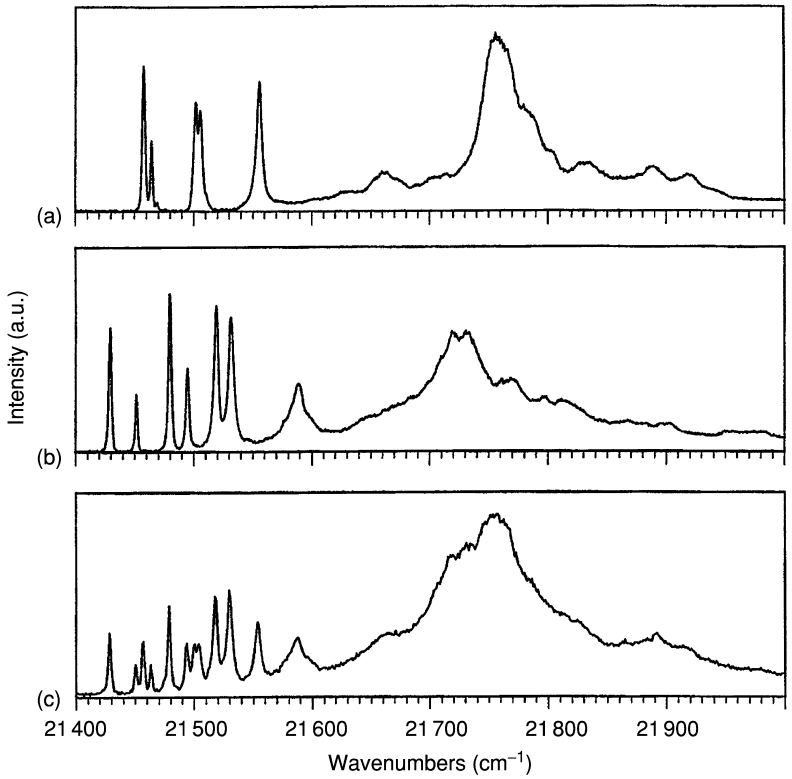

Fig. 18.14 *Site-elective excitation spectra of the* $^7F_0$–$^5L_0$ *transitions in* 0.1% Cm^{4+}:CeF_4 *at* 4.3 K. (*a*) *The spectrum of* Cm^{4+} *ions on site* A *recorded with emission at* 16 603 cm^{-1}; (*b*) *the spectrum of* Cm^{4+} *on site B recorded with emission at* 16 584 cm^{-1}; *and* (*c*) *the excitation spectrum without emission selection. The broad features in the high-energy range are due to vibronic transitions.* (*Reprinted with permission from Liu et al.,* 1994*b*. *Copyright* 1994, *American Institute of Physics.*)

et al., 1983) seems unlikely to be rationalized by assuming appreciable *J*-mixing. For Bk^{4+}, the $J = 0$ character is more than 99.5%, but the contribution from the pure $^8S_{7/2}$ is reduced to 75.5% (Brito and Liu, 2000).

Systematic analysis of the free-ion and crystal-field interactions in AnF_4 (An = U–Bk) provides a useful comparison of the trends in free-ion parameter values between those that would have been expected based on parameters computed using *ab initio* methods and those obtained from fitting the experimental data. As shown in Fig. 18.15, when plotted as a function of atomic number, the model free-ion parameters for An^{4+} exhibit similar increasing trends as those predicted by Hartree–Fock calculations. However, the normalized Hartree–Fock-based values of F^k were typically found to show a steeper slope than those obtained in fitting the experimental data.

Table 18.11 *Energy-level parameters for tetravalent actinide ions in actinide tetrafluorides* (*in* cm^{-1}) (*Liu* et al., 1994*a*,*b*).[a]

	U^{4+}	Np^{4+}	Pu^{4+}	Am^{4+}	Cm^{4+}	Bk^{4+}
F^2	44 784	47 630	50 000	51 824(47)	53 051(38)	55 300
F^4	43 107	42 702 ($0.896F^2$)	44 500 ($0.89F^2$)	$0.89F^2$	$0.893F^2$	$0.88F^2$
F^6	25 654	29 623 ($0.622F^2$)	30 500 ($0.61F^2$)	$0.61F^2$	$0.619F^2$	$0.60F^2$
ζ	1761(3)	2021(4)	2315(7)	2604(6)	3017(5)	3244
α	34.74	34.89	35	35	35	34
β	−767.3	−743.2	−740	−740	−740	−740
γ	913.9	890.7	900	900	900	1000
T^2		200	200	200	200	200
T^3		50	50	50	50	50
T^4		50	50	50	50	50
T^6		−360	−360	−360	−360	−360
T^7		425	425	425	425	425
T^8		340	340	340	340	340
$M^{0,b}$	0.775	0.877	0.984	1.094	1.204	1.314
M^2	0.434	0.489	0.546	0.608	0.671	0.733
M^4	0.294	0.340	0.381	0.424	0.468	0.512
$P^{2,c}$	2715(94)	2700	2200	1623(71)	633(96)	1064
B_0^2	1183(28)	1127(92)	1127	1302(59)	1209(75)	1150
B_2^2	29(27)	45	45	45	45	45
B_0^4	−2714(99)	−2818 (193)	−2818	−2822	−2820	−2720
B_2^4	3024(71)	3090 (171)	3090	3219(135)	3304(99)	3000
B_4^4	−3791(53)	−3584 (170)	−3584	−3337(101)	−3243(90)	−3275
B_0^6	−1433(148)	−1427 (382)	−1427	−1500	−1500	−1700
B_2^6	1267(101)	1267	1267	1400	1400	1500
B_4^6	−1391(93)	−1147 (181)	−1147	−1147	−1142	−1200
B_6^6	1755(82)	1819 (129)	1819	1819	1820	1800
σ^d	31	41	30	31	28	27
n^d	69	57	23	61	38	25

[a] The values in parentheses are errors in the indicated parameters.
[b] The M^k values were assigned in each case based on *ab initio* calculation and were not varied.
[c] P^2 was varied freely, P^4 and P^6 were constrained by ratios $P^4 = 0.5P^2$, $P^6 = 0.1P^2$.
[d] Deviation (σ) and number of assigned levels (n), see Table 18.4, footnote c.

It has been shown that a significant change in the ratios of F^4/F^2 and F^6/F^2 from U^{4+} to Np^{4+} is required to fit the experimental data (Carnall *et al.*, 1991; Liu *et al.*, 1994b). However, in the analysis of the transneptunium ions, the ratios of F^4/F^2 and F^6/F^2 could be held constant. In this context, values of F^2

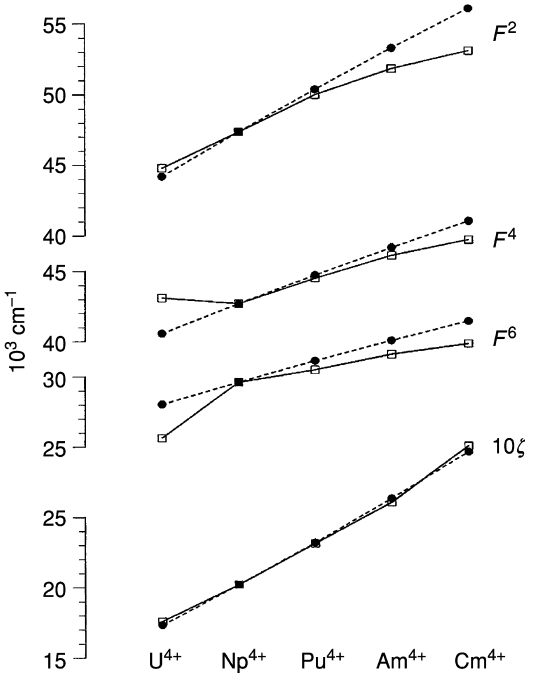

Fig. 18.15 *Systematic trends in free-ion parameters of the effective-operator Hamiltonian for AnF_4 ($An = U$ through Bk). The dots (•) connected by the dashed lines are calculated using Hartree–Fork methods, and the squares (□) connected by solid lines are from fitting experimental data. All values are normalized to those for NpF_4.* (*Reprinted with permission from Liu* et al., 1994a,b. *Copyright* 1994, *American Institute of Physics.*)

for all the ions studied exhibited a functional (but not linear) increase with atomic number. It is important to note that the values of F^2 for all transneptunium members of the AnF_4 series would be poorly estimated based solely on linear projections from U^{4+} or Np^{4+}. Similar to the An^{3+} series, a regular behavior appears to be characteristic of the transneptunium actinide tetrafluorides. The computed values of ζ_{5f} from fitting the experimental data are generally quite consistent with *ab initio* values normalized to agree with the empirical value for NpF_4. In comparison to the An^{3+} series, the slope found for the variation of F^k for An^{4+} as a function of atomic number is reduced. This is particularly evident for F^2 in Fig. 18.15 and provides the rationale for increasingly similar energies found in the lower energy free-ion states of iso-f-electron An^{3+} and An^{4+} spectra as a function of increasing atomic number.

The parametric free-ion electrostatic interaction parameters F^k for UF_4 and NpF_4 are a few percent larger than those that have been determined by fitting spectroscopic data for the tetravalent chlorides and bromides listed in Table 18.10, and those for UF_4 are smaller than the gaseous free-ion values for UV

(Van Deurzen *et al.*, 1984), as expected. Indeed all the free-ion parameter values used in the analysis of AnF_4 spectra are fully consistent with those available from other analysis of An^{4+} spectra in a variety of crystal environments (Krupa, 1987).

For tetravalent actinide ions, it is useful to emphasize that the crystal field is no longer a small interaction relative to that of the free ion, but is capable of radically transforming the energy level scheme without any change in magnitude in the free-ion interaction parameters. This is readily evident in comparing the parameters and energy level schemes for UCl_4 and Cs_2UCl_6. One of the consequences of this change in the hierarchy of interactions that comprise the theoretical model is that there is a decreased sensitivity in energy level structure calculations to the values of the F^k integrals in the analysis of An^{4+} compared to An^{3+} and Ln^{3+} spectra. This is a direct result of the stronger crystal-field and spin–orbit interactions. Recognition of this fact is important because it explains the relatively uncertain F^k values obtained from fitting experimental data. In most cases, very few free-ion states are actually included in the calculation. Indeed, those states that are included tend to be the lowest-energy states in the configuration and to exhibit the smallest J-mixing that would aid in defining the parameters.

Most of the experimental data from absorption spectra include contributions from An^{4+} ions on two crystallographic sites. One of the basic aspects of modeling the AnF_4 crystal field spectra is the reliance, not only on the results of a model calculation of the crystal field parameters in the actual C_2 symmetry, but also the assumption that for purposes of interpreting the observed energy level structure, it is possible to use an approximate C_{2v} symmetry. It was shown that the predictions that were made as a result of this approximation could be directly related to the observed structure and were consistent with the few available measurements that had been obtained independently. In fact, as shown in Table 18.11, very little change in crystal field parameter values over the series was required. This again confirms the arguments in Section 18.4.3 on using the descent-of-symmetry method to simplify the analysis of crystal field spectra of lanthanide and actinide ions in crystals of low symmetry.

In the history of f-element spectroscopy, theoretical interpretations of the crystal-field splitting of the $^8S_{7/2}$ ground state in a half-filled shell of the f^7 configuration have been contradictory. The lanthanides in such a configuration are Eu^{2+}, Gd^{3+}, and Tb^{4+}; and the actinide ions include Am^{2+}, Cm^{3+}, and Bk^{4+}. Early arguments were focused on the Gd^{3+} ion because the ground state crystal-field splitting observed in EPR experiments was less than 0.5 cm^{-1} (Hubert *et al.*, 1985) and could not be interpreted by the crystal field theory. A series of mechanisms were considered but failed to provide a consistent interpretation (Wybourne, 1966; Newman, 1970, 1975). However, the $^8S_{7/2}$ ground-state splittings in the actinide ions is much larger than that of the Gd^{3+}. For Am^{2+} and Cm^{3+}, the observed splitting varies from 2 to 20 cm^{-1}

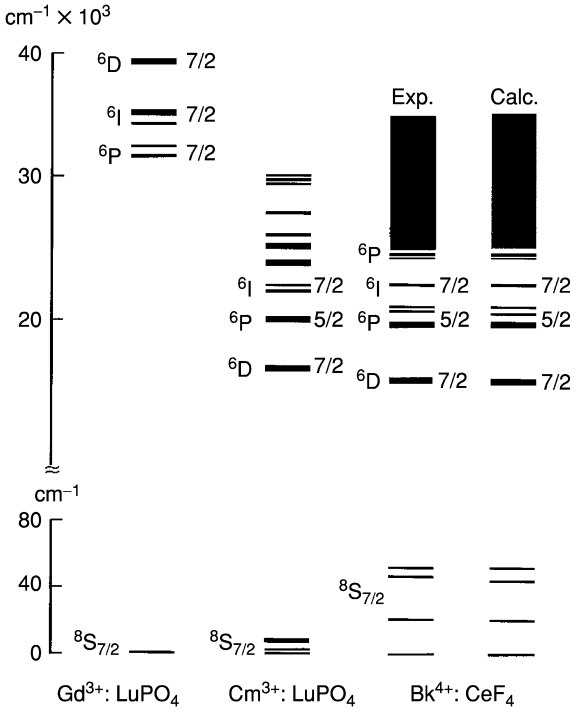

Fig. 18.16 *Partial energy level diagrams of Gd^{3+}, Cm^{3+}, and Bk^{4+} based on computed and experimental crystal field energies.* (*Reprinted with permission from Brito and Liu,* 2000. *Copyright* 2000, *American Institute of Physics.*)

(Edelstein and Easley, 1968; Liu *et al.*, 1993; Murdoch *et al.*, 1996; Edelstein, 2002), while for Bk^{4+} it is on the order of 60 cm^{-1} (Liu *et al.*, 1994b; Brito and Liu, 2000).

As a summary of previous work on the $5f^7$ ion, a comparison of the crystal-field splittings of Gd^{3+}, Cm^{3+}, and Bk^{4+} ions including the ground-state splitting is shown in Fig. 18.16. For the $5f^7$ systems, no additional mechanisms other than the crystal-field interaction are needed to provide a satisfactory interpretation to the observed splitting in the $^8S_{7/2}$ ground state of actinide ions (Liu *et al.*, 1993; Brito and Liu, 2000). As indicated in Section 18.4.2, the observed crystal-field splittings must be attributed to the contributions of the mixture of other *LS* terms into the ground state free-ion wave function (see equation (18.39)) and nonzero off-diagonal matrix elements between different *J*-multiplets. Because of the large energy gaps from the ground state to the excited multiplets of Gd^{3+}, the excited state *LS* components in the ground state is small, and *J*-mixing is also negligible in this case. However, for the actinide ions in $5f^N$ configurations, as discussed in Section 18.3, the ground-state wave

functions contains considerable *LS* components of the excited states, and thus lead to much larger splittings that should not occur for a pure *S*-state.

18.7 SPECTRA AND ELECTRONIC STRUCTURE OF DIVALENT ACTINIDE IONS AND ACTINIDES IN VALENCE STATES HIGHER THAN 4+

Although spectra of actinide compounds and solutions exhibiting other than the 3+ and 4+ valence states are well known, systematic analyses of the electronic structure in other valence states are very tentative now. Extensive analysis is limited to a few isolated cases. However, tabulations of electrostatic (Varga *et al.*, 1970) and spin–orbit integrals (Lewis *et al.*, 1970), computed using *ab initio* methods, have been published, and the relative energies of electronic configurations occurring within the usual spectral range of interest to chemists have been estimated from free-ion spectra (Brewer, 1971a,b).

The electrostatic and spin–orbit interactions in any given valence state are expected to vary systematically across the series. However, in the trivalent and tetravalent series it was necessary to introduce effective operators to explicitly screen the effects of configuration interaction to obtain good correlation with the experiment. In the absence of these correction terms, the values of the Slater integrals obtained in fitting the data exhibited a much more erratic behavior when plotted as a function of Z. In the discussion of 2+ and high valent actinides, it should be noted that the role of second-order correction terms has not been studied in detail for these oxidation states. What is clear is that the importance of both spin–orbit coupling and crystal-field interactions relative to the electrostatic interaction increases with increasing valence.

One of the reasons for introducing the theoretical interpretation of trivalent and tetravalent spectra in some detail was to provide the basis for discussing models appropriate to other valence states. Although detailed models have yet to be constructed, and may lead to revision of some of the values given here, it is advantageous to introduce a generalizing element into the discussion and relate available spectra to this central theme rather than approach each different actinide ion as a unique entity.

It has been realized for An^{2+} that the interactions appear to be of the same relative magnitude as for An^{3+}; however for An^{4+} and An^{5+} the crystal-field interaction becomes, relatively, much more important, and extraction of well-defined parameters for the free-ion and crystal-field interactions becomes more difficult. In An^{3+} spectra, the correction terms H_{corr} act mainly on the electrostatic part of the free-ion Hamiltonian, although some provision for second-order magnetic effects are included. In this discussion it is assumed that it is not necessary to modify the magnitudes of the terms associated with H_{corr} in treating other valence states. Since the crystal-field splitting is computed using a single-particle model, corrections to E_{cf} may be required as the relative magnitude of the crystal field increases.

In early attempts to develop a systematic interpretation of trivalent actinide and lanthanide spectra, initial sets of F^k and ζ_{nf} for some members of the series had to be estimated. This was done by linear extrapolation based on the fitted parameters that were available from the analyses of other individual spectra. As more extensive data and improved modeling yielded better determined and more consistent F^k and ζ_{nf} values for the 3+ actinides (and lanthanides), it became apparent that the variation in the parameters was nonlinear, as indicated for F^2 (5f,5f) in Fig. 18.4. This nonlinearity could also be observed in the values of parameters obtained from the *ab initio* calculations. The difference between the *ab initio* and fitted values of parameters (ΔP) appears to exhibit a much more linear variation with Z than do the parameter values. Consequently, ΔP has been adopted as the basis for a useful predictive model (Carnall *et al.*, 1966; Crosswhite, 1977; Crosswhite and Crosswhite, 1984).

For the trivalent actinides the values of ΔP are not constant over the series, but use of a single average value over a group of four or five elements is not an unreasonable approximation. Thus, in developing a predictive model for the F^k and ζ_{nf} parameters, an attempt is made to establish average values of ΔP for a particular valence state and type of crystal-field interaction. The energy level structure computation based on the predicted parameters can be compared to that observed, and then appropriate modifications sought by a fitting procedure where necessary.

18.7.1 Divalent actinide-ion spectra

Efforts to prepare divalent actinide compounds and analyze their spectra have been less successful than was the case for lanthanides, where the divalent ion for each member of the series could be stabilized in CaF_2 (McClure and Kiss, 1963). In both Am^{2+}:CaF_2 and Es^{2+}:CaF_2 (Edelstein *et al.*, 1966, 1967, 1970; Baybarz *et al.*, 1972), intense absorption bands were observed. These bands could be attributed to either f→d or charge-transfer transitions. The presence of divalent actinide ions in these cases was established by measurements of the electron paramagnetic resonance spectra, not on the basis of the observed optical spectra. In contrast to the more intense absorption bands reported for Es^{2+}:CaF_2, weak absorption bands consistent with the intensities expected for f→f transitions were identified in the 10 000–20 000 cm^{-1} region in both $EsCl_2$ and Es^{2+}:$LaCl_3$ (Fellows *et al.*, 1978). The relatively narrow band structure exhibited by the Es^{2+} halides was also found to be characteristic of the Cf^{2+} halides (Peterson *et al.*, 1977; Wild *et al.*, 1978).

Although it was not possible to stabilize Cm^{2+} in CaF_2 under the same conditions that yielded for Am^{2+}:CaF_2, evidence for the formation of both Am^{2+} and Cm^{2+} has been obtained in solution in pulse radiolysis studies; however, as in the spectrum of Am^{2+}:CaF_2, the absorption bands were broad and intense. The nature of the absorption process is therefore not clear. A charge-transfer process cannot be excluded (Sullivan *et al.*, 1976).

Because the available spectroscopic results for divalent actinides are fragmentary, a consistent interpretation that accounts for all observations and predicts the energies of other bands that might be accessible to observation will be adopted. The basic aspects of this tentative model can be deduced in part from available data for divalent lanthanide spectra.

The free-ion spectra of Ce III and Pr IV are known. Initial estimates of F^k and ζ_{4f} values appropriate to Ln^{2+} in condensed phases can be made by assuming that the change observed in these parameters for iso-f-electron couples such as Ce III/Pr IV (both $4f^2$) will also be characteristic of the couple Ce^{2+}/Pr^{3+} in condensed phases. This suggests a reduction of 20–30% in comparing values of F^k and ζ_{4f} for divalent compared to isoelectronic trivalent-ion cases. Comparing the results for Eu^{2+}:CaF_2 (Downer *et al.*, 1983) with those for Gd^{3+}:LaF_3 (Carnall *et al.*, 1971), the parameters for Eu^{2+} ($4f^7$) are 82–86% of those for Gd^{3+} ($4f^7$). The little information available on divalent lanthanide ion crystal-field splitting (Dieke, 1968) suggests that the crystal-field interaction is even smaller than for the trivalent case. This also was suggested in an analysis of Eu^{2+} in strontium fluoride (Downer *et al.*, 1983).

Based on the small crystal-field splitting indicated for the divalent lanthanides, it is reasonable to assume as a first-order approximation that the corresponding actinide crystal-field splitting will be small. Although fragmentary, available spectroscopic data for An^{2+} appear to be consistent with this estimate. The initial model can consequently be limited to free-ion considerations. The initial F^k and ζ_{5f} parameters for An^{2+} may be estimated to be 85–90% of those for the iso-f-electronic An^{3+}:$LaCl_3$ ion. The effects of configuration interaction for An^{2+} can be taken to approximate those for An^{3+}. The resulting model energy level schemes for An^{2+} are plotted in Fig. 18.17 where the overlap of the $5f^{N-1}6d$ and $5f^N$ configurations is also indicated (Brewer, 1971a,b).

Examining the range of energies in which f→f transitions might be observed, it is seen from the figure that the largest 'optical windows' are expected in Am^{2+}, Cf^{2+}, and Es^{2+}. In Np^{2+}, Pu^{2+}, Cm^{2+}, and Bk^{2+}, it is probable that f→f transitions will only be observed in the infrared range. This of course assumes that the $5f^N$ is consistently the ground state configuration. Transitions resulting from the promotion of f→d would be expected to result in intense (allowed) absorption bands such as those observed in Ln^{2+} spectra (McClure and Kiss, 1963). The much weaker f→f transitions occurring in the same energy range as the allowed transitions would be masked, so the optical window corresponding to the pure f→f energy spectrum will be somewhat smaller than that for the gaseous free-ion f→d transition energies indicated in Fig. 18.17 (Brewer, 1971a,b). The computed level structure for Cf^{2+} and Es^{2+} agree with the experimental results, but indicate the existence of bands not yet reported.

Systematic energy level calculations are of considerable importance in predicting the energies at which luminescence might be observed. In general, the longest-lived luminescence will originate from the state with the largest energy gap between it and the next lower-energy state. Based on the computed large

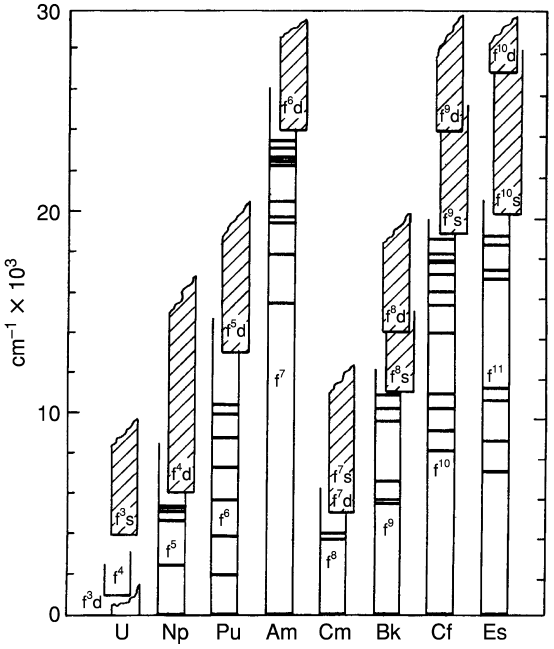

Fig. 18.17 *Estimated ranges of energies in which 5f–5f transitions in An^{2+} may be experimentally observed.*

energy gap between the ground ($^8S_{7/2}$) and first excited ($^6P_{7/2}$) states in Am^{2+} ($5f^7$), isolated Am^{2+} sites would be expected to exhibit luminescence near 14 000 cm^{-1} (Edelstein *et al.*, 1966; Edelstein and Easley, 1968; Edelstein, 1991).

18.7.2 Spectra of actinide ions in the pentavalent and hexavalent states

The actinide ions with well-defined valence states greater than VI are confined to the light half of the 5f series. A large number of stable compounds are known, and spectra have been recorded in solution, in solids, and in gas phase. However, there have been relatively few attempts to develop detailed energy level analyses. Although Hartree–Fock type calculations of F^k and ζ_{nf} can be carried out for any arbitrary state of ionization of an actinide ion, the relative importance of the ligand (or crystal) field must also be established to develop a correlation for experimentally observed transition energies. *Ab initio* models of the ligand field are characteristically very crude. The spectra of penta- and higher-valent actinides are strong crystal field cases and the development of correction terms for first-order crystal field model may well be essential to any detailed analysis.

Two types of ionic structure are normally encountered in the higher-valent species: the actinyl ions AnO_2^+ and AnO_2^{2+} (Denning, 1992; Matsika and Pitzer,

2001; Denning *et al.*, 2002), and halides such as UCl_5, $CsUF_6$, and PuF_6. Mixed oxohalide complexes are also known. In the actinyl ions (An = U, Np, Pu, Am) the axial field imposed by the two nearest-neighbor (−y1) oxygen atoms plays a dominant role in determining the observed energy level structure (Eisenstein and Pryce, 1966; Bell, 1969). The analysis of spectra of higher-valent actinide halides is also based on a strong ligand-field interaction, but the symmetry is frequently found to be octahedral or distorted octahedral (Goodman and Fred, 1959; Eisenstein and Pryce, 1960; Kugel *et al.*, 1976; Eichberger and Lux, 1980). Typical iso-f-electronic penta- and higher-valent actinide species are shown in Table 18.12, where X is a halide ion.

Aqueous solution spectra characteristic of the NpO_2^+ and PuO_2^{2+} ions, both having the $5f^2$ electronic structure, are shown in Fig. 18.18. Some qualitative similarities in band patterns for these iso-f-electronic ions appear to exist, but detailed analysis of the observed structure in terms of a predictive model is tentative. Charge-transfer bands for NpO_2^{2+} (20 800 cm^{-1}), PuO_2^{2+} (19 000 cm^{-1}), and AmO_2^{2+} (∼18 000 cm^{-1}) have been identified (Jørgensen, 1970). Spectra of the actinyl ions and the molar absorptivities of the more intense bands in aqueous solution have been tabulated (Carnall, 1973, 1982). The charge-transfer transitions in crystalline $CsNpO_2Cl_4$ and $CsNpO_2(NO_3)$ as reported by Denning *et al.* (1982) are apparently much lower than that predicted for NpO_2^{2+} (20 800 cm^{-1}). In their analysis, Denning *et al.* (1982) assigned five charge-transfer bands of $CsNpO_2Cl_4$ and $CsNpO_2(NO_3)$ between 13 000 and 20 000 cm^{-1}.

Attempts to interpret the spectra of the penta- and hexahalides of the actinides have used the effective-operator Hamiltonian discussed in Sections 18.3 and 18.4. However, the results are limited primarily to U^{5+} and Np^{6+}, both having the $5f^1$ configuration and Np^{5+} and Pu^{6+} with the $5f^2$ configuration. The magnitude of the spin–orbit interaction is known for U v. Its free-ion spectrum has been interpreted in terms of a coupling constant, $\zeta_{5f} = 2173.9$ cm^{-1}, based on a $^2F_{5/2} \rightarrow {}^2F_{7/2}$ energy difference of 7608.6 cm^{-1} (Kaufman and Radziemski, 1976). The optical properties of Np and Pu ions and compounds were analyzed by Edelstein (1992). The spectra of several complex pentavalent uranium halide

Table 18.12 *Some iso-f-electron penta- and higher-valent actinide species.*[a]

Number of 5f electrons =	0	1	2	3	4
	UO_2^{2+} Np VIII UF_6 UCl_6	UO_2^{+} NpO_2^{2+} Pu VIII NpF_6 UX_6^{-} UF_5	PuO_2^{2+} NpO_2^{+} PuF_6 NpX_6^{-}	AmO_2^{2+} PuO_2^{+} PuX_6^{-}	AmO_2^{+}

[a] X, halide ion.

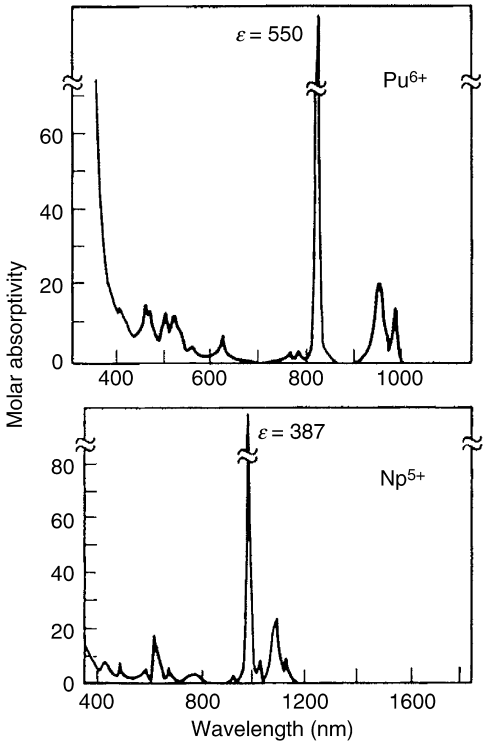

Fig. 18.18 *Aqueous solution absorption spectra of* PuO_2^{2+} (Pu^{6+}) *and* NpO_2^{+} (Np^{5+}).

compounds appear in the literature and, based on representative crystallographic determinations, the site symmetry usually is close to octahedral. The combined effect of the spin–orbit and octahedral ligand-field interactions is to split the parent ^2F state into five components whose irreducible double group labels are indicated in Fig. 18.19.

The energy level structures of several actinide 4+, 5+, and 6+ compounds with the $5f^1$ ion at a site of octahedral (or approximated as octahedral) symmetry are compared in Table 18.13. As indicated in Table 18.13, there has been considerable variation in the ligand field parameters deduced by different investigators from absorption spectra in which the energies of observed features are surprisingly consistent. The case of UCl_5, which has a dimeric structure that gives rise to approximately octahedral U^{5+} sites, is particularly interesting because the spectra of solutions (UCl_5 in $SOCl_2$) (Karraker, 1964), of a single crystal (Leung and Poon, 1977), and of the vapor phase, $(UCl_5)_2$ or $UCl_5 \cdot AlCl_3$ (Gruen and McBeth, 1969), all give absorption features that are similar to both the relative intensities of the transitions and their energies. The importance of the nearest-neighbor coordination sphere in determining the spectra, essential

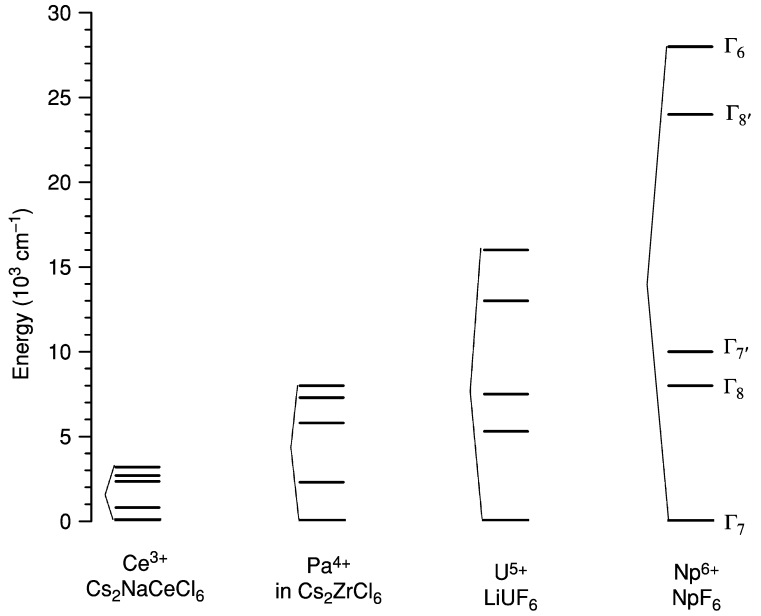

Fig. 18.19 *Comparison of crystal-field splittings of the $5f^1$ states of actinide ions in various hosts.*

to the exclusion of the effects of long-range order, is consistent with the behavior expected for strong octahedral bonding. However, more evidence is needed to justify the assignments and to establish uniquely the limits over which the ligand field parameters may vary.

The spectra of $CsUF_6$ (Reisfeld and Crosby, 1965) and $CsNpF_6$ (Hecht *et al.*, 1979) have been reported and analyzed, and that of $CsPuF_6$ has been measured (Morss *et al.*, 1983). However, the treatment of $CsUF_6$, which has been considered to be a model for other cases of distorted octahedral symmetry, has been questioned both experimentally (Ryan, 1971) and on theoretical grounds. Both Leung (1977) and Soulie (1978) have pointed out that there is actually a very significant distortion of the O_h symmetry originally assumed for $CsUF_6$ (Reisfeld and Crosby, 1965), with D_{3d} symmetry providing the basis for a much improved interpretation. If electrostatic interaction parameters of the same order of magnitude as those suggested by Poon and Newman (1982) are utilized for $CsNpF_6$, together with the D_{3d} ligand field parameters for $CsUF_6$, and further extrapolation of these results is carried out to provide values for the $CsPuF_6$ case, the resulting energy level structure is that indicated in Fig. 18.20. The general aspects of this predicted structure appear to be consistent with available experimental data. Aside from the structure of the ground state, a relatively isolated $^3F_2$ state in $CsNpF_6$ should be observed. However, with the

Table 18.13 *Energy parameters for* $An^{4+,\ 5+,\ 6+}$ *compounds* (in cm^{-1}).[a]

	$(5f^1)$ Pa^{4+}: Cs_2ZrCl_6[b]	$(5f^1)$ UCl_5[c]	$(5f^1)$ $CsUF_6$[d]	$(5f^1)$ NpF_6[e]	$(5f^2)$ $CsNpF_6$[f]	$(5f^2)$ PuF_6[g]	$(5f^3)$ $CsPuF_6$[f]
F^2					48 920	36 026 (2 472)	51 760
F^4					42 300	72 458 (3 054)	44 200
F^6					27 700	40 535 (3 877)	29 120
ζ	1539.6	1559 (115)	1910.2 (13)	2448.4 (33)	2200	2551 (46)	2510
α					30 000	[35 500]	30 000
β					−660	[−664]	−660
γ					700	[744]	700
B_0^2			534.2 (139)		534.2		543.2
B_0^4	6945.3	13 479 (1 125)	−14 866 (66)	44 553 (211)	−14 866	48 377(803)	−14 866
B_0^6	–162.7	–158.6 (745)	3305 (78)	7992 (105)	3305	8690(180)	3305
σ[h]		370	33	73		54.2	

[a] Values in parentheses are errors in the indicated parameters. Values in brackets were not allowed to vary in the parameter fitting.
[b] Piehler *et al.* (1991).
[c] Leung and Poon (1977).
[d] Ryan (1971).
[e] Goodman and Fred (1959).
[f] Estimated parameter values shown. In addition to those parameters tabulated, the following were included: $P^2 = 500$, $P^4 = P^6 = 0$ (for both $CsNpF_6$ and $CsPuF_6$); $T^2 = 200$, $T^3 = 50$, $T^4 = 100$, $T^6 = -300$, $T^7 = 400$, $T^8 = 350$ (for $CsPuF_6$ only).
[g] Edelstein (1992). $M^0 = 0.987$, $M^2 = 0.55$, $M^4 = 0.384$, $P^2 = 573$, $P^4 = 524$, $P^6 = 1173$.
[h] Deviation as defined in footnote c of Table 18.4.

exception of this $^3F_2$ state, neither the spectrum of $CsNpF_6$ nor that of $CsPuF_6$ is expected to exhibit any extensive, easily recognizable band structure. A relatively high density of excited states is predicted and detailed analysis will be difficult.

The actinide hexafluorides, UF_6, NpF_6, and PuF_6, form a unique group of volatile actinide molecular species. They are not regarded as strongly bonded since the metal–fluorine distances tend to be rather large (~1.98 Å) (Claassen, 1959). The combination of well-characterized spectroscopic and magnetic (Goodman and Fred, 1959; Hutchison and Weinstock, 1960; Edelstein, 1992) results for NpF_6 and PuF_6 has served to establish a reasonable basis for the energy level analysis in octahedral symmetry summarized in Table 18.13. A consistent set of F^k and ζ_{5f} parameters can be combined with the crystal field for NpF_6 to yield an estimate of the parameters set for PuF_6 and AmF_6. However, in terms of the free-ion interaction parameters, no consistent results have been

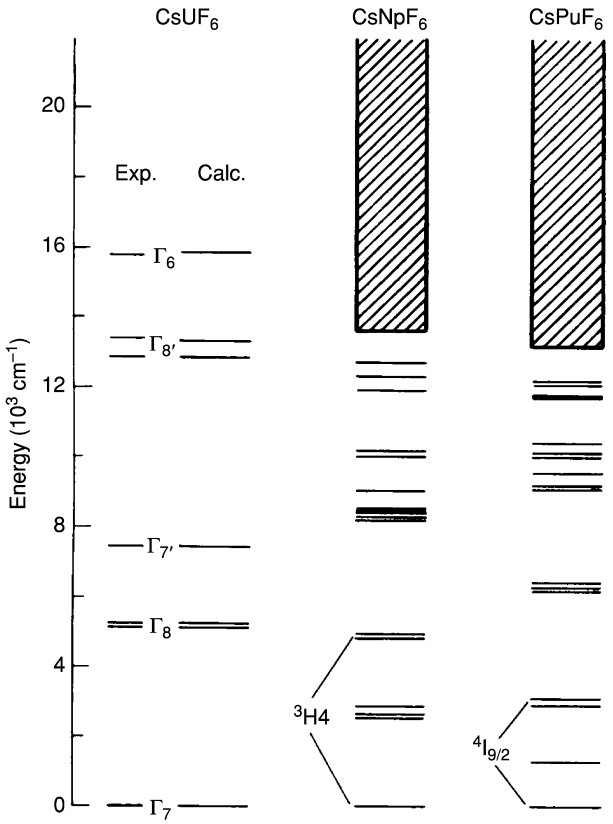

Fig. 18.20 *Computed energy levels schemes for $CsUF_6$, $CsNpF_6$, and $CsPuF_6$. The cross-hatched areas indicate that a relative dense energy structure is predicted.*

achieved when the parameters are varied in fitting of the observed energy levels of PuF_6 (Edelstein, 1992). As listed in Table 18.13, the value of F^2 for PuF_6 is reduced by greater than 50% from its Hartree–Fock value and F^4 is greater than the calculated Hartree–Fock value (Wadt, 1987). In comparison with Hartree–Fock values and the parameters for NpF_6, the empirical values for F^6 and ζ seem to be of reasonable magnitude. The energies of some of the lower-lying states in NpF_6 and PuF_6 are shown in Fig. 18.21. The two upper levels of NpF_6 at 23 500 and 28 000 cm^{-1} were not well resolved in absorption spectra (Steindler and Gerding, 1966) and the uncertainty in assigning these two levels could result in uncertainties in the spin–orbit and crystal field parameters. The indicated structure is consistent with the principal features in the absorption spectrum of PuF_6 (Kugel *et al.*, 1976) as shown in Fig. 18.22. Detection of luminescence in the selective excitation of NpF_6 and PuF_6 and at energies in

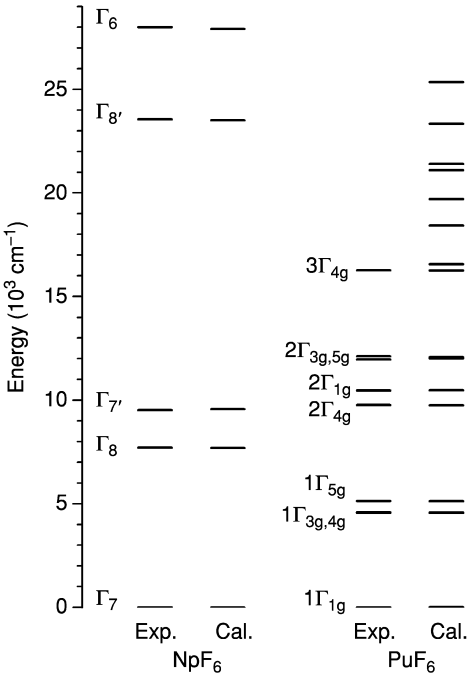

Fig. 18.21 *Comparison of observed and computed energy level schemes for NpF_6 (data from Goodman and Fred,* 1959) *and PuF_6 (data from Edelstein,* 1992). *Analysis of near-infrared spectra of matrix-isolated NpF_6 was also reported* (*Mulford* et al., 1991)

agreement with the energy gaps between the predicted ground and first excited states in both spectra has been reported (Beitz *et al.*, 1982).

18.7.3 Charge-transfer transitions and structure of actinyl ions

In addition to electronic transitions from $5f^N$ to excited configurations, an electron may be excited from a ligand to a 5f orbital, creating a charge-transfer state, with a configuration consisting of $5f^{N+1}$ plus a ligand 'hole'. The spectra of UO_2^{2+}, UF_6, and Np^{7+} shows typical charge-transfer transitions for the actinide series since, in contrast to the transitions between states within the $5f^N$ configuration which characterize most of the actinide spectra discussed in previous sections; the above species contain no f-electrons in open shells. The energies of these states are highly ligand-dependent and, especially in organic systems, they can be at a lower energy than the $5f^{N-1}6d$ states. For lighter actinide ions in oxygen environments, actinyl ions are formed through charge-transfer bonding (Jørgensen, 1957). The most extensive studies of ion-to-ligand charge transfer have been conducted on uranyl (UO_2^{2+}) ion in various solutions and compounds (Denning *et al.*, 1982, 2002; Denning, 1992). Fig. 18.23 shows

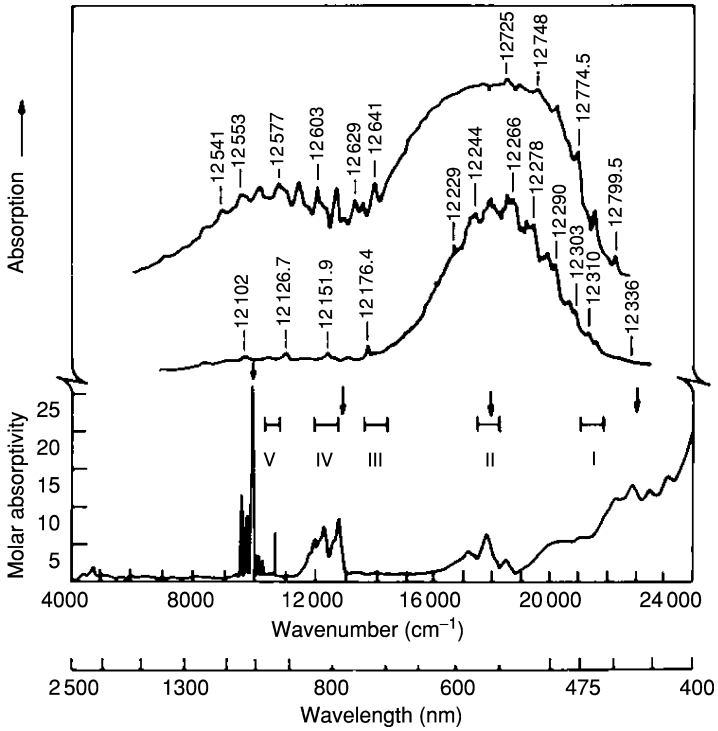

Fig. 18.22 *The absorption spectrum of PuF_6. Arrows indicate regions reported to show vibrational structure. Bars indicate regions examined by intra-cavity laser absorption:* I, 455–470; II, 550–574; III, 697–729; IV, 786–845; V, 918–971 nm. *At the top is a densitometer trace of the high-resolution absorption spectrum of PuF_6 in the* 781–830 nm *region obtained in multipass experiments. Data from Kugel* et al. (1976).

the energy level structure of UO_2^{2+} charge-transfer states in comparison with that of the U^{6+} and O^{2-} ions. The lowest-energy level of the excited charge-transfer states starts at (20 000 cm^{-1} for uranyl ion and at (14 000 cm^{-1} for neptunyl ion (NpO_2^{2+}), which is below the energy levels of several 5f states of the Np^{6+} core (Denning *et al.*, 1982, 2002). In the neptunyl case, energy levels of different origins, namely $5f^N$, $5f^{N-1}6d$, and ion–ligand charge transfer, may overlap in the same energy region, and thus make spectrum analysis difficult. Emission from charge-transfer states of actinide ions in condensed phase is relatively rare except for the case of uranyl (UO_2^{2+}) ions, which often exhibit a strong luminescence in solution. This is because of the large energy gap between its ground and excited charge-transfer states that suppresses quenching due to nonradiative phonon relaxation (Riseberg and Moos, 1968).

The spectra of UO_2^{2+} compounds with a characteristic structure in the visible–ultraviolet range below 400 nm are commonly observed charge-transfer

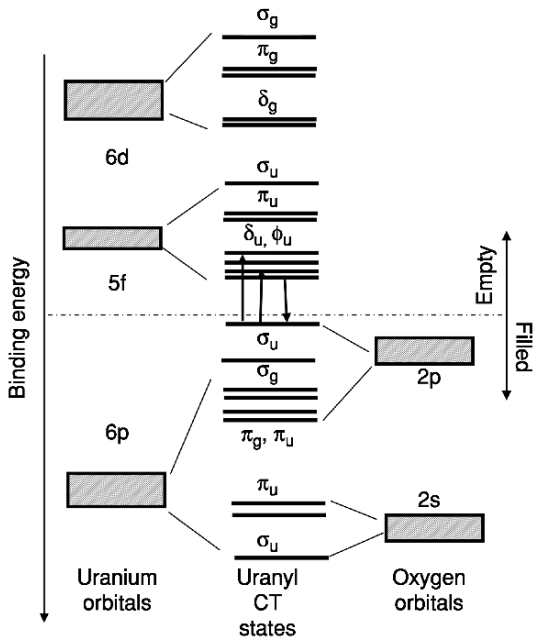

Fig. 18.23 *Illustration of electronic energy level scheme of uranyl ion* UO_2^{2+}.

transitions in the actinide series. Analyses of crystal spectra such as that for $Cs_2UO_2Cl_4$ are now available (Denning *et al.*, 1980, 1982; Denning, 1992). Because of the energy gap between the emitting and ground states as shown in Fig. 18.23 is much larger than the vibration energies, in many cases including uranyl species in solutions, fluorescence emission is often the dominant channel of relaxation from the lowest level of the excited charge-transfer states. Fig. 18.24(a) shows the fluorescence spectrum of $UO_2Cl_4^{2-}$:Cs_2ZrCl_6 single crystal at 20 K (Metcalf *et al.*, 1995). The ZPL is accompanied by a progression of vibronic lines due to the O–U–O stretching and bending modes, which characterize the uranyl structure and are relatively insensitive to the environment of the uranyl ion in the equatorial plane. Usually, the linear dioxo cation O–U–O is coordinated by an additional four to six ligand ions in its equatorial plane. The vibrational frequencies of different modes of the complexed ion can be determined directly from the spectrum. They are typically 820, 900, and 240 cm^{-1} for the symmetric, asymmetric, and bending modes of the UO_2^{2+} ion, respectively. As to the nature of the uranyl bonding, variation of the vibrational frequencies is correlated with the energy levels of the charge-transfer states (Denning, 1992). The spectrum of the uranyl ion in single crystals of $UO_2Cl_4^{2-}$:Cs_2ZrCl_6 exhibits extremely sharp line widths, indicating that the uranyl ions in the crystal have highly identical local structure so that

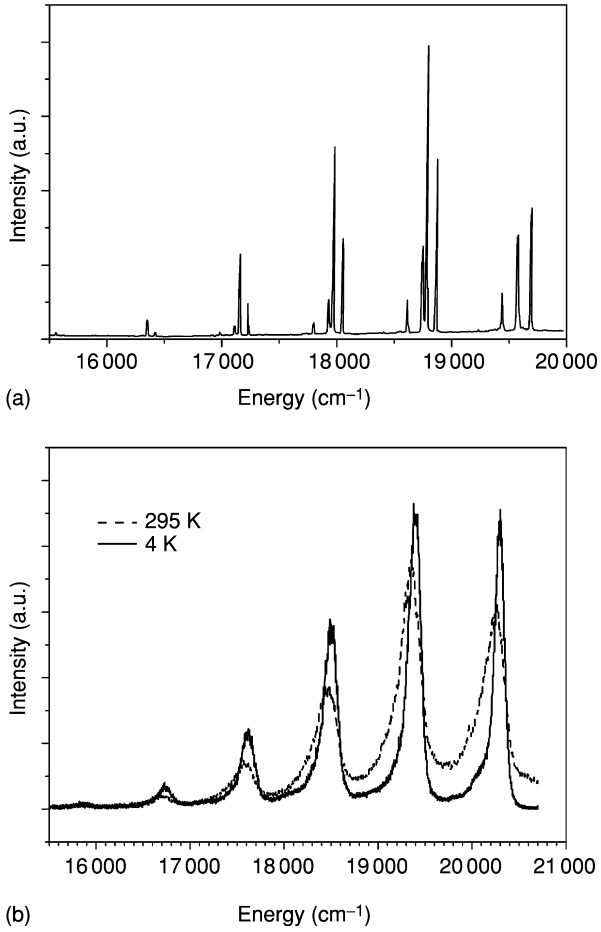

Fig. 18.24 *Spectra of uranyl charge-transfer vibronic transitions:* (*a*) *fluorescence spectrum of* UO_2^{2+} in Cs_2ZrCl_6 *at* 20 K (*data from Metcalf* et al., 1995) *and* (*b*) *fluorescence spectra of* UO_2^{2+} *in* B_2O_3 *glass at* 4 *and* 295 K.

inhomogeneous line broadening induced by structure defects is not significant. If structure variation and impurity phases exist, inhomogeneous line broadening would obscure the features due to different vibrational modes. Fig. 18.24(b) shows the emission spectra of uranyl in B_2O_3 glass matrix at 4 and 295 K. In comparison with Fig. 18.24(a), the lines become much broader, whereas the changes in the overall spectral profile and line locations are insignificant. Given the nature of charge-transfer states, it is apparent that the energy levels of charge-transfer states are more sensitive to local structure disordering than that of the 5f−5f transitions. Therefore, in structurally disordered environments such as glasses and solutions, inhomogeneous line broadening obscures

observation of separated lines of the asymmetric and bending modes. Only the progression of the symmetric mode, up to five quanta of phonon sidebands, is often observed. Based on the theory of ion–phonon interaction (Huang and Rhys, 1950), the spectra of charge-transfer vibronic transitions of uranyl species may be theoretically simulated using a model proposed by Liu *et al*. (2002). The Huang–Rhys parameter of the uranyl vibronic coupling is typically in the range of 1.0–1.5.

For the closely related case of NpO_2^{2+} ion doped into single-crystal $Cs_2UO_2Cl_4$, detailed spectroscopic studies have identified a single electronic transition belonging to the $5f^1$ configuration, but the other structure observed is similar in origin to that reported for UO_2^{2+}, i.e. transitions to molecular-orbital states (Stafsudd *et al*., 1969; Jørgensen, 1982; DeKock *et al*., 1985). Extensive analyses of the absorption and fluorescence spectra of UF_6 have been published, and are covered in a review (Carnall, 1982). In the visible to near-ultraviolet range, the character of the spectrum is similar to that of UO_2^{2+}.

18.8 RADIATIVE AND NONRADIATIVE ELECTRONIC TRANSITIONS

18.8.1 Intensity of 5f–5f transitions

A systematic understanding of the energy level structure for An^{3+} serves as a foundation upon which to base the interpretation of other physical measurements. Considerable success has now been achieved in developing a parameterized model of f → f transition intensities.

The intensity of an absorption band can be defined in terms of the area under the band envelope normalized for the concentration of the absorbing ion and the path length of light in the absorbing medium. A proportional quantity, the oscillator strength P, has been tabulated for trivalent actinide-ion absorption bands in aqueous solution. The experimentally determined oscillator strengths of transitions can in turn be related to the mechanisms by which light is absorbed (Condon and Shortley, 1963; Reid, 2000):

$$P = \frac{8\pi^2 mc\sigma}{3he^2(2J+1)}\left(\chi\overline{F}^2 + n\overline{M}^2\right) \tag{18.51}$$

where $\overline{F}$and $\overline{M}$ are, respectively, the matrix elements of the electric dipole and magnetic dipole operators joining the initial state J to a final state J', $\chi = (n^2+2)^2/9n$ and n is the refractive index of the medium, σ is the energy of the transition (cm^{-1}), and the other symbols have their usual meanings.

Only a few transitions observed for the 3+ actinide ions have any significant magnetic dipole character; however, the matrix elements of $\bar{M}^2$ can be evaluated directly from the knowledge of the eigenvectors of the initial (ΨJ) and final ($\Psi' J'$) states. Following the results of Condon and Shortley (1963), the magnetic dipole operator is given as

$$M = -\frac{e}{2mc}\sum_i (l_i + 2s_i). \tag{18.52}$$

The matrix elements of the operator in equation (18.51) can then be written as

$$\overline{M}^2 = \frac{e^2}{4m^2c^2}\langle \Psi J \| L + 2S \| \Psi' J' \rangle^2. \tag{18.53}$$

The nonzero matrix elements, which should be calculated in the intermediate coupling scheme, will be those diagonal in the quantum numbers τ, S, and L. The selection rule on J is $\Delta J = 0, \pm 1$.

The Judd–Ofelt theory (Judd, 1962; Ofelt, 1962) has successfully addressed the problem of computing the matrix elements of $\overline{F}^2$, and can be written in the form:

$$\overline{F}^2 = e^2 \sum_{k=2,4,6} \Omega_k \left\langle \Psi J \left\| \mathbf{U}^{(k)} \right\| \Psi' J' \right\rangle^2 \tag{18.54}$$

where Ω_k are three parameters which in practice are evaluated from measured band intensities. These parameters involve the radial parts of the f^N wave functions, the wave functions of perturbing configurations such as $5f^{N-1}6d$, and the interaction between the central ion and the immediate environment. Since the Ω_k parameters contain many contributions, model calculations are not possible. Nevertheless, the relative simplicity of the intensity calculations using equation (18.51) have resulted in extremely useful analyses of experimental data. The matrix elements in equation (18.54) may be calculated using the SPECTRA program. For the trivalent actinide ions, the matrix elements of $\mathbf{U}^{(k)}$ have been tabulated (Carnall, 1989) for states of $5f^3$ to $5f^{12}$ configurations with energies up to 40 000 cm^{-1}. It should be noted that the intensity theory presented here is applied only to the free-ion multiplets, and the empirical values for the intensities of these multiplets are obtained by integrating over the band intensities in solution.

Judd (1962) showed that the theory could successfully reproduce the observed intensities of bands of Nd^{3+} and Er^{3+} in aqueous solution ($RE(H_2O)_x$ where x is 8 or 9) throughout the optical range, and that the intensity parameters Ω_k computed from first principles were consistent with those derived from fitting experimental data. Later systematic treatments of the intensities observed in the spectra of all aquated Ln^{3+} ions have confirmed and extended the original correlation (Carnall *et al.*, 1968; Carnall, 1979a) and, more recently, it was found that a similar systematic treatment of band intensities for aquated An^{3+}-ion spectra could be successfully carried out with only Ω_4 and Ω_6 treated as variables (Carnall *et al.*, 1984). The emphasis on aquated f^N-ion spectra comes from the ability to identify many relatively isolated bands with single or very limited numbers of *SLJ* states, the corresponding unambiguous quantitative nature of the oscillator-strength calculation, and the wide range of data

available, i.e. most members of the 4f and 5f series can be readily obtained as trivalent aquated ions in dilute acid solution. Intensity correlations for Ln^{3+} ion in many different host crystals, as well as in vapor complexes, have been developed (Beitz, 1994b; Reid, 2000). For the actinides, systematic and quantitative examination of transition intensities is presently restricted to aquated An^{3+}.

Examination of Fig. 18.8 shows that, particularly for U^{3+}, Np^{3+}, and Pu^{3+}, the density of states is high and few of the observed bands can be uniquely identified. Both the relative intensities of observed transitions and the density of states decrease in magnitude with increasing atomic number. Starting with aquated Cm^{3+}, the heavy-actinide aquated-ion spectra are all amenable to intensity analyses with excellent correlation found between observed oscillator strengths and intensities computed using the Judd parameterization (Carnall *et al.*, 1983). The oscillator strengths of aquated An^{3+} bands tend to be a factor of 10−100 greater than those observed for the lanthanides, Starting with aquated Bk^{3+}, there is an apparent transition to a heavy-lanthanide-like character in the spectra, with no bands being disproportionately intense. Analysis reveals that the trends in the intensity parameter values over the series can be correlated with the extent to which higher-lying opposite-parity configurations like $f^{N-1}d$ are mixed into the f^N configuration. There is much less mixing of $f^{N-1}d$ states into $5f^8(Bk^{3+})$ than in $5f^3(U^{3+})$ which it is consistent with the energy level structures of the $f^{N-1}d$ and f^N configurations of the two ions. An example of the type of correlation obtained between experiment and theory for aquated An^{3+} was previously discussed for aquated Cm^{3+} (Carnall and Rajnak, 1975). Figs. 18.25 and 18.26 compare the observed absorption spectra of U^{3+} and Cf^{3+} in dilute perchloric acid, respectively. These spectra are from the work of Carnall (1992) and have been published, along with those of other An^{3+} ions, with split abscissa scales to highlight weakly absorbing transitions (Beitz, 1994b). Also shown in Figs. 18.25 and 18.26 as vertical bars are the centers of gravity expected for the actinide ion's 5f electron states based on the free-ion parameters established for trivalent actinide ions in single crystals of lanthanum trichloride. It is evident in Fig. 18.26 that the free-ion states provide an excellent basis for interpretation and assignment of the parity-forbidden f–f absorption bands of Cf^{3+}. The very strong absorption bands that occur in the blue and ultraviolet spectral ranges of the U^{3+} spectrum can be assigned as arising from parity-allowed transitions. In addition, it is evident that the f–f absorption bands of U^{3+} at longer wavelengths are significantly more intense than those of the comparatively heavy actinide ion Cf^{3+}. Qualitatively, the high intensity of U^{3+} f–f transitions can be attributed to interaction with the low-lying opposite-parity states of U^{3+}. Put another way, the f-electron states of light actinide ions contain a larger contribution from opposite-parity states than is the case for heavier actinide ions.

Band intensities of spectra such as those shown in Figs. 18.25 and 18.26 have been analyzed systematically (Carnall and Crosswhite, 1985; Carnall *et al.*, 1985;

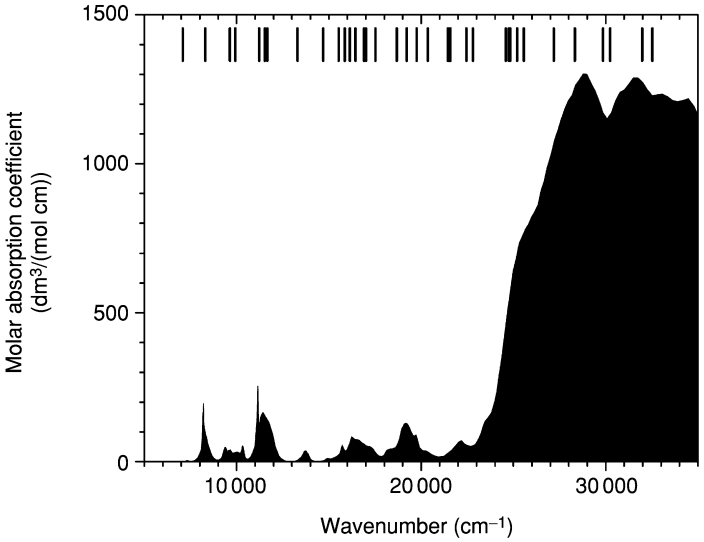

Fig. 18.25 *Optical absorption spectrum of* U^{3+} *in dilute acid solution* (*shaded curve*) *compared to the* 5*f electron free-ion state energies from studies on* U^{3+} *in* $LaCl_3$ (*vertical bars*). *Data from Carnall* (1992).

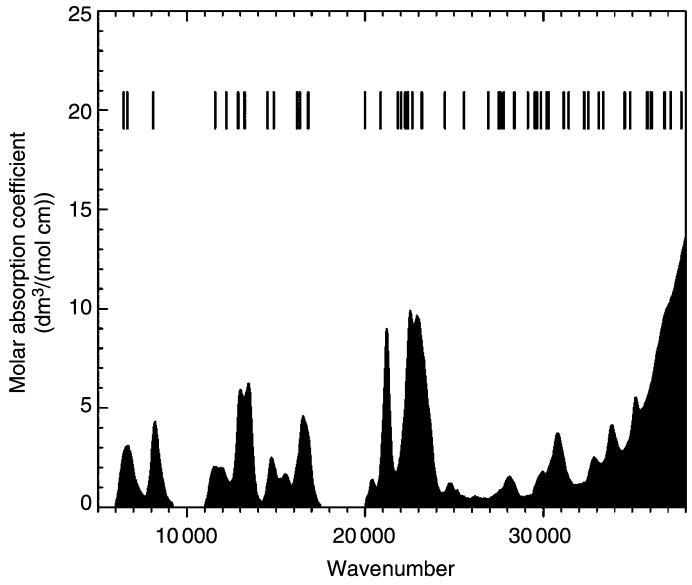

Fig. 18.26 *Optical absorption spectrum of* Cf^{3+} *in dilute acid solution* (*shaded curve*) *compared to the* 5*f electron free-ion state energies from studies on* Cf^{3+} *in* $LaCl_3$ (*vertical bars*). *Data from Carnall* (1992).

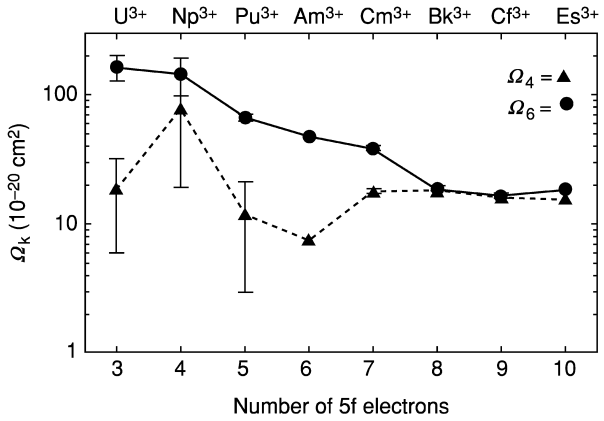

Fig. 18.27 *Trends in the values of the Judd–Ofelt theory Ω_4 and Ω_6 parameters across the trivalent actinide ion series.* (*Data from Carnall and Crosswhite,* 1985*; Carnall* et al., 1985*; Beitz,* 1994b).

Beitz, 1994b) from the f–f transition intensities using the Judd–Ofelt formalism (see equation (18.54)). The results of these analyses for aquated U^{3+} through aquated Es^{3+}, based on a fixed value of the Judd–Ofelt parameter Ω_2 at 1×10^{-20} cm^2, are shown in Fig. 18.27. The difficulty in uniquely determining band areas for the strongly overlapping bands of light actinide ions results in large error estimates for these ions. The Judd–Ofelt parameters for aquated trivalent lanthanide ions become nearly constant in value beginning at neodymium and continuing across the series of lanthanide elements (Carnall, 1979a). A similar trend is evident in Fig, 18.27 beginning at Bk^{3+} for aquated trivalent actinide ions. Few opportunities exist for experimentally establishing Ω_2 values for trivalent actinide ions. One such case is found in the branching ratios for emission from the $^5D_1$ state of aquated Am^{3+}. Partial measurement of those ratios led Beitz (1994a) to conclude that an Ω_2 value of 7×10^{-20} cm^2 was consistent with the Ω_4 and Ω_6 values shown in Fig. 18.27 (Beitz, 1994a). Görller-Walrand and Binnemans (1998) have reviewed the application of Judd–Ofelt theory to lanthanide and actinide f–f transitions.

18.8.2 Florescence lifetimes

One reason of interest for determining absorption intensity correlations is that, once the parameters of the Judd–Ofelt theory are evaluated, they can be used to compute the radiative lifetime of any excited state of interest via the Einstein expression

$$A(\Psi J, \Psi' J') = \frac{64\pi^2\sigma^3}{3h(2J+1)}\left(\chi'\overline{F}^2 + n^3\overline{M}^2\right) \tag{18.55}$$

where $|\Psi J\rangle$ and $|\Psi' J'\rangle$ are the initial and final states, A is the rate of relaxation of ΨJ by radiative processes, and $\overline{F}^2$ and $\overline{M}^2$ are the terms defined in equations (18.52) and (18.54). The observed fluorescent lifetime of a particular excited state, τ_T, is determined by the sum of the inverse of the radiative and nonradiative lifetimes. Usually the nonradiative relaxation mechanisms are dominant. Thus

$$(\tau_T)^{-1} = A_T(\Psi J) + W(\Psi J) \tag{18.56}$$

where A_T (ΨJ) is the total radiative relaxation rate from state $|\Psi J\rangle$, that is, the sum of the rates of radiative decay to all states with energy less than that of $|\Psi J\rangle$. If τ_R (calc) is the (computed) total radiative lifetime of $|\Psi J\rangle$, then τ_R (calc) $= [A\ (\Psi J)]^{-1}$. Similarly, $W_T(\Psi J)$ is a total rate summed over all nonradiative relaxation processes. The magnitude of the energy gap between a fluorescing state and the next lower-energy state appears to play a major role in determining the nonradiative lifetime of that state; shorter empirical fluorescent lifetimes are correlated with narrower gaps for the same fluorescing level in different systems.

On the basis of the existence of relatively large energy gaps in the spectra of some of the heavier actinides (Fig. 18.8), experiments were initiated and luminescence lifetimes were successfully measured in solution for some of the excited states of aquated Bk^{3+} and Es^{3+} (Beitz *et al.*, 1981), as well as aquated Cm^{3+} (Beitz and Hessler, 1980) and aquated Am^{3+} (Beitz *et al.*, 1987). As indicated in Fig. 18.28, which shows the lower energy level structure for the heavier aquated

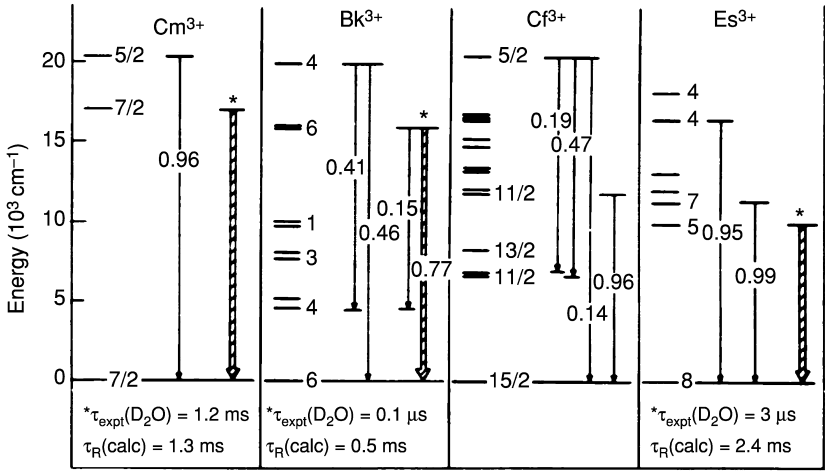

Fig. 18.28 *Energy level schemes and selected branching ratios for radiative relaxation for Cm^{3+} through Es^{3+}.*

An^{3+} ions, only in aquated Cm^{3+} does the observed lifetime of 1.2 ms in D_2O (Kimura *et al.*, 2001) compare well with the computed radiative lifetime, $\tau_R = 1.3$ ms. With smaller energy gaps, the nonradiative relaxation rate clearly becomes rate-determining. Inability to observe a luminescing state for aquated Cf^{3+} in preliminary experiments suggests that lifetimes may be in the nanosecond time range (Beitz *et al.*, 1981; Carnall *et al.*, 1983).

In addition to computing radiative lifetimes, it is instructive to establish the most probable pathway for fluorescence from a given state. Thus the branching ration, β_R, from a given relaxing state to a particular final state is

$$\beta_R(\Psi J, \Psi' J') = \frac{A(\Psi J, \Psi' J')}{A_T(\Psi J)}. \tag{18.57}$$

As indicated in Fig. 18.28 for Cf^{3+}, $\beta_R = 0.47$ for emission from an excited ($J = 5/2$) state to a lower-lying ($J = 11/2$) state, whereas $\beta_R = 0.14$ for emission to the ground state. In the case of $J = 5/2$ state, it would be appropriate to monitor for luminescence near 13 000 cm^{-1} as well as near 20 000 cm^{-1}.

18.8.3 Nonradiative phonon relaxation

The identification of the mechanisms of nonradiative relaxation of actinide ions in solution as well as in solids remains an important area for research (Hessler *et al.*, 1980; Liu and Beitz, 1990a,b). The nonradiative relaxation rate between crystal field energy levels belonging to different multiplets is predominantly determined by temperature, the energy gap, and the lattice phonon modes of the particular host crystal (Riseberg and Moos, 1968; Miyakawa and Dexter, 1970). With the assumption that the phonons involved are of equal energy, a commonly used expression for the temperature-dependent multiphonon relaxation rate is (Riseberg and Moos, 1968)

$$W(T) = W(0)\left[\frac{\exp(\hbar\omega_m/kT)}{\exp(\hbar\omega_m/kT) - 1}\right]^{\Delta E/\hbar\omega_m}, \tag{18.58}$$

where $\hbar\omega_m$ is the maximum phonon energy the lattice vibrations that couples to the electronic transition of the metal ion, ΔE is the energy gap between the populated state and the next low-lying state, and $W(0)$ is the spontaneous transition rate at $T = 0$ when the phonon modes are all initially in their ground state. At low temperatures where $\hbar\omega_m \gg kT$, nonradiative relaxation rate is dominated by $W(0)$, which can be expressed as a simple exponential function depending on the energy gap, ΔE

$$W(0) = C\exp(-\alpha\Delta E/\hbar\omega_m), \tag{18.59}$$

where C and α are empirical parameters which are characteristic of the particular crystal. Known as the energy gap law, this exponential dependence of the transition rate on the energy gap has been used to describe quite generally the

energy gap dependence of multiphonon transitions rates for the 4f and 5f states (Riseberg and Moos, 1967, 1968).

Extensive experimental results for lanthanide systems are available for comparison with those obtained for actinide ions. It should be possible to explore bonding differences between selected actinides and lanthanides by examining their excited state relaxation behavior. Because of smaller electrostatic interaction and larger spin–orbit coupling and crystal-field splittings, the energy gaps between different *J*-multiplets of actinide ions are much smaller than that of the isoelectronic lanthanide ions. Therefore, phonon-induced nonradiative relaxation in actinide systems is more efficient than in the lanthanide systems. Except for a few cases, such as the $^6D_{7/2}$ state of Cm^{3+} and Bk^{4+}, that have a large energy gap to the low-lying states, the lifetime of most 5f–5f electronic transitions of actinide ions in solids and solutions are predominantly determined by nonradiative relaxation. A direct comparison of the use of the energy gap law for Cm^{3+} in $LaCl_3$ and the trivalent rare earth ions in $LaCl_3$ has been reported (Illemassene *et al.*, 1997). A comparison of the emitting state lifetimes of Cm^{3+} in various crystals is given in Fig. 18.16. A summary of spectroscopic studies of Cm^{3+} in crystals $LaCl_3$, $LuPO_4$, ThO_2, Cs_2NaYCl_6, and $CsCdBr_3$ was given in a review paper (Edelstein, 2002). The lifetimes of the actinide ions with the $5f^7$ configuration (Cm^{3+}, Bk^{4+}) are roughly consistent with the energy gap law in that for the hosts $LuPO_4$, ThO_2, and in CeF_4, only one or at most two levels luminesce. For the heavier halide hosts, the vibrational spread is small and the crystal field strength is relatively small so many more levels luminesce.

Early studies on multiphonon relaxation of 5f states of aquated trivalent actinide ions have been reviewed (Yusov, 1993; Beitz, 1994a) and compared to similar work on 4f states of aquated trivalent lanthanide ions (Beitz, 1994b). Aquated ions are those whose inner coordination sphere consists only of water molecules. Systematic studies of the 5f state luminescence lifetimes of aquated trivalent actinide ions began in 1980 with the work of Beitz and Hessler (1980) who reported the luminescence emission spectra of $^{248}Cm^{3+}$ in dilute perchloric or hydrochloric acid as well as luminescence lifetimes in H_2O and D_2O solutions. They assigned the emission as arising from the electronically excited $^6D_{7/2}$ state of Cm^{3+} based on a study of the solution absorption spectrum of Cm^{3+} in perchloric acid (Carnall and Rajnak, 1975). A subsequent study by Beitz and coworkers on the luminescence of $^{244}Cm^{3+}$ in dilute acid solution showed that speciation studies on ultratrace levels of Cm^{3+} could be carried out using elementary laser-induced fluorescence techniques (Beitz *et al.*, 1988). Laser-induced luminescence studies also have been reported on Am^{3+} (Beitz *et al.*, 1987; Yusov, 1990; Thouvenot *et al.*, 1993b; Kimura and Kato, 1998), Bk^{3+} (Carnall *et al.*, 1984) and Es^{3+} (Beitz *et al.*, 1983) in dilute acid solutions and as well as additional studies on aquated Cm^{3+} (Yusov, 1987; Kimura and Choppin, 1994; Kimura *et al.*, 1996, 1997). In all cases, the observed luminescence bands were assigned as arising from a 5f state lying at or below the energy

of the exciting photons and that, among all such states, in addition possessed the largest ΔE value. The reported 5f state emission spectra of aquated trivalent actinide ions are in good agreement with the calculated free-ion states of trivalent actinide ions doped into lanthanum trichloride (Carnall, 1992).

Aquated actinide ions are prototypical species for the investigation of coordination complexes that form as ligands other than water become associated with an actinide ion. It should be appreciated that the coordination sphere of trivalent actinide ions is dynamic unless there is an exceptionally strong ligand bonding. For example, using nanosecond laser excitation, there are no reports of emission from aquated actinide ions that differ as to the number of coordinated water molecules, which suggests that the coordination environment of aquated actinide ions reaches equilibrium on the submicrosecond timescale. In the case of aquated actinide ions, interest naturally exists as to the number of inner-sphere coordinated water molecules, and luminescence studies have been reported that provide a measure of that number.

Kimura and Choppin (1994) doped Cm^{3+} into a series of solid-hydrated lanthanum compounds and determined the influence of the number of inner-sphere coordinated water molecules on the observed Cm^{3+} luminescence lifetimes. Their data are plotted in Fig. 18.29 where the solid line expresses the resulting correlation as

$$n_{H_2O} = 0.65k_{obs} - 0.88 \tag{18.60}$$

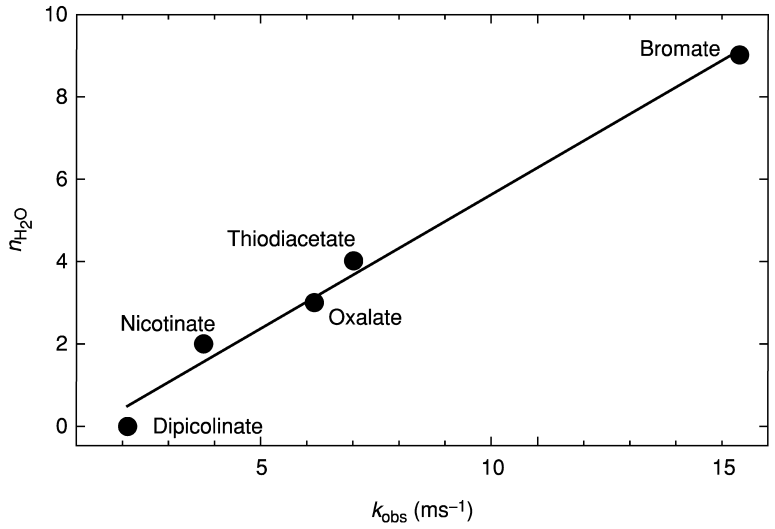

Fig. 18.29 *Observed $^{248}Cm^{3+}$ luminescence decay rate, $k_{obs,}$ from Cm^{3+} doped into a series of solid-hydrated lanthanum compounds at Cm:La = 1:6.9 × 10^3 as a function of the number of inner-sphere coordinated water molecules, n_{H_2O}. Data from Kimura and Choppin* (1994).

where n_{H_2O} is the number of inner-sphere coordinated water molecules and k_{obs} is the measured luminescence lifetime in units of ms^{-1}. Analysis of the data in Fig. 18.29 using equation (18.60) results in a calculated 95% confidence limit of $\pm$ 0.74 for n_{H_2O} values, if one assumes that there is no error as to the number of inner-sphere coordinated water molecules in a given compound. The correlation embodied in equation (18.60) should be valid as long as there is no contribution from ligands other than H_2O or HDO to de-excitation of the emitting state and the purely radiative decay rate of the emitting state remains essentially unchanged across the series of compounds. The value of n_{H_2O} for aquated Cm^{3+} reported by Kimura and Choppin was 9.2 $\pm$ 0.5 water molecules.

Subsequently, Kimura and Kato (1998) studied aquated and complexed $^{241}Am^{3+}$ luminescence via its $^5D_1 \rightarrow {}^7F_1$ transition. They reported $k_{obs} = 24.6 \pm 0.6$ ns for aquated Am^{3+} in H_2O and 162 $\pm$ 4 ns for Am^{3+} in 99.9% D_2O. They adopted a different analysis procedure based on the assumption that the number of inner-sphere water molecules is 9 for aquated Am^{3+} and aquated Cm^{3+}. With that assumption and from the linear correlation they observed between the observed luminescence decay rate, k_{obs}, and the deuterium mole fraction in H_2O–D_2O mixtures, they determined

$$n_{H_2O} = 2.56 \times 10^{-4} k_{obs} - 1.43 \tag{18.61}$$

for the case of aquated Am^{3+} and

$$n_{H_2O} = 0.612\, k_{obs} - 0.48 \tag{18.62}$$

for the case of aquated Cm^{3+}. Subsequently, Kimura and coworkers studied the luminescence lifetimes of Am^{3+} and Cm^{3+} of unstated actinide isotopic composition at 25°C (Kimura *et al.*, 2001). They reported lifetime values for aquated Am^{3+} in H_2O of 25 $\pm$ 0.75 and 160 $\pm$ 5 ns for aquated Am^{3+} in 99.95% D_2O along with the values of 65 $\pm$ 2 μs for aquated Cm^{3+} in H_2O and 1200 $\pm$ 36 μs for aquated Cm^{3+} in 99.95% D_2O. These values together with equations (18.61) and (18.62) give $n_{H_2O} = 8.9$ for aquated Cm^{3+} and $n_{H_2O} = 8.8$ for aquated Am^{3+}. On the basis of preferential solvation in the nonaqueous solutions, an estimate of the Gibbs free energy of transfer of Am^{3+} and Cm^{3+} ions from aqueous to nonaqueous solutions also was obtained using the observed luminescence lifetimes in mixtures of water and organic solvents.

Due to its spectroscopy and photophysics, Cm^{3+} is the trivalent actinide ion most commonly studied in solution using luminescence techniques. As noted earlier, luminescence from three other aquated trivalent actinide ions has been reported. Selected lifetime values from these studies are shown in Table 18.14. In nearly all cases where the stated measurement errors were 5% or less of the observed value and the lifetime was at least a factor of 10 longer than the excitation pulse width, the reported lifetime values are concordant at the 95% confidence level. The seeming exception occurs for Cm^{3+} in D_2O solution. Beitz and Hessler (1980) reported that the luminescence lifetime of Cm^{3+} in 1 M $DClO_4$ solution was 940 $\pm$ 40 μs, whereas Kimura and coworkers reported

Table 18.14 *Selected 5f state luminescence lifetimes, τ, for actinide ions in dilute acid solution at ambient temperature.*[a]

Actinide ion	*Emitting state*[b]	*τ in H_2O*	*τ in D_2O*
U^{4+}	$^1S_0$	<20 ns	
Am^{3+}	$^5D_1$	22 ± 3 ns	160 ± 5 ns
Cm^{3+}	$^6D_{7/2}$	65 ± 3 μs	1200 ± 36 μs
Bk^{3+}	$^7F_6$		100 ± 20 ns
Es^{3+}	$^5F_5$	1.05 ± 0.05 μs	2.87 ± 0.09 μs

[a] See text for selection basis and literature references.
[b] Term symbols for emitting states from the work of Carnall and coworkers (Carnall *et al.*, 1991; Carnall, 1992).

that the lifetime of aquated Cm^{3+} in 0.01 M $DClO_4$ was 1200 ± 36 μs (Kimura *et al.*, 2001). Both studies reported that the lifetime of Cm^{3+} in H_2O was 65 μs. Beitz and Hessler used triply distilled D_2O that was 99% D_2O by near-infrared absorption spectroscopy to make up their solutions whereas Kimura and coworkers used as-received 99.95% D_2O. The work of Kimura and coworkers provides evidence that the observed luminescence lifetime of Cm^{3+} in a mixture of H_2O and D_2O is given by the expression

$$k_{obs} = (1 - \chi)\, k_{H_2O} + \chi\, k_{D_2O} + C, \tag{18.63}$$

where k_{obs} is the observed Cm^{3+} luminescence lifetime in a mixture of H_2O and D_2O in which χ is the deuterium mole fraction of the solution, C is a constant, and k_{H_2O} and k_{D_2O} are the luminescence decay rates of Cm^{3+} in 100% H_2O and 100% D_2O solutions, respectively. Taking into account the stated errors in the measured luminescence lifetimes and equation (18.63), the reported 940 ± 40 and 1200 ± 36 μs Cm^{3+} lifetime values in heavy water solutions agree with each other at the 95% confidence level given the differing degree of solvent deuteration in the two studies.

Reported lifetimes for the $^5D_1$ state of aquated Am^{3+} in H_2O are more discordant which can be attributed primarily to the use of excitation pulses whose width was not insignificant compared to the luminescence decay time of aquated Am^{3+}. The value reported by Beitz (1994a) is selected for inclusion in Table 18.14 because a deconvolution procedure was used to correct for the finite excitation pulse width. The lifetimes reported by Kimura and coworkers for Cm^{3+} and Am^{3+} (Kimura *et al.*, 2001) in D_2O were selected for inclusion in Table 18.14 because of the higher level of solution deuteration in their studies in comparison with earlier studies by others.

A limit for the luminescence lifetime of the $^1S_0$ state of U^{4+} in 1 M perchloric acid has been reported (Kiarshima *et al.*, 2003) and is included in Table 18.14. Based on their excitation and emission spectra, the energy gap between the U^{4+} emitting state and its next lower 5f state is comparable to the Cm^{3+} energy gap. In consequence, one might have expected that nonradiative decay would

only moderately diminish the observed lifetime of the $^1S_0$ state. However, Kiarshima and coworkers report that the luminescence lifetime of the $^1S_0$ state of aquated U^{4+} is <20 ns. Evidently the $^1S_0$ state is primarily quenched by processes other than those that are responsible for the nonradiative decay of the observed 5f emitting states of aquated trivalent actinide ions. Candidate processes for U^{4+} include intersystem crossing to a lower-lying opposite-parity state of U^{4+} and electron transfer to or from neighboring ligands.

Insight into the factors influencing the nonradiative decay of emitting 5f states of aquated trivalent actinide ions can be obtained by plotting the data of Table 18.14 for such ions semilogarithmically as shown in Fig. 18.30. The solid and dashed lines are fits of the data for ions in H_2O and D_2O, respectively, to equation (18.59). Use of this equation is justified ($\hbar\omega_m \gg kT$) if energy is transferred to a stretching or bending vibrational modes of water at ambient temperature. The resulting fit values for $(\alpha/\hbar\omega_m)$ are 6.23×10^{-4} cm for H_2O solutions and 7.52×10^{-4} cm for D_2O solutions. Based on equation (18.59), nonradiative decay occurs primarily to stretching vibrational modes of water for Es^{3+} and Cm^{3+}. However, the currently available data for aquated trivalent actinide ions in H_2O are too less to determine if energy transfer to bending vibrational modes of water makes a significant contribution to the overall nonradiative decay rate at low values of ΔE as might be expected from recent studies on multiphonon-induced nonradiative decay in single crystals (Ermeneux *et al.*, 2000).

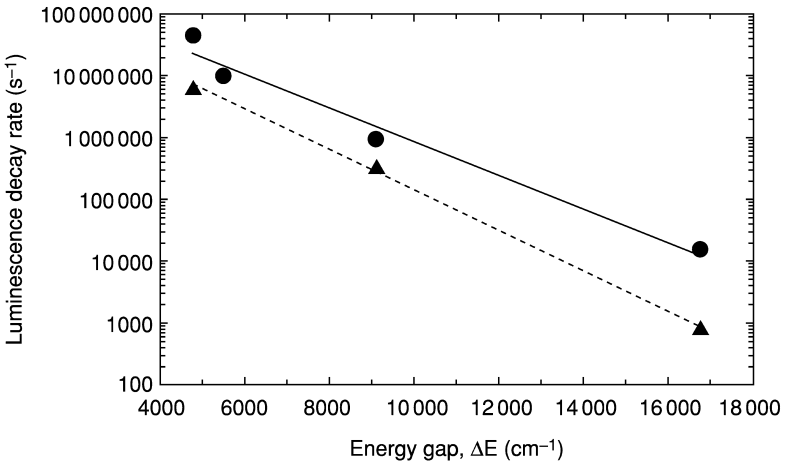

Fig. 18.30 *Energy gap law plot of the luminescence decay rates from Table* 18.14 *of aquated trivalent actinide ions in H_2O* (•) *and D_2O* (▲) *solutions. The solid and dashed lines are fits of equation* (18.59) *to the observed data for H_2O and D_2O solutions, respectively.*

18.8.4 Ion–ion interaction and energy transfer

The success of the single-particle model for interpretation of the solid-state actinide spectra is largely due to the localized nature of the 5f electrons. In the modeling of $5f^N$ electronic energy level structure, the coupling between neighboring f-element ions is neglected even for actinides in stoichiometric compounds, although ion–ion interaction induced band structure and cooperative pair transitions have been observed in lanthanide compounds (Cone and Meltzer, 1987) and are expected to be more significant in the actinide compounds because of more extended 5f orbitals (Fig. 18.3). However, the effects of ion–ion interactions on the excited state dynamics such as luminescence decay are very significant even in dilute crystals with actinide doping level below 1% (Liu and Beitz, 1990a). As a result of ion–ion interactions, luminescence emission from a $5f^N$ state is usually observed only in dilute crystals. The excited state lifetime and the luminescence decay dynamics are strongly dependent on the actinide ion concentration as well as on sample temperature. Fig. 18.31 shows the $^5D_1$ luminescence decay of 0.1 at% Cm^{4+} (a) and 5 at% Cm^{4+} (b) in crystalline CeF_4 at 4 K. There is an obvious deviation from a single exponential decay for the 0.1 at% Cm^{4+}:CeF_4 sample and the decay rate in the long time range is approximately $5 \times 10^3\ s^{-1}$. In the 5 at% Cm^{4+}:CeF_4 sample, most Cm^{4+} ions relaxed from the excited state within 15 μs. At long times, behavior similar

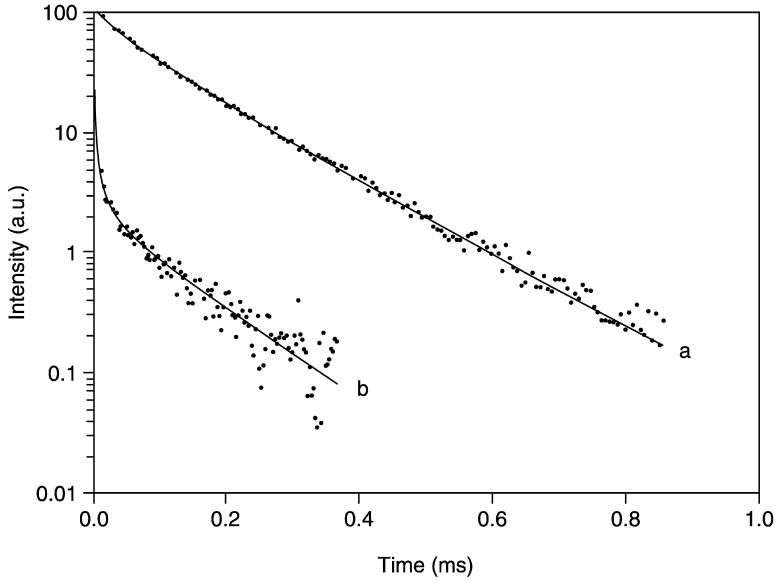

Fig. 18.31 *Nonexponential fluorescence decays of Cm^{3+} ions in CeF_4 induced by interionic excitation energy transfer.* (*a*) *the $^5D_1$ fluorescence decay of* 0.1% (*atom*) *Cm^{4+}:CeF_4 at* 4 K*; and* (*b*) *the $^5D_1$ fluorescence decay of* 5% (*atom*) *Cm^{4+}:CeF_4 at* 4 K. (*Reprinted with permission from Liu and Beitz,* 1990b. *Copyright* 1990, *Elsevier.*)

to that of the 0.1 at% Cm^{4+}:CeF_4 sample is due to the contribution from Cm^{4+} ions at isolated sites where energy transfer is improbable.

The theory of energy transfer of luminescent ions in solids has been developed for interpretation of sensitized luminescence (Förster, 1948; Dexter, 1953). This theory is based on the assumption that the rate of excitation energy transfer (W_{da}) from a donor, d, to an acceptor, a, depends on the distance between d and a, R_{da}, as

$$W_{da} = \alpha\left(\frac{R_0}{R_{da}}\right)^s, \tag{18.64}$$

where the parameter α contains the matrix elements of the interaction between d and a, and R_0 is the distance between the nearest neighbors. These matrix elements depend on the transition probabilities as well as the energy mismatches if d and a do not have identical excitation energy levels. In equation (18.64), s takes an integer value of 6, 8, or 10 for electric dipole–dipole, dipole–quadrupole, or quadrupole–quadrupole interactions, respectively. For the simple case where energy-transfer processes are irreversible, the luminescence decay rate may be evaluated using

$$\frac{dP_d}{dt} = -\kappa P_d - \sum_a W_{da} P_d, \tag{18.65}$$

where P_d is the probability of excitation of the donor, κ is for the intrinsic decay rate, and the summation is over all possible acceptors. In f-element ions in dielectric crystals, the donors and acceptors are the same. It is often difficult, especially for the doped crystals or structurally disordered solids, to perform the lattice summation over the occupied acceptor sites in equation (18.65). Inokuti and Hirayama (1965) first obtained a general approximate solution for ion concentration $c \ll 1$:

$$\ln\frac{P(0)}{P(t)} = \kappa t + c\Gamma(1 - 3/s)(\alpha t)^{3/s}, \tag{18.66}$$

where $\Gamma(1 - 3/s)$ is the gamma function and other quantities are the same as defined in equations (18.64) and (18.65). The solid line in Fig. 18.31 are fitted results using the Inokuti and Hirayama model.

Although nonexponential luminescence decay is the direct consequence of ion–ion interactions that are easy to measure by experiment, there are different microscopic mechanisms that may not be revealed in detail in the analysis of the decay dynamics alone. Analysis of energy level structure is often critical in understanding the energy-transfer processes. For actinide and lanthanide ions in insulating crystals, resonant migration excitation of excitation among the identical ions is common, and if there is inhomogeneous line broadening, phonon-assisted (phonon absorption from or emission to the lattice) energy-transfer results in temperature-dependent spectral diffusion as well as nonexponential luminescence decay (Yen, 1987). In many cases, energy transfer occurs in such a way that the donor gives the acceptor a part of its excitation energy and

nonradiatively relaxes to an intermediate state, whereas with this amount of energy the acceptor is excited into the same or a different intermediate state. This type of energy transfer is called cross-relaxation. As shown in Fig. 18.31, the nonexponential decay of Cm^{4+} in the $^5D_1$ level is dependent on the Cm^{4+} doping level. The mechanism for the nonexponential decay is mainly due to the cross-relaxation into the low-lying excited states of $^7F_{3,4}$ states (Liu and Beitz, 1990a). A special type of cross-relaxation is up-conversion energy transfer. In this process, the donor and acceptor are both in metastable states while the donor relaxes into a low-lying state and the acceptor is further excited into a high-lying state. This energy-transfer process enables emission of a photon with energy higher than the initial excitation energy. Instead of emission of a higher energy photon, this type of energy transfer may end up with energy lost to the lattice or lead to ionization, a process called annihilation.

Extensive studies of the microscopic mechanisms of ion–ion interactions and various consequences of energy-transfer processes have been done for lanthanide ions and detailed reviews of the previous work have been published (Cone and Meltzer, 1987; Yen, 1987). Much less work has been conducted on actinide systems. Many experimental results from the actinide systems may be interpreted using the same framework developed from modeling the lanthanide systems, such as those of Cm^{4+}:CeF_4 (Liu and Beitz, 1990a,b). The excited state dynamics of both U^{3+} and U^{4+} ion in a host crystal of Ba_2YCl_7 was recently reported. It is shown that energy transfer induced up-conversion of U^{4+} excitation leads to strong luminescence from the $^1I_6$ state at 19 600 cm^{-1} (Karbowiak *et al.*, 2003). Consistent with the observations in analyses of crystal-field splittings and ion–phonon coupling, ion–ion interactions in the actinide systems with the same level of ion concentration are much stronger than that in the lanthanide systems. This explains in general the more significant nonexponential decay and quenching of actinide luminescence emission.

ACKNOWLEDGMENTS

We dedicate this chapter to the memory of William T. Carnall who was our actinide spectroscopy mentor, colleague, and friend. We also thank him for permission to base our present work on the chapter that he coauthored in the second edition of this work. This work was performed under the auspices of the Office of Basic Energy Sciences, Office of Science, U.S. Department of Energy under contract W-31-109-ENG-38.

REFERENCES

Auzel, F., Hubert, S., Delamoye, P., and Hussonnois, M. (1982) *J. Lumin.*, **26**, 251–62.
Auzel, F. and Malta, O. L. (1983) *J. Phys.*, **44**, 201–6.
Axe, J. D., Stapleton, H. J., and Jeffiries, C. D. (1961) *Phys. Rev.*, **121**, 1630–7.

Baybarz, R. D., Asprey, L. B., Strouse, C. E., and Fukushima, E. (1972) *J. Inorg. Nucl. Chem.*, **34**, 3427–31.
Beitz, J. V. and Hessler, J. P.(1980) *Nucl. Technol.*, **51**, 169–77.
Beitz, J. V., Carnall, W. T., and Wester, D. W. (1981) in *Lawrence Berkeley Laboratory Report LBL-12441*, Lawrence Berkeley Laboratory, Berkeley, CA, pp. 108–10.
Beitz, J. V., Williams, C. W., and Carnall, W. T. (1982) *J. Chem. Phys.*, **76**, 2756–7.
Beitz, J. V., Wester, D. W., and Williams, C. W. (1983) *J. Less Common Metals*, **93**, 331–8.
Beitz, J. V., Jursich, G., and Sullivan, J. C. (1987) in *Rare Earths 1986, Proc. of the 17th Rare Earth Research Conference*, vol. 1 (eds. H. B. Silber, L. R. Morss, and L. E. DeLong), Elsevier Sequoia, Lausanne, p. 301.
Beitz, J. V., Bowers, D. L., Doxtader, M. M., Maroni, V. A., and Reed, D. T. (1988) *Radiochim. Acta*, **44/45**, 87–93.
Beitz, J. V. (1994a) *J. Alloys Compds*, **207/208**, 41–50.
Beitz, J. V. (1994b) in *Handbook on the Physics and Chemistry of Rare Earths,* vol. 18 (eds. K. A. Gschneidner Jr, L. Eyring, G. R. Choppin, and G. H. Lander), North-Holland, Amsterdam, pp. 159–95.
Beitz, J. V., Williams, C. W., and Liu, G. K. (1998) *J. Alloys Compds*, **271**, 850–3.
Bell, J. T. (1969) *J. Inorg. Nucl. Chem.*, **31**, 703–10.
Blaise, J., Fred, M. S., Carnall, W. T., Crosswhite, H. M., and Crosswhite, H. (1983) *ACS Symp. Ser.*, **216**, 173–98.
Brewer, L. (1971a) *J. Opt. Soc. Am.*, **61**, 1101–11.
Brewer, L. (1971b) *J. Opt. Soc. Am.*, **61**, 1666–82.
Brewer, L. (1983) in *Systematics and the Properties of the Lanthanides,* Reidel, Boston, pp. 17–63.
Brito, H. F. and Liu, G. K. (2000) *J. Chem. Phys.*, **112**, 4334–41.
Brown, D. (1968) *Halides of the Lanthanides and Actinides,* John Wiley, New York.
Brown, D., Whittaker, B., and Edelstein, N. (1974) *Inorg. Chem.*, **13**, 1805–8.
Brown, D., Lidster, P., Whittaker, B., and Edelstein, N. (1976) *Inorg. Chem.*, **15**, 511–14.
Carnall, W. T., Walker, A., and Neufeldt, S. J. (1966) *Inorg. Chem.*, **5**, 2135–40.
Carnall, W. T., Fields, P. R., and Rajnak, K. (1968) *J. Chem. Phys.*, **49**, 4412–23.
Carnall, W. T., Fields, P. R., and Sarup, R. (1969) *J. Chem. Phys.*, **51**, 2587–91.
Carnall, W. T., Fields, P. R., and Sarup, R. (1971) *J. Chem. Phys.*, **54**, 1476–9.
Carnall, W. T. (1973) in *Gmelin Handbuch der Anorganishce Chemie,* Vol. *Transurane A2*, Verlag Chemie, Weinheim, pp. 49–80.
Carnall, W. T. Rajnak, and K. (1975) *J. Chem. Phys.*, **63**, 3510–14.
Carnall, W. T. (1979a) in *Handbook on the Physics and Chemistry of the Rare Earths,* vol. 3 (eds. K. A. Gschneidner Jr, and L. Eyring) North-Holland, Amsterdam, pp. 171–208.
Carnall, W. T. (1979b) *NATO Adv. Study Inst. Ser., Ser. C: Math. Phys. Sci.*, **44**, 281–307.
Carnall, W. T. (1982) in *Gmelin Handhuch der Anorganischen Chemie,* 8th edn., Uranium Suppl. A5, Springer-Verlag, Berlin, pp. 69–161.
Carnall, W. T., Beitz, J. V., Crosswhite, H., Rajnak, K., and Mann, J. B. (1983) in *Systematics and the Properties of the Lanthanides* (ed. S. P. Sinha), Reidel, Dordrecht, pp. 389–450.
Carnall, W. T., Beitz, J. V., and Crosswhite, H. (1984) *J. Chem. Phys.*, **80**, 2301–8.

Carnall, W. T. and Crosswhite, H. M. (1985) *Argonne National Laboratory Report ANL-84-90,* Argonne National Laboratory, Argonne, IL, 154 pp.
Carnall, W. T., Crosswhite, H., and Rajnak, K. (1985) in *Rare Earths Spectroscopy* (eds. B. Jezowska-Trzebiatowska, J. Legendziewicz, and W. Strek), World Scientific Publishing, Singapore, pp. 267–97.
Carnall, W. T. (1989) *Argonne National Laboratory Report ANL-89/39,* Argonne National Laboratory, Argonne, IL, p. 285.
Carnall, W. T., Goodman, G. L., Rajnak, K., and Rana, R. S. (1989) *J. Chem. Phys.*, **90**, 3443–57.
Carnall, W. T., Liu, G. K., Williams, C. W., and Reid, M. F. (1991) *J. Chem. Phys.*, **95**, 7194–203.
Carnall, W. T. (1992) *J. Chem. Phys.*, **96**, 8713–26.
Claassen, H. H. (1959) *J. Chem. Phys.*, **30**, 968–9.
Condon, E. U. and Shortley, G. H. (1963) *The Theory of Atomic Spectra,* Cambridge University Press, Cambridge.
Cone, R. L. and Meltzer, R. S. (1987) in *Spectroscopy of Solids Containing Rare Earth Ions* (eds. A. A. Kaplyanskii and R. M. Macfarlane), North-Holland, Amsterdam, pp. 481–556.
Conway, J. G. (1964) *J. Chem. Phys.*, **41**, 904–5.
Copland, G. M., Newman, D. J., and Taylor, C. D. (1971) *Journal of Physics B: Atomic and Molecular Physics*, **4**, 1605–10.
Cowan, R. D. and Griffin, C. D. (1976) *J. Opt. Soc. Am.*, **66**, 1010–14.
Cowan, R. D. (1981) *The Theory of Atomic Structure and Spectra,* University of California Press, Berkeley.
Crosswhite, H. M., Dieke, G. H., and Carter, W. J. (1965) *J. Chem. Phys.*, **43**, 2047–54.
Crosswhite, H., Crosswhite, H. M., and Judd, B. R. (1968) *Phys. Rev.*, **174**, 89–94.
Crosswhite, H. M., Crosswhite, H., Kaseta, F. W., and Sarup, R. (1976) *J. Chem. Phys.*, **64**, 1981–5.
Crosswhite, H. M. (1977) *Colloq. Int. CNRS*, **255**, 65–9.
Crosswhite, H. M., Crosswhite, H., Carnall, W. T., and Paszek, A. P. (1980) *J. Chem. Phys.*, **72**, 5103–7.
Crosswhite, H. M. (1982) in *Gmelin Handbuch der Anorganischen Chemie,* 8th edn, Uranium Suppl. A5, Springer-Verlag, Berlin, pp. 1–68.
Crosswhite, H. M. and Crosswhite, H. (1984) *J. Opt. Soc. Am. B*, **1**, 246–54.
de Bruin, T. L., Klinkenberg, P. F. A., and Schuutmans, P. (1941) *Z. Phys.*, **118**, 58–87.
DeKock, R. L., Baerends, E. J., Boerrigter, P. M., and Snijders, J. G. (1985) *Chem. Phys. Lett.*, **105**, 308–16.
Delamoye, P., Rajnak, K., Genet, M., and Edelstein, N. (1983) *Phys. Rev. B*, **28**, 4923–30.
Denning, R. G., Norris, J. O. W., Short, I. G., Snellgrove, T. R., and Woodwark, D. R. (1980) in *ACS Symposium Series: Lanthanide and Actinide Chemistry and Spectroscopy,* vol. 131 (ed. N. Edelstein), American Chemical Society, Washington, DC, pp. 313–30.
Denning, R. G., Norris, J. O. W., and Brown, D. (1982) *Mol. Phys.*, **46**, 287–364.
Denning, R. G. (1992) in *Structure and Bonding,* vol. 79 (ed. M. J, Clarke), Springer-Verlag, Berlin, pp. 215–76.

Denning, R. G., Green, J. C., Hutchings, T. E., Dallera, C., Tagliaferri, A., Giarda, K., Brookes, N. B., and Braicovich, L. (2002) *J. Chem. Phys.*, **117**, 8008–20.
Dexter, D. L. (1953) *J. Chem. Phys.*, **21**, 836–50.
Dick, B. G. and Overhauser, A. (1958) *Phys. Rev.*, **112**, 90–103.
Dieke, G. H. (1968) *Spectra and Energy Levels of Rare Earth Ions in Crystals,* John Wiley, New York.
Downer, M. C., Cordero- Montalvo, C. D., and Crosswhite, H. (1983) *Phys. Rev. B*, **28**, 4931–43.
Edelstein, N., Easley, W., and McLaughlin, R. (1966) *J. Chem. Phys.*, **44**, 3130–1.
Edelstein, N., Easley, W., and McLaughlin, R. (1967) *Adv. Chem. Ser.*, **71**, 203–10.
Edelstein, N. and Easley, W. (1968) *J. Chem. Phys.*, **48**, 2110–15.
Edelstein, N., Conway, J. G., Fujita, D. K., Kolbe, W., and McLaughlin, R. (1970) *J. Chem. Phys.*, **52**, 6425–6.
Edelstein, N., Brown, D., and Whittaker, B. (1974) *Inorg. Chem.*, **13**, 563–7.
Edelstein, N. M. (1979) in *Organometallics of the f-elements* (eds. T. J. Marks and R. D. Fischer), Reidel, Dordrecht, pp. 37–79.
Edelstein, N. (1987) *J. Less Common Metals*, **133**, 39–51.
Edelstein, N. M. (1991) *Eur. J. Solid State Inorg. Chem.*, **28**, 47–55.
Edelstein, N. (1992) in *Transuranium Elements: A Half Century* (eds. L. R. Morss and J. Fuger), American Chemical Society, Washington, DC, pp. 145–58.
Edelstein, N., Kot, W. K., and Krupa, J. C. (1992) *J. Chem. Phys.*, **96**, 1–4.
Edelstein, N. M. (1995) *J. Alloys Compds*, **223**, 197–203.
Edelstein, N. (2002) *Proc. SPIE-Int. Soc. Opt. Eng.*, **4766**, 8–21.
Eichberger, K. and Lux, F. (1980) *Ber. Bunsenges. Phys. Chem.*, **84**, 800–7.
Eisenstein, J. C. and Pryce, M. H. L. (1960) *Proc. Roy. Soc. A*, **255**, 181–98.
Eisenstein, J. C. and Pryce, M. H. L. (1966) *J. Res. NBS*, **70A**, 165–7.
Eremin, M. V. (1989) in *Spectroscopy of Crystals* (ed. A. A. Kaplyanskii), Nauka, Leningrad, p. 30.
Ermeneux, F. S., Goutaudier, C., Moncorge, R., Sun, Y., Cone, R. L., Zannoni, E., Cavalli, E., and Bettinelli, M. (2000) *Phys. Rev. B*, **61**, 3915–21.
Esterowitz, L., Bartoli, F. J., Allen, R. E., Wortman, D. E., Morrison, C. A., and Leavitt, R. P. (1979) *Phys. Rev. B*, **19**, 6442–55.
Faucher, M. D., Moune, O. K., Garcia, D., and Tanner, P. (1996) *Phys. Rev. B*, **53**, 9501–4.
Fellows, R. L., Peterson, J. R., Young, J. P., and Haire, R. G. (1978) in *The Rare Earths in Modern Science and Technology* (eds. G. J. McCarthy and J. J. Ryne), Plenum, New York, pp. 493–9.
Förster, T. (1948) Ann. Phys.(Germany), **2**, 55-75.
Fred, M. (1967) in *Lanthanide/Actinide Chemistry,* vol. 71 (eds. P. R. Fields and T. Moeller) ACS Adv. Chem. Ser. American Chemical Society, Washington, DC, pp. 180–202.
Garcia, D. and Faucher, M. (1995) in *Handbook on the Physics and Chemistry of Rare Earths,* vol. 21 (eds. K. A. Gschneidner Jr and L. Eyring), Elsevier, Amsterdam, p. 263.
Gerloch, M. and Slade, R. C. (1973) *Ligand-Field Parameters,* Cambridge University Press, Cambridge.
Goldschmidt, Z. B. (1978) in *Handbook on the Physics and Chemistry of Rare Earths,* vol. 1 (eds. K. A. Gschneidner Jr and L. Eyring), North-Holland, New York, pp. 1–172.

Goodman, G. L. and Fred, M. (1959) *J. Chem. Phys.*, **30**, 849–50.
Görller-Walrand, C., Behets, M., Porcher, P., Moune-Minn, O. K., and Laursen, I. (1985) *Inorg. Chim. Acta*, **109**, 83–90.
Görller-Walrand, C. and Binnemans, K. (1996) in *Handbook on the Physics and Chemistry of Rare Earth,* vol. 23 (eds. K. A. Gschneidner Jr and L. Eyring), Elsevier, Amsterdam.
Görller-Walrand, C. and Binnemans, K. (1998) in *Handbook on the Physics and Chemistry of Rare Earths,* vol. 25 (eds. K. A. Gschneidner Jr and L. Eyring), Elsevier, Amsterdam, pp. 101–264.
Gruen, D. M. and McBeth, R. L. (1969) *Inorg. Chem.*, **8**, 2625–33.
Hansen, J. E., Judd, B. R., and Crosswhite, H. (1996) *At. Data and Nucl. Data Tables*, **62**, 1–49.
Hartree, D. R. (1957) *The Calculation of Atomic Structures,* John Wiley, New York.
Hecht, H. G., Varga, L. P., Lewis, W. B., and Boring, A. M. (1979) *J. Chem. Phys.*, **70**, 101–8.
Hessler, J. P., Brundage, R. T., Hegarty, J., and Yen, W. M. (1980) *Opt. Lett.*, **5**, 348–50.
Huang, K. and Rhys, A. (1950) *Proc. Roy. Soc. A*, **204**, 406–23.
Hubert, S., Emery, J., Edelstein, N., and Fayet, J. C. (1985) *Solid State Commun.*, **54**, 1085–90.
Hubert, S., Thouvenot, P., and Edelstein, N. (1993) *Phys. Rev. B*, **48**, 5751–60.
Hüfner, S. (1978) *Optical Spectra of Transparent Rare Earth Compounds,* Academic Press, New York.
Hutchison, C. A. and Weinstock, B. (1960) *J. Chem. Phys.*, **32**, 56–61.
Illemassene, M., Murdoch, K. M., Edelstein, N. M., and Krupa, J. C. (1997) *J. Lumin.*, **75**, 77–87.
Inokuti, M. and Hirayama, F. (1965) *J. Chem. Phys.*, **43**, 1978–89.
Johnston, D. R., Satten, R. A., Schreiber, C. L., and Wong, E. Y. (1966a) *J. Chem. Phys.*, **44**, 3141–3.
Johnston, D. R., Satten, R. A., and Wong, E. Y. (1966b) *J. Chem. Phys.*, **44**, 687–91.
Jørgensen, C. K. (1957) *Acta Chem. Scand.*, **11**, 166–78.
Jørgensen, C. K. (1959) *Mol. Phys.*, **2**, 96–108.
Jørgensen, C. K. (1962) *Orbits in Atoms and Molecules,* Academic Press, London.
Jørgensen, C. K., Pappalardo, R., and Schmidtke, H. H. (1963) *J. Chem. Phys.*, **39**, 1422–30.
Jørgensen, C. K. (1970) *Prog. Inorg. Chem.*, **12**, 101–52.
Jørgensen, C. K. (1975) in *Structure and Bonding,* vol. 22, Springer-Verlag, New York, pp. 49–81.
Jørgensen, C. K. (1980) *Isr J. Chem.*, **19**, 174–92.
Jørgensen, C. K. (1982) *Chem. Phys. Lett.*, **89**, 455–8.
Judd, B. R. (1962) *Phys. Rev.*, **127**, 750–61.
Judd, B. R. (1963a) *Proc. Phys. Soc.*, (*London*) **82**, 874–81.
Judd, B. R. (1963b) *Operator Techniques in Atomic Spectroscopy,* McGraw-Hill, New York.
Judd, B. R. (1966) *Phys. Rev.*, **141**, 4–14.
Judd, B. R. (1968a) *Phys. Rev.*, **173**, 40–3.
Judd, B. R. (1968b) *Phys. Rev.*, **173**, 39–40.
Judd, B. R., Crosswhite, H. M., and Crosswhite, H. (1968) *Phys. Rev.*, **169**, 130–8.

Judd, B. R. (1975) *Angular Momentum Theory for Diatomic Molecules,* Academic Press, New York.
Judd, B. R. (1977a) *Phys. Rev. Lett.*, **39**, 242–4.
Judd, B. R. (1977b) *J. Chem. Phys.*, **66**, 3163–70.
Judd, B. R. (1979) *J. Lumin.*, **18–19**, 604–8.
Judd, B. R. and Crosswhite, H. (1984) *J. Opt. Soc. Am. B*, **1**, 255–60.
Judd, B. R. and Suskin, M. A. (1984) *J. Opt. Soc. Am. B*, **1**, 261–5.
Judd, B. R. (1988) in *Handbook on the Physics and Chemistry of Rare Earths,* vol. 11 (eds. K. A. Gschneidner Jr and L. Eyring), North-Holland, Amsterdam, pp. 81–195.
Judd, B. R. and Lo, E. (1996) *At. Data Nucl. Data Tables*, **62**, 51–75.
Kanellakopulos, B. and Fischer, R. D. (1973) in *Gmelin Handhuch der Anorganischen Chemie, Transurane A2,* Verlag Chemie, Weinheim, pp. 1–48.
Karbowiak, M., Drozdzynski, J., Murdoch, K. M., Edelstein, N. M., and Hubert, S. (1997) *J. Chem. Phys.*, **106**, 3067–77.
Karbowiak, M., Mech, A., and Drozdzynski, J. (2003) *Phys. Rev. B*, **67**, 195108–17.
Karraker, D. G. (1964) *Inorg. Chem.*, **3**, 1618–22.
Kaufman, V. and Radziemski, L. J. (1976) *J. Opt. Soc. Am.*, **66**, 599–601.
Kiarshima, A., Kimura, T., Tochiyama, O., and Yoshida, Z. (2003) *Chem. Commun.*, **2003**, 910–11.
Kimura, T. and Choppin, G. R. (1994) *J. Alloys Compds*, **213/214**, 313–17.
Kimura, T., Choppin, G. R., Kato, Y., and Yoshida, Z. (1996) *Radiochim. Acta*, **72**, 61–4.
Kimura, T., Kato, Y., and Choppin, G. R. (1997) in *Recent Progress in Actinides Separation Chemistry, Proc. Workshop on Actinides Solution Chemistry*, WASC '94, Tokai, Japan, September 1–2, 1994, pp. 149–64.
Kimura, T. and Kato, Y. (1998) *J. Alloys Compds*, **271–273**, 867–71.
Kimura, T., Nagaishi, R., Kato, Y., and Yoshida, Z. (2001) *Radiochim. Acta*, **89**, 125–30.
Kramers, H. A. (1930) *Proc. Amsterdam Acad.*, **33**, 959.
Krupa, J. C., Hubert, S., Foyentin, M., Gamp, E., and Edelstein, N. (1983) *J. Chem. Phys.*, **78**, 2175–9.
Krupa, J. C. (1987) *Inorg. Chim. Acta*, **139**, 223–41.
Krupa, J. C. and Carnall, W. T. (1993) *J. Chem. Phys.*, **99**, 8577–84.
Kugel, R., Williams, C., Fred, M., Malm, J. G., Carnall, W. T., Hindman, J. C., Childs, W. J., and Goodman, L. S. (1976) *J. Chem. Phys.*, **65**, 3486–92.
Larionov, A. L. and Malkin, B. Z. (1975) *Opt. Spektrosk.*, **39**, 1109–13.
Leung, A. F. (1977) *J. Phys. Chem. Solids*, **38**, 529–32.
Leung, A. F. and Poon, Y. M. (1977) *Can. J. Phys.*, **55**, 937–42.
Levin, L. I. and Cherpanov, V. I. (1983) *Sov. Phys.: Solid State*, **25**, 394–9.
Lewis, W. B., Mann, J. B., Liberman, D. A., and Cromer, D. T. (1970) *J. Chem. Phys.*, **53**, 809–20.
Liu, G. K. and Beitz, J. V. (1990a) *Phys. Rev. B*, **41**, 6201–12.
Liu, G. K. and Beitz, J. V. (1990b) *J. Lumin.*, **45**, 254–6.
Liu, G. K., Beitz, J. V., and Carnall, W. T. (1992) in *Transuranium Elements: A Half Century* (eds. L. R. Morss and J. Fuger), American Chemical Society, Washington, DC, pp. 181–6.
Liu, G. K., Beitz, J. V., and Huang, J. (1993) *J. Chem. Phys.*, **99**, 3304–11.

Liu, G. K., Carnall, W. T., Jones, R. P., Cone, R. L., and Huang, J. (1994a) *J. Alloys Compds*, **207–208**, 69–73.
Liu, G. K., Carnall, W. T., Jursich, G., and Williams, C. W. (1994b) *J. Chem. Phys.*, **101**, 8277–89.
Liu, G. K., Cao, R., Beitz, J. V., and Huang, J. (1996) *Phys. Rev. B*, **54**, 483–7.
Liu, G. K., Beitz, J. V., Huang, J., Abraham, M. M., and Boatner, L. A. (1997a) *J. Alloys Compds*, **250**, 347–51.
Liu, G. K., Huang, J., and Abraham, M. M. (1997b) *Phys. Rev. B*, **55**, 8967–72.
Liu, G. K., Li, S. T., Zhorin, V. V., Loong, C.-K., Abraham, M. M., and Boatner, L. A. (1998) *J. Chem. Phys.*, **109**, 6800–8.
Liu, G. K. (2000) in *Crystal Field Handbook* (eds. D. J. Newman and B. K. C. Ng), Cambridge University Press, Cambridge, pp. 65–82.
Liu, G. K., Chen, X. Y., and Huang, J. (2002) *Mol. Phys.*, **101**, 1029–36.
Loh, E. (1966) *Phys. Rev.*, **147**, 332.
Mackey, D. J., Runciman, W. A., and Vance, E. R. (1975) *Phys. Rev. B*, **11**, 211–18.
Malek, C. K. and Krupa, J. C. (1986) *J. Chem. Phys.*, **84**, 6584.
Malkin, B. Z., Ivanenko, Z. I., and Aizenberg, I. B. (1970) *Fiz. Tverd. Tela (USSR)*, **12**, 1873–80.
Malkin, B. Z. (1987) in *Spectroscopy of Solids Containing Rare Earth Ions* (eds. A. A. Kaplyanskii and R. M. Macfarlane), North-Holland, Amsterdam, pp. 13–50.
Marvin, H. H. (1947) *Phys. Rev.*, **71**, 102–10.
Matsika, S. and Pitzer, R. M. (2001) *J. Chem. Phys.*, **105**, 637–45.
Matsika, S., Zhang, Z., Brozell, S. R., Blaudeau, J.-P., Wang, Q., and Pitzer, R. M. (2001) *J. Phys. Chem. A*, **105**, 3825–8.
McClure, D. S. and Kiss, Z. (1963) *J. Chem. Phys.*, **39**, 3251–7.
Metcalf, D. H., Dai, S., Del Cul, G. D., and Toth, L. M. (1995) *Inorg. Chem.*, **34**, 5573–7.
Miyakawa, T. and Dexter, D. L. (1970) *Phys. Rev. B*, **1**, 2961–9.
Morosin, B. (1968) *J. Chem. Phys.*, **49**, 3007–12.
Morrison, J. C. (1972) *Phys. Rev. A*, **6**, 643–50.
Morrison, C. A. and Leavitt, R. P. (1982) in *Handbook on the Physics and Chemistry of Rare Earths,* vol. 5 (eds. K. A. Gschneidner Jr and L. Eyring), North-Holland, Amsterdam, pp. 461–692.
Morss, L. R., Williams, C. W., and Carnall, W. T. (1983) *ACS Symp. Ser.*, **216**, 199–210.
Morss, L. R. (2005) in this volume, see Chapter 19.
Moune, O. K., Faucher, M. D., and Edelstein, N. (2002) *J. Lumin.*, **96**, 51–68.
Mulford, R. N., Dewey, H. J., and Barefield II, J. E. (1991) *J. Chem. Phys.*, **94**, 4790–6.
Murdoch, K. M., Edelstein, N. M., Boatner, L. A., and Abraham, M. M. (1996) *J. Chem. Phys.*, **105**, 2539–46.
Murdoch, K. M., Nguyen, A. D., Edelstein, N. M., Hubert, S., and Gacon, J. C. (1997) *Phys. Rev. B*, **56**, 3038–45.
Murdoch, K. M., Cavellec, R., Simoni, E., Karbowiak, M., Hubert, S., Illemassene, M., and Edelstein, N. M. (1998) *J. Chem. Phys.*, **108**, 6353–61.
Nave, S., Haire, R. G., and Huary, P. G. (1983) *Phys. Rev. B*, **28**, 2317–27.
Newman, D. J. (1970) *Chem. Phys. Lett.*, **6**, 288–90.
Newman, D. J. (1971) *Adv. Phys.*, **20**, 197–256.
Newman, D. J. (1975) *J. Phys. C: Solid State Phys.*, **8**, 1862–8.
Newman, D. J. and Ng, B. (1989a) *J. Phys.: Condensed Matter*, **1**, 1613–19.

Newman, D. J. and Ng, B. (1989b) *Rep. Prog. Phys.*, **52**, 699–763.
Newman, D. J. and Ng, B. (2000) in *Crystal Field Handbook* (eds. D. J. Newman and B. Ng), Cambridge University Press, Cambridge, pp. 140–59.
Nielson, C. W. and Koster, G. F. (1963) *Spectroscopic Coefficients for the pn, dn, and fn Configurations,* MIT Press, Cambridge.
Ofelt, G. S. (1962) *J. Chem. Phys.*, **37**, 511–20.
Peterson, J. R. (1976) in *Gmelin Handhuch der Anorganischen Chemie,* 8th edn, Uranium Suppl. A5, Springer-Verlag, Berlin, pp. 57–84.
Peterson, J. R., Fellows, R. L., Young, J. P., and Haire, R. G. (1977) *Radiochem. Radioanal. Lett.*, **31**, 277–82.
Piehler, D., Kot, W. K., and Edelstein, N. (1991) *J. Chem. Phys.*, **94**, 942–8.
Poon, Y. M. and Newman, D. J. (1982) *J. Chem. Phys.*, **77**, 1077–9.
Poon, Y. M. and Newman, D. J. (1983) *J. Phys. B: At. Mol. Phys.*, **16**, 2093–101.
Racah, G. (1949) *Phys. Rev.*, **76**, 1352–65.
Rajnak, K. and Wybourne, B. G. (1963) *Phys. Rev.*, **132**, 280–90.
Rajnak, K. and Wybourne, B. G. (1964) *J. Chem. Phys.*, **41**, 565–9.
Rana, R. S., Cordero- Montalvo, C. D., and Bloembergen, N. (1984) *J. Chem. Phys.*, **81**, 2951–2.
Reid, M. F. and Richardson, F. S. (1984) *Mol. Phys.*, **51**, 1077–94.
Reid, M. F. and Richardson, F. S. (1985) *J. Chem. Phys.*, **63**, 95.
Reid, M. F. (1987) *J. Chem. Phys.*, **87**, 2875–84.
Reid, M. F. (2000) in *Crystal Field Handbook* (eds. D. J. Newman and B. Ng), Cambridge University Press, Cambridge, pp. 190–226.
Reisfeld, M. J. and Crosby, G. A. (1965) *Inorg. Chem.*, **4**, 65–70.
Richman, I., Kisliuk, P., and Wong, E. Y. (1967) *Phys. Rev.*, **155**, 262–7.
Riseberg, L. A. and Moos, H. W. (1967) *Phys. Rev. Lett.*, **25**, 1423–6.
Riseberg, L. A. and Moos, H. W. (1968) *Phys. Rev.*, **174**, 429–38.
Rotenberg, M., Bivins, R., Metropolis, R. B. N., and Wooten, J. K. Jr (1959) *The 3-j and 6-j Symbols,* MIT Press, Cambridge.
Ryan, J. L. (1971) *J. Inorg. Nucl. Chem.*, **33**, 153–77.
Satten, R. A., Schreiber, C. L., and Wong, E. Y. (1983) *J. Chem. Phys.*, **78**, 79–87.
Seijo, L. and Barandiaran, Z. (2001) *J. Chem. Phys.*, **115**, 55554–60.
Shen, Y. and Bray, K. L. (1998) *Phys. Rev. B*, **58**, 5305–13.
Slater, J. C. (1960) *Quantum Theory of Atomic Structure,* McGraw-Hill, New York.
Sobelman, I. I. (1972) *Theory of Atomic Spectra,* Pergamon, Oxford.
Soulie, E. (1978) *J. Phys. Chem. Solids*, **39**, 695–8.
Stafsudd, O. M., Leung, A. F., and Wong, E. Y. (1969) *Phys. Rev.*, **180**, 339–43.
Steindler, M. J. and Gerding, T. J. (1966) *Spectrochim. Acta*, **22**, 1197–200.
Stevens, K. W. H. (1952) *Proc. Phys. Soc.*, (*London*) **A65**, 209–15.
Suger, J. (1963) *J. Opt. Soc. Am.*, **53**, 831–5.
Sullivan, J. C., Gordon, S., Mulac, W. A., Schmidt, K. H., Cohen, D., and Sjoblom, R. (1976) *Inorg. Nucl. Chem. Lett.*, **12**, 599–601.
Thouvenot, P., Hubert, S., and Edelstein, N. (1993a) *Phys. Rev. B*, **48**, 5751–60.
Thouvenot, P., Hubert, S., Moulin, C., Decambox, P., and Mauchien, P. (1993b) *Radiochim. Acta*, **61**, 15–21.
Thouvenot, P., Hubert, S., and Edelstein, N. (1994) *Phys. Rev. B*, **50**, 9715–20.
Tinkham, M. (1964) *Group Theory and Quantum Mechanics,* McGraw-Hill, New York.

Tissue, B. M. and Wright, J. C. (1987) *Phys. Rev. B*, **36**, 9781–9.
Van Deurzen, C. H. H., Rajnak, K., and Conway, J. G. (1984) *J. Opt. Soc. Am. B*, **1**, 45–7.
van Pieterson, L., Reid, M. F., Burdick, G. W. and Meijerink, A. (2002a) *Phys. Rev. B*, **65**, 045114.
van Pieterson, L., Reid, M. F., Burdick, G. W. and Meijerink, A. (2002b) *Phys. Rev. B*, **65**, 045113.
Varga, L. P., Brown, J. D., Reisfeld, M. J., and Cowan, R. D. (1970) *J. Chem. Phys.*, **52**, 4233–41.
Wadt, W. R. (1987) *J. Chem. Phys.*, **86**, 339–46.
Weissbluth, M. (1978) *Atoms and Molecules,* Academic Press, New York.
Wild, J. F., Hult, E. K., Lougheed, R. W., Hayes, W. N., Peterson, J. R., Fellows, R. L., and Young, J. P. (1978) *J. Inorg. Nucl. Chem.*, **40**, 811–16.
Worden, E. F. J., Blaise, J., Trautmann, N., and Wyart, J. F. (2005) in this volume, see Chapter 16.
Wyart, J. F., Kaufman, V., and Suger, J. (1980) *Phys. Scr.*, **22**, 389–96.
Wybourne, B. G. (1965a) *Spectroscopic Properties of Rare Earths,* Wiley Interscience, New York.
Wybourne, B. G. (1965b) *J. Opt. Soc. Am.*, **55**, 928–35.
Wybourne, B. G. (1966) *Phys. Rev.*, **148**, 317–27.
Yen, W. M. (1987) in *Spectroscopy of Solids Containing Rare Earth Ions* (eds. A. A. Kaplyanskii and R. M. Macfarlane), North-Holland, Amsterdam, pp. 185–249.
Yusov, A. B. (1987) *Radiokhimiya*, **29**, 118–21.
Yusov, A. B. (1990) *J. Radioanal. Nucl. Chem.*, **143**, 287–94.
Yusov, A. B. (1993) *Radiokhimiya*, **35**, 3–25.
Zhorin, V. V. and Liu, G. K. (1998) *J. Alloys Compds*, **275–277**, 137–41.